

UNIVERSITÄTSKLINIKUM HAMBURG-EPPENDORF

I. Medizinische Klinik und Poliklinik

Prof. Dr. med. Ansgar W. Lohse

The role of B cells in a mouse model of autoimmune hepatitis

Dissertation

zur Erlangung des Grades eines Doktors der Medizin
an der Medizinischen Fakultät der Universität Hamburg.

vorgelegt von:

Lena Amrei Schlott
aus Hamburg

Hamburg 2021

urn:nbn:de:gbv:18-ediss-99929

**Angenommen von der
Medizinischen Fakultät der Universität Hamburg am: 22.03.2022**

**Veröffentlicht mit Genehmigung der
Medizinischen Fakultät der Universität Hamburg.**

Prüfungsausschuss, der/die Vorsitzende: Prof. Dr. Linda Diehl

Prüfungsausschuss, zweite/r Gutachter/in: Prof. Dr. Johannes Herkel

Contents

1	List of abbreviations	7
2	Introduction	9
2.1	Immune tolerance to self.....	9
2.1.1	Mechanisms of self-tolerance	9
2.1.1.1	Clonal deletion and receptor editing.....	10
2.1.1.2	Anergy.....	11
2.1.1.3	Regulatory T cells.....	11
2.1.1.4	Clonal ignorance.....	13
2.2	Autoimmunity.....	14
2.2.1	Breach of tolerance.....	14
2.2.2	Drivers of autoimmunity	15
2.2.2.1	T cells.....	15
2.2.2.2	B cells.....	17
2.3	Local and systemic autoimmune diseases.....	18
2.3.1	Organ-specific autoimmunity: Autoimmune hepatitis.....	19
2.3.2	Systemic autoimmunity: Systemic lupus erythematosus	20
2.4	Mouse model of AIH – Alb-iGP_Smarta.....	21
2.4.1	Introduction of the model	21
2.4.2	Basic characterization of the Alb-iGP_Smarta mouse model	23
2.5	Mouse models to examine the role of B cells in AIH	24
2.5.1	CD19-iGP_Smarta.....	24
2.5.2	Alb-/CD19-iGP_Smarta	26
2.6	Objectives.....	26
2.6.1	Examining the role of autoantigen-presentation by B cells for the development of AIH	26

2.6.2	Examining the role of autoantigen-presentation by B cells for the development of systemic autoimmunity.....	27
3	Material & Methods.....	28
3.1	Instruments.....	28
3.2	Material.....	29
3.3	Software.....	34
3.4	Buffer and other solutions.....	34
3.5	Laboratory animals.....	36
3.6	Methods.....	37
3.6.1	Organ sampling.....	37
3.6.2	Cell isolation.....	38
3.6.2.1	Cell isolation from the spleen, thymus and lung.....	38
3.6.2.2	Cell isolation from the liver.....	38
3.6.2.3	Cell isolation from the kidney.....	38
3.6.3	Flow cytometry.....	39
3.6.4	Histology.....	39
3.6.4.1	Haemalum and eosin (H&E).....	39
3.6.4.2	Periodic Acid Schiff (PAS).....	40
3.6.5	Immunohistochemistry.....	40
3.6.6	Indirect immunofluorescence staining of serum autoantibodies.....	41
3.6.7	Measurement of transaminases.....	41
3.6.8	Statistical analysis.....	41
4	Results.....	42
4.1	The role of B cells in a mouse model for AIH: Alb-/CD19-iGP_Smarta mice.....	42
4.1.1	Autoantigen-presentation by B cells shapes the repertoire of autoreactive T cells.....	42
4.1.1.1	Flow cytometry gating strategy for T cell analysis.....	42
4.1.1.2	Antigen-specific Smarta T cells are not deleted when autoantigen is expressed in B cells or hepatocytes.....	43

4.1.1.3	Co-expression of autoantigen in B cells and hepatocytes does not alter the Foxp3 ⁺ Treg frequency in Alb-/CD19-iGP_Smarta mice	46
4.1.2	Autoantigen-presentation by B cells results in a diverse autoantibody production.....	48
4.1.2.1	Flow cytometry gating strategy for CD19 ⁺ B220 ⁺ B cells.....	48
4.1.2.2	B cell numbers are not altered in mice co-expressing the autoantigen in B cells and hepatocytes	48
4.1.2.3	Autoantigen-presentation by B cells results in a diverse autoantibody pattern	49
4.1.3	Co-expression of antigen in B cells and hepatocytes leads to the formation of ELT in the liver, but not to liver inflammation in young Alb-/CD19-iGP_Smarta mice ..	51
4.1.3.1	ELT can be found in the liver of Alb-/CD19-iGP_Smarta mice	51
4.1.3.2	Alb-/CD19-iGP_Smarta mice show no exacerbated liver damage	52
4.1.4	Lymphocyte composition in Alb-/CD19-iGP_Smarta mice is not sex-dependent.....	53
4.2	Characterization of the CD19-iGP_Smarta mouse model of autoantigen-presentation by B cells.....	54
4.2.1	Development of immunological processes in eight-week-old CD19-iGP_Smarta mice	54
4.2.1.1	Presence of antigen-specific Smarta T cells, reduction of Tregs and formation of ELT in the lungs of CD19-iGP_Smarta mice.....	54
4.2.1.1.1	Formation of lymphatic structures in the lungs of CD19-iGP_Smarta mice	55
4.2.1.1.2	Autoantigen-presentation by B cells leads to presence of antigen-specific Smarta cells and a reduction of Tregs in the lungs of CD19-iGP_Smarta mice	57
4.2.1.1.3	Autoantigen-presentation by B cells leads to reduced B cell frequencies in the lungs of CD19-iGP_Smarta mice	58
4.2.1.2	Reduced amount of B cells in the liver of CD19-iGP_Smarta mice	59
4.2.1.3	Kidneys of CD19-iGP_Smarta mice show an age-related increase in intraglomerular cell number	60

4.2.2	Systemic autoimmune disease in CD19-iGP_Smarta mice.....	61
4.2.2.1	Characterization of autoimmune pathology in CD19-iGP_Smarta mice	61
4.2.2.2	Increase of T cells with reduced frequency of Tregs in diseased CD19-iGP_Smarta mice.....	64
4.2.2.2.1	Increase of T cells in diseased CD19-iGP_Smarta mice.....	64
4.2.2.2.2	Reduction of Tregs in diseased CD19-iGP_Smarta mice.....	67
4.2.2.3	Reduction of the overall B cell frequency but increase of the Plasma cell frequency in diseased CD19-iGP_Smarta mice.....	67
4.2.2.3.1	Age-related reduction of B cells in CD19-iGP_Smarta mice	68
4.2.2.3.2	Higher frequency of Plasma cells in diseased CD19-iGP_Smarta mice	69
4.2.2.3.3	B cell activation marker expression is elevated in diseased CD19-iGP_Smarta mice	73
4.2.3	Disease development and severity in CD19-iGP_Smarta mice is not sex-dependent.....	75
5	Discussion	77
5.1	Autoantigen-presenting B cells in experimental AIH.....	77
5.2	Systemic autoimmune disease induction by autoantigen-presenting B cells	81
6	Summary	88
7	Zusammenfassung	89
8	Bibliography	91
9	List of figures	97
10	List of tables.....	101
11	Acknowledgements.....	101
12	Curriculum Vitae	102
13	Eidesstattliche Versicherung.....	103

1 List of abbreviations

ACK	ammonium-chloride-potassium
AIH	autoimmune hepatitis
AIRE	autoimmune-regulator
ALT	alanine aminotransferase
APC	antigen presenting cell
AST	aspartate aminotransferase
BAFF	B cell survival factor
BCL-6	B cell leukemia/lymphoma 6
BCR	B cell receptor
B _{eff}	B effector cell
CD	cluster of differentiation
CLIP	class II-associated invariant chain peptide
cTEC	cortical thymic epithelial cell
CTLA-4	cytotoxic T-lymphocyte-associated protein 4
D	diversity
DC	dendritic cell
DMSO	dimethyl sulfoxide
DNA	desoxyribonucleic acid
DNase	desoxyribonuclease
EAE	experimental autoimmune encephalomyelitis
EDTA	ethylenediaminetetraacetic acid
ELT	ectopic lymphoid tissue
FACS	fluorescence-activated cell sorting
FCS	fetal calf serum
FDC	follicular dendritic cell
FOXP3	forkhead box protein 3
GATA3	GATA binding protein 3
GP	glycoprotein
HCL	hydrochloric acid
IFN γ	interferon gamma
IgE	immunoglobulin E
IgG	immunoglobulin G
IL	interleukin
J	joining
MFI	mean fluorescence intensity
MHC	major histocompatibility complex
MOG	myelin oligodendrocyte glycoprotein
mRNA	messenger ribonucleic acid
mTEC	medullary thymic epithelial cell
PAS	periodic acid schiff
PBS	phosphate buffered saline
PFA	paraformaldehyde
RCF	relative centrifugal force
ROR γ	RAR-related orphan receptor gamma
SLE	systemic lupus erythematosus
TBX21	T-box 21
TCR	T cell receptor
T _{eff}	T effector cells
T _{FH}	T follicular helper cell
TGF β	transforming growth factor beta

T_H1..... *T helper 1*
T_H17..... *T helper 17*
T_H2..... *T helper 2*
TNF α *tumour necrosis factor alpha*
Treg..... *regulatory CD4 T cell*
TSA *tissue specific antigen*
V..... *variable*

2 Introduction

2.1 Immune tolerance to self

The human immune system defends the body against a broad spectrum of different germs. To be able to do so, the innate immune system reacts instantly to infections preventing fast spreading of pathogens. In addition, the adaptive immune system, mainly consisting of B and T cells, initiates a specific response to pathogens to ensure their effective clearance and maintains a memory response to enable faster and more specific reaction upon reinfection.

Therefore, during the maturation of T and B cells in the thymus and bone marrow, a recombination of the variable (V), diversity (D) and joining (J) genes takes place to generate a vast repertoire of different B cell receptors (BCRs) and T cell receptors (TCRs) with allelic exclusion ensuring that each cell has only one specific receptor (Nossal, 1994, Goodnow et al., 2005). This random process enables T and B cells to react to a wide range of structures, in particular peptides. But it also bears a high risk: 20 to 50 % of TCRs and BCRs generated by V(D)J recombination bind with a potentially dangerous affinity to self-antigen (Ignatowicz et al., 1996, Zerrahn et al., 1997, Laufer et al., 1996, Wardemann et al., 2003). However, only up to 5 % of the population of western countries develop autoimmune diseases, which evolve from a reaction of the immune system against self-antigens. This shows that the organism developed mechanisms of self-tolerance in order to prevent a reaction of T and B cells against their host (Murphy and Weaver, 2016).

In the following, the most important self-tolerance mechanisms are described. They are derived from the findings in animal models, human cell culture experiments and the analysis of genetic defects causing autoimmune diseases and immunodeficiencies.

2.1.1 Mechanisms of self-tolerance

The generation of self-tolerance is based on a multilevel system of several checkpoints, with each of them being able to eliminate or disarm a certain amount of potentially autoreactive lymphocytes, and which taken together can effectively prevent autoimmune reactions. (Goodnow et al., 2005) In reverse conclusion, the failure of one of the mechanisms usually does not lead to the onset of autoimmunity but a deficiency in several mechanisms is needed to break tolerance.

The checkpoints of self-tolerance can be categorized in those taking place during the maturation of T and B cells in thymus and bone marrow, which are called central tolerance mechanisms. These include clonal deletion and receptor editing.

In addition there are mechanisms of peripheral tolerance, which can be again divided into cell intrinsic mechanisms including induction of anergy and extrinsic regulation of autoreactive cells through regulatory cells, mainly regulatory cluster of differentiation (CD) 4 T cells (Tregs) (Goodnow et al., 2005).

2.1.1.1 Clonal deletion and receptor editing

Clonal deletion is the most important mechanism of central tolerance. It ensures the apoptotic cell death of most T and B cells bearing a TCR or BCR recognizing self-antigen due to V(D)J recombination.

In the bone marrow, maturing B cells are exposed to self-antigens. At this stage, the B cells are especially sensitive to tolerance induction, so that only low antigen concentrations are needed to induce a cell intrinsic program leading to apoptosis of the antigen recognizing B cells (Nossal and Pike, 1975, Metcalf and Klinman, 1977). If crosslinking of the BCR is too strong, intracellular signalling exceeds a certain threshold, which causes the internalization of the BCR and an intermission of the ongoing maturation program (Nemazee and Hogquist, 2003, Hartley et al., 1993, Fields and Erikson, 2003). As a consequence, the B cell is not able to express homing receptors needed for the entry into secondary lymphoid organs and up-regulates the expression of pro-apoptotic factors. However, the cell is not immediately deleted, but instead the VJ recombination is continued giving the cell a chance to escape apoptosis through editing its receptor via light chain replacement (Nemazee and Hogquist, 2003, Hartley et al., 1993, Mackay et al., 2003, Jankovic et al., 2004). If the B cell fails to edit its BCR to a less self-reactive kind, it will die within one to two days (Hartley et al., 1993, Strasser and Bouillet, 2003, Tiegs et al., 1993). Clonal deletion and receptor editing mainly prevent the formation of B cells recognizing systemic antigens, as these are displayed in the bone marrow (Goodnow et al., 2005). Nevertheless, many B cells binding self-antigen with only low affinity escape these mechanisms and may develop into antibody-producing plasma cells. Still, in most cases this does not lead to the onset of autoimmunity but the formation of autoantibodies to some extent is rather normal (Nossal, 1994).

In the thymus, potentially autoreactive T cells are mainly deleted while receptor editing plays a less important role than in B cell development (Nemazee and Hogquist, 2003). Those T cells binding to peptides presented on major histocompatibility complex (MHC) by cortical thymic epithelial cells (cTECs) trigger intrinsic maturation signals and stop V(D)J recombination, so that no further editing is possible. The positively selected immature T cells then migrate to the thymic medulla, where they encounter medullary thymic epithelial cells (mTECs) and dendritic cells (DCs) also presenting self-peptide on MHC, but this time

accompanied by costimulatory molecules. Strong binding of the TCR to MHC/self-peptide complexes now induces apoptotic cell death (Palmer, 2003). One special feature in T cell development is that due to the autoimmune-regulator (AIRE) transcription factor mTECs are not only able to present thymic antigens but also peripheral antigens which are specifically restricted to certain tissues. This enables tolerance induction to systemic as well as tissue-specific antigens already at this state (Anderson and Su, 2016).

2.1.1.2 Anergy

As already mentioned above, not all potentially autoreactive T and B cells are deleted in the primary lymphoid organs. Lymphocytes that bind antigen with only low affinity or bind antigens that are not displayed in bone marrow or thymus may escape clonal deletion and end up in the periphery. Especially for T cells, additional tolerance mechanisms are important, as all T cells leaving the thymus have been selected with a moderate degree of self-reactivity by the cTECs (Goodnow et al., 2005). Under steady-state conditions in the absence of pro-inflammatory stimuli, such T cells are either inactivated in the periphery or may develop into regulatory lymphocytes as described in 2.1.1.3 (Murphy and Weaver, 2016).

In B cells, peripheral inactivation of autoreactive cells is due to a decreased display of self-reactive BCRs, decreased BCR signalling and an increased threshold for activation (Benschop et al., 2001, Goodnow et al., 2005). In T cells, peripheral antigen recognition under non-inflammatory conditions leads to the upregulation of inhibitory receptors, which in turn suppress the response to self-peptides and inhibit activation through co-stimulatory molecules of antigen presenting cells (APCs) (Goodnow et al., 2005). Thus, these cells fail to respond to their specific antigen, a state which is called anergy. Anergic lymphocytes have a reduced life span of only a few days showing that anergy and deletion are not two separate mechanisms but shading into each other (Fulcher and Basten, 1994, Nossal, 1994).

2.1.1.3 Regulatory T cells

The most important extrinsic regulation of self-recognizing lymphocytes happens through regulatory lymphocytes, of which the CD4 positive, forkhead box protein 3 (FOXP3) positive Tregs play the most important role. This group of cells consists of two different subsets, the thymic derived Tregs and peripheral derived Tregs which can differentiate from naïve T cells in the periphery. Two characteristic markers of both these subsets are the FOXP3 transcription factor as well as CD25, the interleukin (IL) 2 receptor alpha chain (Murphy and Weaver, 2016).

One very important stimulus for Tregs is IL-2, as it is required for sustained FOXP3 and CD25 expression. Moreover, IL-2 enhances the suppressive function and promotes survival and expansion of Tregs (Fontenot et al., 2005, Shevach et al., 2006, Laurence et al., 2007). As IL-2 is produced by activated effector T cells, it facilitates a natural feedback control in which Tregs not only provide control of potentially self-reactive lymphocytes but also of overflowing reactions to pathogens (Sakaguchi et al., 2008).

Thymus derived Tregs mature in the thymus and make up 10-15 % of the circulating CD4 T cell population (Murphy and Weaver, 2016). In contrast to the other T cell subpopulations, they are already mature and antigen-primed when leaving the thymus and need no further activation process to receive the effector status (Sakaguchi et al., 1982, Itoh et al., 1999). T cells with a high affinity to thymic MHC-II/self-peptide ligands may be selected to develop into Tregs and thereby become resistant to clonal deletion (van Santen et al., 2004). The strong binding of the TCR to MHC-II/self-peptide on thymic stromal cells switches on a transcriptional regulation program leading to Treg development, with FOXP3 stabilizing the Treg phenotype and enabling the suppressive activity. Presentation of tissue-specific antigens (TSAs) by mTECs due to AIRE also enables the development of Tregs specific for TSAs (Sakaguchi et al., 2008).

Peripheral derived Tregs can evolve from activated naïve T cells in the periphery under the influence of the cytokine transforming growth factor beta (TGF β) in the absence of IL-6 (see 2.2.2.1). This is usually the case in the absence of infection, as IL-6 is produced by innate immune cells in the presence of pathogens. FOXP3 also plays an important role in peripheral Treg induction, as it blocks other transcription factors facilitating the activation and differentiation of T effector cells (T_{eff}), and instead converts them into Tregs (Sakaguchi et al., 2008, Murphy and Weaver, 2016).

Tregs are usually located in the regional lymph nodes of those tissues containing the antigens they are specific for, but may also migrate to inflamed tissues, infectious sites and tumours similar to the T_{eff} cells (Samy et al., 2005, Belkaid et al., 2002). Even though both Tregs and T_{eff} cells can be activated by the same antigens, the Treg activation takes place at much lower antigen concentrations (Takahashi et al., 1998), allowing a tonic suppression of self-reactive T cells and prohibiting molecular mimicry (see 2.2.1).

The suppressive function of Tregs is not only directed against the activities of T_{eff} cells but also against the proliferation and differentiation of naïve T cells as well as the function of natural killer cells, B cells, macrophages, osteoclasts and DCs (Sakaguchi et al., 2008).

Furthermore, they can suppress T cells irrespective of whether they share antigen-specificity or not, as long as the recognized antigen derives from the same tissue or is presented by the same APC (Takahashi et al., 1998). Suppression by Tregs can be executed in three different ways: They can out-compete naïve T cells by consumption of IL-2 due to their constitutive expression of the high affinity receptor for IL-2. Moreover, Tregs can down-regulate the stimulatory function of DCs. Through inhibitory molecules like cytotoxic T-lymphocyte-associated protein 4 (CTLA-4) which binds the co-stimulatory ligands of APCs, Tregs can interfere with effective co-stimulation of T_{eff} cells by DCs. Furthermore, Tregs can suppress via secretion of the inhibitory cytokines TGFβ and IL-10. TGFβ blocks T cell cytokine production, proliferation as well as their killing ability. IL-10 also suppresses cytokine production, especially of IL-2, tumour necrosis factor alpha (TNFα) and IL-5, and in addition reduces the expression of MHC and co-stimulatory molecules on APCs (Sakaguchi et al., 2008, Murphy and Weaver, 2016).

Besides the FOXP3⁺ Tregs there are some other FOXP3⁻ cell populations like T helper 3 or T regulatory 1 cells that also express immunosuppressive cytokines characteristic for Tregs, especially IL-10. These are among others enriched in intestinal tissues, but since they are not very relevant for this work they are not further discussed here (Murphy and Weaver, 2016).

2.1.1.4 Clonal ignorance

Despite all the above described mechanisms to delete or inactivate self-recognizing lymphocytes, some of these potentially self-reactive cells fail for some reason to interact with the self-antigen and therefore escape any tolerance mechanism. This can be due to a very low affinity to the self-antigen so that any induced signalling stays below the threshold. Another reason can be that the self-recognizing lymphocyte is not encountering its antigen because they are separated from each other, a condition called sequestration. Both these circumstances lead to ignorance of autoantigens by potentially pathogenic autoreactive clones. If for any reason the circumstances change, for example if the threshold for activation is lowered due to more co-activating factors, or if the barrier of sequestration is broken, both likely to occur upon infection or inflammation in general, former ignorant self-recognizing lymphocytes may be activated and induce autoimmunity (Nossal, 1994, Murphy and Weaver, 2016).

2.2 Autoimmunity

Autoimmunity is defined as the “response to self-antigens or antigens associated with the commensal microbiota” and may lead to autoimmune diseases, which are discussed in 2.3. The concept of autoimmunity was first presented by Paul Ehrlich in the beginning of the 20th century and since then, the factors causing the onset of autoimmunity have been the subject of intensive research. It is now believed that the development of autoimmunity and autoimmune diseases results from a combination of genetic susceptibility, the breakdown of tolerance mechanisms and environmental triggers that in many cases cause the outbreak of disease (Murphy and Weaver, 2016).

2.2.1 Breach of tolerance

The dysfunction of one or several checkpoints of self-tolerance can lead to autoimmune reactions of T cells, B cells or both. The reasons of these dysfunctions can be genetic defects but also environmental causes, for example infectious diseases. Possible mechanisms that breach self-tolerance and lead to the development of autoimmune diseases are the reversal of anergy or clonal ignorance, cross-reactions due to molecular mimicry between autoantigens and pathogen-derived antigens and the lack or dysfunction of Tregs (Murphy and Weaver, 2016).

An anergic cell is not able to react to co-stimulatory signals under physiological circumstances and can therefore not be activated. However, anergy is not an ultimate condition but can be reversible if the immunological signalling was strong enough (Goodnow et al., 1991). In inflammatory conditions, when concentrations of pro-inflammatory cytokines, co-stimulatory molecules and numbers of APCs and activated T and B cells are increased, anergic lymphocytes might get activated to proliferate and differentiate (Murphy and Weaver, 2016).

By the same token, ignorant lymphocytes can be activated, if the barrier of antigen sequestration was broken. A common and striking example for this is the formation of autoantibodies against nuclear antigens in systemic lupus erythematosus (SLE, see 2.3.2). This disease is characterized by extracellular release of nuclear antigens, due to inadequate clearance of apoptotic cells by the mononuclear phagocytic system. This increased concentration and availability of antigen can lead to the activation of previously ignorant T and B cells and the formation of autoantibodies. This can also induce a feed forward loop, as activated lymphocytes as well as immune complexes consisting of autoantibodies and autoantigens increase the formation and release of pro-inflammatory cytokines, which in turn promotes apoptotic cell death and therefore the release of more nuclear antigens

(Tsubata, 2017, Murphy and Weaver, 2016). An ignorant B cell can also be activated when its recognized antigen changes into an immunogenic form. This occurs for instance when monomeric Immunoglobulin G (IgG) in the blood, which alone cannot crosslink the BCR and therefore cannot activate B cells, forms immune complexes, which can crosslink the BCR (Murphy and Weaver, 2016).

Another way to break B or T cell tolerance is by cross-reaction or molecular mimicry. If a foreign pathogen resembles a self-antigen, which is called molecular mimicry, the cognate T and B cells will not only react to the pathogen but also to the similar host structure (Fujinami et al., 1983).

A pathogen derived molecule may also bind to a host structure, for example an enzyme. A B cell recognizing the pathogen via its BCR internalizes the complex of pathogen and enzyme and presents peptides of both on MHC-II, thereby also providing help to self-reactive T cells which could otherwise not be activated (Mamula et al., 1994).

Probably one of the most severe defects in self-tolerance concerns the extrinsic regulation of self-recognizing lymphocytes through regulatory cells, especially Tregs. If due to genetic mutations the function of Tregs is impaired, their number is reduced, or even completely absent, this will almost always lead to the emergence of various autoimmune diseases (Murphy and Weaver, 2016).

2.2.2 Drivers of autoimmunity

The drivers of autoimmunity and autoimmune diseases are the cells of the adaptive immune system, B and T cells, even though the cells of the innate immune system are usually also involved. Autoreactive CD4 T cells differentiate into different T helper cells, which recruit and activate cells of the innate immune system, such as neutrophils and macrophages, and co-stimulate B cells. These in turn develop into plasma cells that secrete antibodies, which may activate the complement system causing cell death, initiate chemokine and cytokine release and form immune complexes. In the following, the different types of T helper cells as well as the different maturation stages and functions of B cells are described. The development of CD8 T cells into cytotoxic T cells, which trigger apoptotic cell death in a contact-dependent manner, is neglected here, as it is of minor importance for this work.

2.2.2.1 T cells

After previous activation and three to four days of proliferation stimulated by IL-2, CD4 T cells differentiate into T_{eff} cells, which are also called T helper cells and do not need further co-stimulation to execute their effector functions.

They can be classified into different subclasses of which the T helper 1 (T_H1), T helper 2 (T_H2), T helper 17 (T_H17) and T follicular helper cells (T_{FH}) cells are described in more detail here. Whether a T cell develops into one of these subclasses, depends on the cytokines released in their environment by cells of the innate immune system or B cells.

A T cell develops into a T_H1 cell under the influence of IL-12. T_H1 cells produce interferon gamma ($IFN\gamma$) and $TNF\alpha$ and thereby and through direct cell-interactions activate and stimulate macrophages. T_H1 cytokines also induce class-switch in B cells to IgG (see 2.2.2.2). The master transcription factor of T_H1 cells is T-bet encoded by the T-box 21 (TBX21) gene as it switches on the genes of $IFN\gamma$ and the IL-12 receptor.

Development into T_H2 cells occurs under the influence of IL-4. T_H2 cells produce the cytokines IL-4, IL-5, IL-10 and IL-13 and promote the function of eosinophils and mast cells as well as B cell class-switch to immunoglobulin E (IgE) to control infections by parasites. Their master transcription factor is GATA binding protein 3 (GATA3) which turns on the transcription of the genes of several cytokines released by T_H2 cells along with its own GATA3 gene to stabilize T_H2 phenotype.

T_H17 cells arise in the presence of $TGF\beta$ together with IL-6 in the absence of IL-4, IL-12 and larger amounts of IL-2. Their name is derived from their production of cytokines of the IL-17 family. Their development requires initial production of IL-21 by the T cell itself, which leads to autocrine stimulation and activation of T_H17 transcription factors, including the master transcription factor RAR-related orphan receptor gamma ($ROR\gamma$), which drives the expression of characteristic T_H17 cytokines. This cell type helps in controlling infections with extracellular bacteria or fungi by engaging the neutrophil response (Cosmi et al., 2014).

T_{FH} cells are one of the newer discovered CD4 T cell populations. It is yet not entirely clear which cytokines are needed for their development, even though IL-6 seems to play an important role. Their master transcription factor is B cell leukemia/lymphoma 6 (BCL-6), which is required for the expression of CXCR5, a chemokine receptor that together with the ICOS receptor is one of the typical T_{FH} cells markers. The main T_{FH} function is to activate B cells and provide help during their affinity maturation in germinal centres. A special feature of T_{FH} cells is that they can either produce cytokines of the T_H1 or T_H2 phenotype, depending on which antibody the B cells are supposed to switch to, which in turn depends on the kind of ongoing infection (Murphy and Weaver, 2016).

2.2.2.2 *B cells*

B cells develop in the bone marrow, yet the B cells leaving the bone marrow are still immature. Most of these immature B cells die, as only a few manage to enter the follicles, the B cell zones of the secondary lymphoid organs, where they receive essential survival signals through the B cell survival factor (BAFF) secreted by follicular dendritic cells (FDCs). Once entered a follicle, they develop into mature B cells.

Upon encounter of their cognate antigen displayed by FDCs or macrophages, they move to the border between the T and B cell zone driven by chemokine attraction. Differentiated T_{FH} cells also migrate there and interact with B cells through MHC-II-TCR binding, co-stimulatory molecules and cytokine secretion, resulting proliferation of the B cell. This interaction also induces the expression of more co-stimulatory molecules and MHC-II complexes on the B cell and enables its survival.

The proliferating B cells form a primary focus where they differentiate first into plasmablasts and then into plasma cells, guaranteeing fast secretion of specific antibodies. This antibody response however consists mainly of IgM and is not highly effective. Therefore, some activated B cells together with T_{FH} cells migrate back to the follicle where they form a germinal centre. Stimulated by the T_{FH} cells, the germinal centre B cells undergo class-switching from IgM to IgG, IgA or IgE depending on which cytokines are produced by the T_{FH} cells. Moreover, somatic hypermutations take place, which are mainly point mutations in the immunoglobulin V-regions genes. Most of these mutations have a negative impact, therefore the germinal centre is filled with apoptotic cells, but some result in a higher antigen affinity of the BCR. Therefore, this process is also called affinity maturation. These germinal centre B cells are positively selected as they receive more proliferation and maturation signals, reduce their proliferation rate and instead enter the growth phase while raising the expression of immunoglobulins on their surface. They exit the germinal centre and evolve into either plasma cells or memory B cells (Murphy and Weaver, 2016).

Plasma cells can be short-lived or long-lived. The short-lived plasma cells stay in the lymph nodes or the red pulp of the spleen, whereas the long-lived plasma cells migrate to the bone marrow where they are responsible for continued antibody production. Antibodies are the main part of the humoral immune response and indispensable for effective pathogen clearance. Their functions include the neutralization of soluble antigens like toxins, opsonisation of pathogens to boost macrophage activity or activation of the complement system, which promotes the inflammatory reaction and induces complement-mediated cell death. The latter together with the formation of immune complexes can cause severe damage in autoimmune diseases.

As opposed to most B cell maturation stages including mature B cells, which carry the markers CD19 and CD20 in humans and CD19 and B220 in mice, respectively, plasma cells no longer carry CD20 (B220) but only CD19 and other specific markers like CD138 (Ribatti, 2017).

Memory B cells are generated to enable a faster and more effective immune response upon reinfection with the same pathogen. They have a very long life span and divide slowly, express immunoglobulins on their surface but do not secrete antibodies.

The expression of MHC-II and co-stimulatory molecules on memory B cells is higher than on mature B cells. Therefore, memory B cells can be activated at lower antigen doses and react faster. They share many markers with activated B cells, but also carry some unique markers like CD27 (Murphy and Weaver, 2016).

It was long believed that antibody production by plasma cells was the only important function of B cells in the adaptive immune response, but now it is known that activated follicular B cells can also differentiate into effector B cells (B_{eff}) that modulate the immune response via cytokine secretion. These B_{eff} cells can be divided into two groups depending on the T helper cell type they had been primed by, and which differ in the type of cytokines they produce. B_{eff} 1 cells had been primed by $T_{\text{H}1}$ cells and produce $\text{IFN}\gamma$ and IL-12, thereby supporting $T_{\text{H}1}$ responses. B_{eff} 2 cells had been primed by $T_{\text{H}2}$ cells and secrete mainly IL-2, IL-13 and IL-4, which promotes $T_{\text{H}2}$ responses (Lund et al., 2005, Harris et al., 2000). Beyond that, a regulatory cell population of B cells has been discovered that supposedly develops from maturing B cells or a distinct B cell subpopulation, the marginal zone B cells. Like Tregs, these regulatory B cells secrete IL-10 and $\text{TGF}\beta$ and thereby suppress immune responses (Mizoguchi and Bhan, 2006).

2.3 Local and systemic autoimmune diseases

Autoimmune episodes can become chronic and manifest as clinical disease that is characterized by tissue damage due the following reasons: As the self-antigen can obviously not easily be cleared and is ubiquitously present, the autoimmune reaction can hardly be limited. Instead, constant autoantigen presence leads to chronic inflammation, which consequently leads to increasing tissue damage and thereby the release of more autoantigens (see 2.2.1). This may also cause the recruitment of more effector cells by a process called epitope spreading. Due to the inflammation and destruction, more self-recognizing B and T cells can react to other autoantigens than the initial ones, as they are now also present in high concentrations and available for the immune system (Powell

and Black, 2001). For these reasons, an autoimmune disease once broken out is very hard to control and usually needs lifelong treatment.

Autoimmune diseases may be categorized in two classes: organ-specific, when the antigen is tissue restricted and therefore the autoimmune reaction is restricted to a certain organ, or systemic, when the antigen is present (almost) everywhere in the body and therefore many organs are affected by the tissue damage (Murphy and Weaver, 2016).

In the following, the autoimmune diseases, which had been most relevant for this study, are briefly introduced: autoimmune hepatitis (AIH) as a form of organ-specific autoimmunity, as well as SLE as one of the most frequent forms of systemic autoimmunity.

2.3.1 Organ-specific autoimmunity: Autoimmune hepatitis

AIH is a chronic inflammatory disease of unknown cause that occurs in all ages and ethnicities with a higher incidence in females (Moritoki et al., 2006, Manns et al., 2015). Genetic as well as environmental factors are likely to be involved in the pathogenesis of the disease (Manns et al., 2015, Manns et al., 2010). During the course of the disease, a breach of T cell tolerance to liver antigen occurs, leading to a destruction of liver parenchyma in the form of necro-inflammatory processes and fibrosis. So far, there is little known about the trigger factors leading to the breach of self-tolerance or the mechanisms determining the severity of the disease. The autoimmune inflammation in the liver may lead to liver cirrhosis, liver cancer or death (Manns et al., 2010, Manns et al., 2015, Krawitt, 2006, Alvarez, 2006). The clinical presentation of the disease ranges from asymptomatic to acute severe cases (Feld et al., 2005, Czaja, 2005, Kessler et al., 2004, Kogan et al., 2002). The main diagnostic criteria of AIH are plasmalymphocytic infiltrations into the liver tissue, presence of serum autoantibodies and hyper IgG globulinemia (Moritoki et al., 2006, Alvarez, 2006, Krawitt, 2006). Typical histological hallmarks are periportal inflammation and interface hepatitis (Moritoki et al., 2006). The autoantibodies secreted by plasma cells are furthermore used to classify the different types of AIH, even though they do not seem to have a pathogenic role (Krawitt, 2006). However, the role of B cells in AIH might be beyond the antibody production, as they may also activate the autoreactive T cells in their role as APCs and expedite inflammation through secretion of pro-inflammatory cytokines (see 2.2.2.2) (DiLillo et al., 2011, Kessel et al., 2008).

AIH is treated with immunosuppressive drugs, classically the corticosteroid prednisone alone or in combination with azathioprine (Summerskill et al., 1975, Larsen, 2008, Luxon, 2008). This rather unspecific therapy has severe side effects including osteopenia, brittle diabetes and opportunistic infections (Summerskill et al., 1975, Uribe et al., 1984, Czaja,

2008). A better understanding of the disease pathogenesis could lead to the development of more specific therapies with less side effects, resulting in a better compliance of patients and a better therapy outcome.

2.3.2 Systemic autoimmunity: Systemic lupus erythematosus

SLE is a multisystemic (which means it affects several organ systems) inflammatory disease and belongs to the lupus disease group (Lo and Tsokos, 2018). The incidence rate of SLE is 1 to 10 per 100,000 persons, with a higher incidence in the ethnic groups of African Americans, Hispanic and Asians and a much higher incidence in females (Pons-Estel et al., 2010, Manzi, 2001, Petri, 2002). An interplay of genetic, environmental and hormonal factors leads to the formation and outbreak of the disease. It is assumed that the breach of self-tolerance is induced by a defective clearance of apoptotic debris as well as aberrant presentation of self-antigen (see 2.2.1) (Lo and Tsokos, 2018). This results in polyclonal B cell activation, an increased number of autoantibody producing plasma cells and high autoantibody serum levels. The autoantibodies are typically directed against nuclear antigens like deoxyribonucleic acid (DNA) and cytoplasmic proteins, which can be found circulating in the blood of SLE patients due to an increased load of apoptotic material. Moreover, circulating immune complex can be deposited in tissues and activate inflammation and tissue damage through stimulation of leukocytic Fc receptors (Frieri, 2013, Frieri, 2002). There is good evidence that B cells play the key role in the development of SLE, as patients not only have high levels of autoantibodies and plasma cells, but also immature and memory B cells as well as plasmablasts. In addition, increased levels of molecules stimulating B cell survival and proliferation as well as B cell produced cytokines can be found (Jacob and Stohl, 2011, Chu et al., 2009).

Symptoms of SLE are complex and variable, ranging from general to tissue restricted symptoms (Frieri, 2013). The immune complexes most frequently deposit in the subendothelial regions of capillaries in the kidneys, causing lupus nephritis, which is one of the most severe complications of SLE and the major predictor of a poor prognosis (Frieri, 2002, de Zubiria Salgado and Herrera-Diaz, 2012). Lupus nephritis clinically manifests with proteinuria, microscopic haematuria and reduced renal function (Cameron, 1999). The diagnostic criteria of SLE include the finding of characteristic autoantibodies such as anti-double-strand-DNA-antibodies, anti-smooth-muscle-antibodies or antinuclear-antibodies (Yu et al., 2014).

Like in AIH and most other autoimmune diseases, the therapy of SLE relies on immunosuppressive drugs, mainly a low daily dose of prednisone (Frieri, 2013). This corticosteroid treatment causes the same side effects as mentioned in 2.3.1. Due to their central role in the development of SLE, B cells are important therapeutic targets.

A specific therapy targeting B cell co-stimulatory molecules or B cell cytokines might provide the possibility to treat SLE without the side effects of less specific immunosuppressive treatment. (Beccastrini et al., 2013, Yildirim-Toruner and Diamond, 2011).

2.4 Mouse model of AIH – Alb-iGP_Smarta

To receive a better understanding of autoimmunity as well as the underlying immunological mechanisms, it proved to be particularly helpful to use mouse models in which diseases are induced that imitate the autoimmune diseases to be examined. To study the formation and development of AIH, our group generated a transgenic mouse model, which combines liver-restricted autoantigen expression with TCR transgenic T cells recognizing the hepatic autoantigen.

2.4.1 Introduction of the model

The mice in this model of AIH express a MHC-II-restricted immunodominant T cell epitope of the Lymphocytic Choriomeningitis Virus glycoprotein (GP₆₁₋₈₀) in hepatocytes. To facilitate MHC-II-presentation of the endogenously expressed GP peptide, a mutant class II-associated invariant chain gene was generated encoding for an invariant chain protein in which the CLIP peptide, i.e. the class II-associated invariant chain peptide, which binds to MHC-II in the rough endoplasmic reticulum to prevent unintentional peptide binding, was replaced by GP₆₁₋₈₀. Thus, a high occupancy of MHC-II-molecules with GP₆₁₋₈₀ peptide was achieved, resulting in effective presentation of the GP₆₁₋₈₀ peptide by cells expressing the mutant invariant chain.

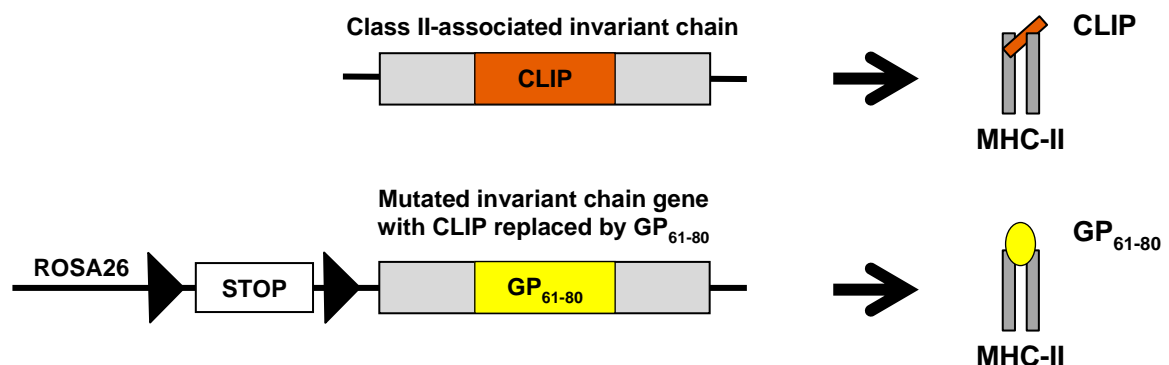


Figure 1: Creation of the mutated iGP gene: The CLIP sequence of the class II-associated invariant chain gene was replaced by the GP₆₁₋₈₀ peptide sequence. In addition, the gene was inserted into the ROSA26 gene with a floxed stop codon put in front.

To facilitate conditional expression of the mutated invariant chain gene, which we called 'iGP', it was inserted into the Rosa26 gene locus together with a floxed stop cassette that prevented its expression (Figure 1).

To enable conditional expression of GP₆₁₋₈₀ by hepatocytes, these mice were bred with mice expressing the cre recombinase under the control of the albumin promoter (Alb-iGP mice). As the cre enzyme removed the floxed stop cassette, the resulting mice expressed the MHC-II-GP complex on hepatocytes. A similar model was described in the paper by Frommer et al. in 2008. The Alb-iGP mice were further crossed with Smarta mice, which possess autoreactive CD4 positive T cells that have a transgenic TCR specific for the GP₆₁₋₈₀ peptide (Oxenius et al., 1998). The resulting triple transgenic Alb-iGP_Smarta mice feature the GP-MHC-II-complex expressed in hepatocytes as well as the cognate Smarta T cells specific for the presented peptide (Figure 2).

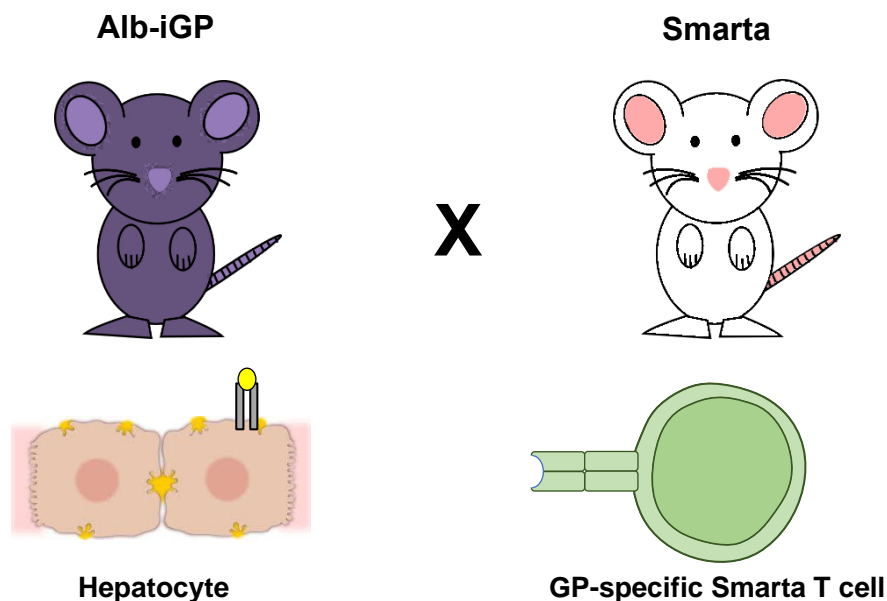


Figure 2: Mouse model of autoimmune hepatitis: Alb-iGP_Smarta mice expressing the GP₆₁₋₈₀ peptide from LCMV in hepatocytes and possessing autoreactive CD4 Smarta T cells specific for this peptide.

2.4.2 Basic characterization of the Alb-iGP_Smarta mouse model

Max Preti analysed the Alb-iGP_Smarta mice and could show that they start to develop autoimmunity by the age of 20 weeks characterized by lymphadenopathy and splenomegaly, elevated serum transaminases, liver inflammation and 50 % disease prevalence at the age of 30 weeks (Figure 3) (Preti, 2019).

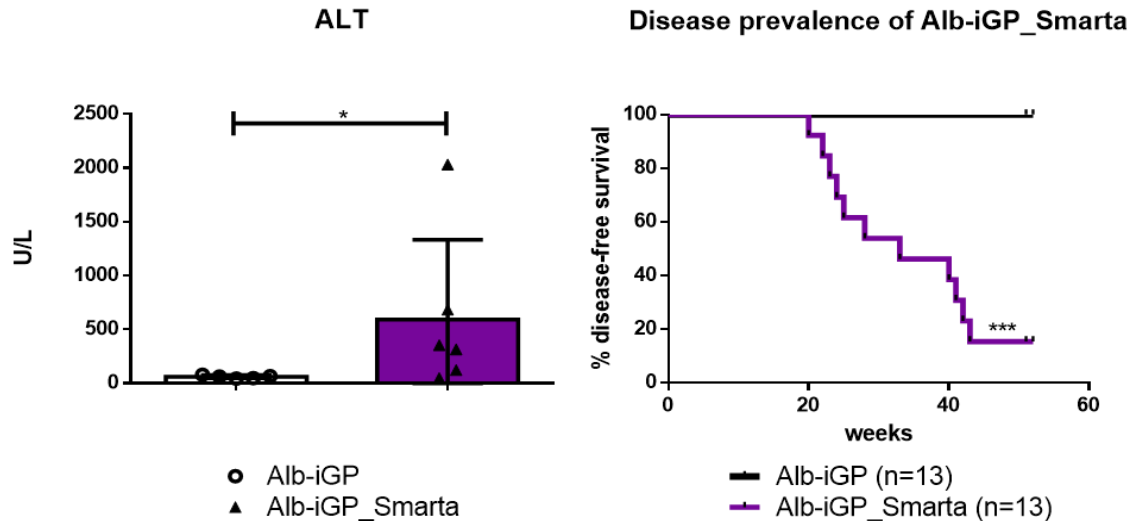


Figure 3: (Left) Serum levels of alanine aminotransferase (ALT) from Alb-iGP_Smarta mice older than 20 weeks with clinical manifestation of the disease compared to 20-week-old Alb-iGP mice. (Right) Disease prevalence of Alb-iGP_Smarta mice compared to Alb-iGP mice. Data obtained from Max Preti (Preti, 2019).

Histological analysis of the liver of young mice in the pre-clinical stage revealed the formation of ectopic lymphoid tissue (ELT) containing separate B and T cell zones (Figure 4). This ELT could be a precondition from which the AIH might develop.

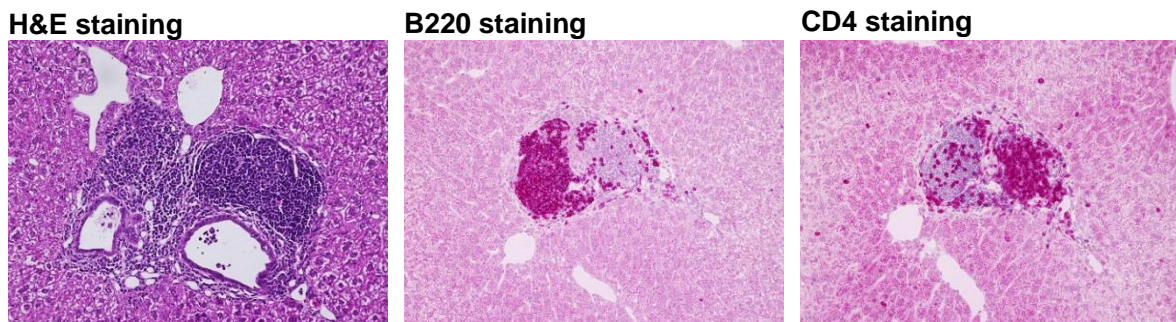
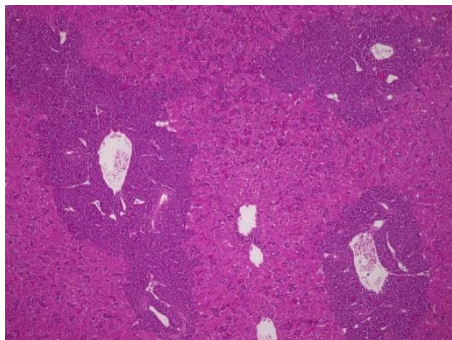


Figure 4: Histology of consecutive liver sections from eight-week-old Alb-iGP_Smarta mice. Haemalaun and eosin (H&E) staining and immunohistochemistry staining for B220 (B cells stained in purple) and CD4 (T cells stained in purple). 200 fold magnification. Data obtained from Max Preti (Preti, 2019).

In an advanced disease stage, histological analysis of the liver of Alb-iGP_Smarta mice revealed large periportal inflammatory infiltrates and interface hepatitis, which are also typical findings for autoimmune hepatitis in human (see 2.3.1.). In immunohistochemical staining, not only CD4 T cells but also a large amount of B cells infiltrating the liver could be found (Figure 5).

H&E staining



B220 staining

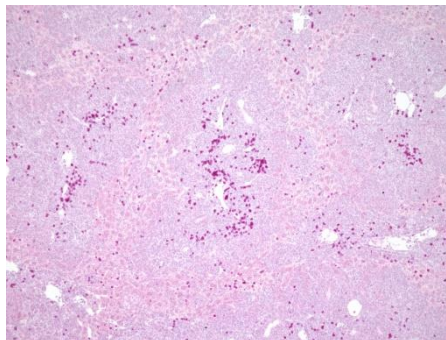


Figure 5: Histology of liver tissue from Alb-iGP_Smarta mice older than 20 weeks with clinical manifestation of the disease. H&E staining and immunohistochemistry staining for B220 (B cells stained in purple). 100 fold magnification. Data obtained from Max Preti (Preti, 2019).

This is also in accordance with the findings in humans where plasmalymphocytic infiltrations into liver tissue are one of the main diagnostic criteria (see 2.3.1). In the current study, we focussed on the further investigation of B cells in the onset and perpetuation of the AIH in the Alb-iGP_Smarta mice.

2.5 Mouse models to examine the role of B cells in AIH

To specifically address the role of B cells in the pathogenesis of AIH, two other mouse lines were created, the CD19-iGP_Smarta and the Alb-/CD19-iGP_Smarta line. These mice allowed us to directly study the role of autoantigen-presentation by B cells in our mouse model of AIH.

2.5.1 CD19-iGP_Smarta

This mouse line was created in a similar way to the Alb-iGP_Smarta mice, with the difference that here, the cre enzyme is expressed under the control of the CD19 promoter leading to the expression of the MHC-II-GP complex in B cells. In addition, the line also possesses the autoreactive Smarta T cells specific for the GP₆₁₋₈₀ peptide (Figure 6). This mouse will be used as control for the below described Alb-/CD19-iGP_Smarta mice, and will also provide information on the effect of autoantigen-presentation by B cells on autoreactive T cell development and behaviour. In a paper by Frommer et al., it has been described that presentation of the autoantigen myelin oligodendrocyte glycoprotein (MOG) by B cells in a mouse model similar to the here described presentation of GP₆₁₋₈₀ led to

peripheral deletion of autoreactive T cells by sensitising them to antigen-induced cell death (Frommer et al., 2008). Thereby, the mice were protected from developing experimental autoimmune encephalomyelitis (EAE). Furthermore, they described a role of B cells in central tolerance, as MOG-specific T cells were drastically reduced in number in the thymus as well as the lymph nodes in mice with MOG-presenting B cells and MOG-specific autoreactive T cells.

Also these mice were protected from developing EAE (Frommer and Waisman, 2010). These findings suggested that B cells can promote central tolerance when acting as APCs.

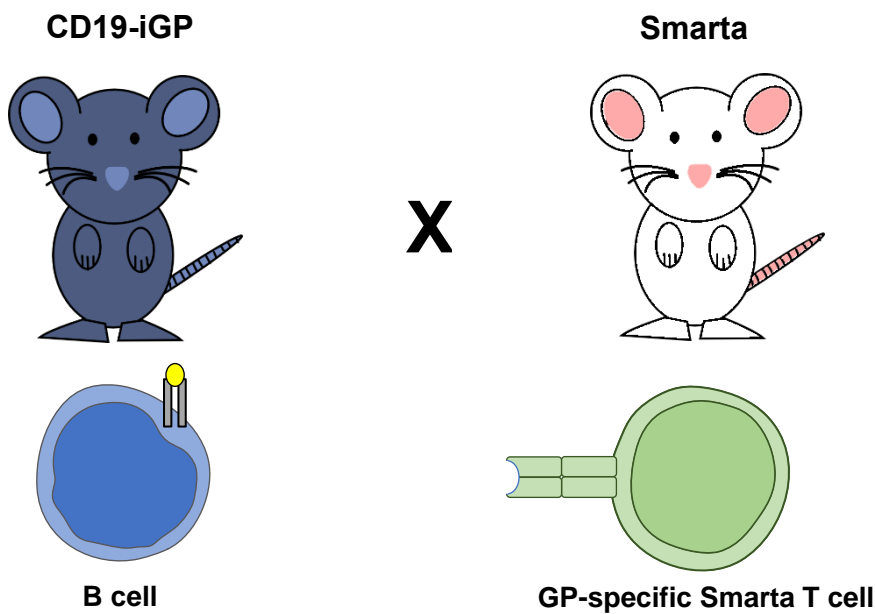


Figure 6: CD19-iGP_Smarta mice expressing the GP₆₁₋₈₀ peptide in B cells and possessing autoreactive CD4 Smarta T cells specific for this peptide.

2.5.2 Alb-/CD19-iGP_Smarta

This mouse line was generated by crossbreeding of the two above described mouse lines. Here, cre expression is under control both of the albumin and the CD19 promoter, resulting in the co-expression of the GP-MHC-II-complex in hepatocytes and B cells.

Also these mice feature the antigen-specific Smarta T cells (Figure 7). We used this line in order to examine the influence of autoantigen-presentation by B cells on the development of AIH.

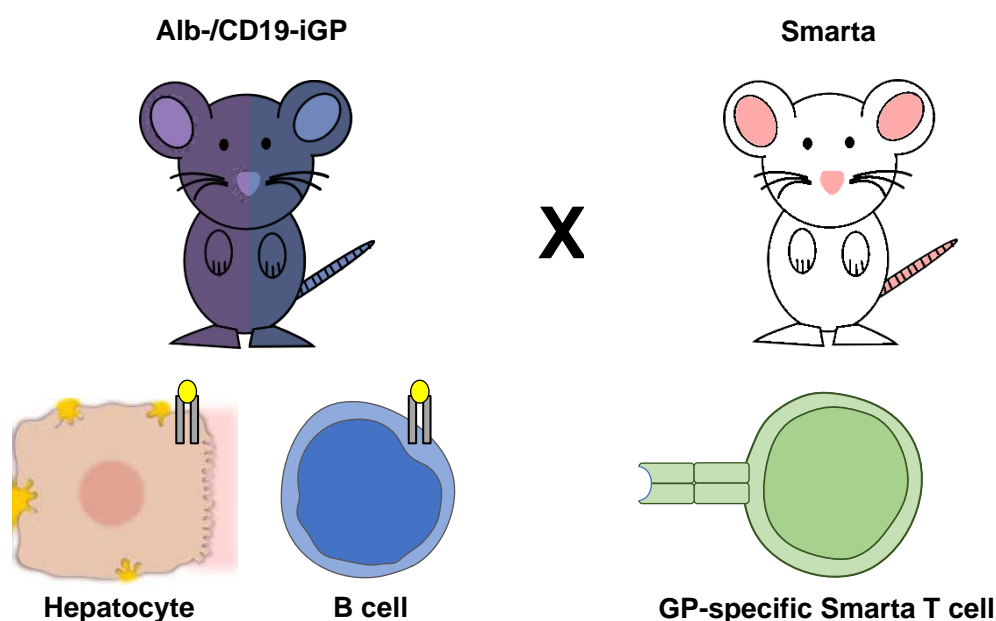


Figure 7: Mouse model to study the role of B cells in autoimmune hepatitis: Alb-/CD19-iGP_Smarta mice expressing the the GP₆₁₋₈₀ peptide in hepatocytes and B cells and possessing autoreactive CD4 Smarta T cells specific for this peptide.

2.6 Objectives

2.6.1 Examining the role of autoantigen-presentation by B cells for the development of AIH

The aim of this work was to examine the influence of autoantigen-presentation by B cells in the development of AIH in a mouse model. We thereby addressed the question, whether this autoantigen-presentation is aggravating the liver disease or leading to increased induction of tolerance and disease protection. The first step was to analyse whether the presentation of autoantigen by B cells influences the T cell differentiation into T_{eff} cells. We also investigated whether T cell tolerance was induced through deletion or functional inactivation of the disease-causing autoreactive T cells or an increased formation of Tregs. Moreover, we analysed the B cell population as well as antibody production.

Liver histology was compared between Alb-iGP_Smarta and Alb-/CD19-iGP_Smarta, as well as control mice, to find out whether there were differences in disease development or severity. In addition, serum transaminases levels were examined as marker for liver damage. Finally, male and female mice were compared to uncover potential sexual dimorphisms.

2.6.2 Examining the role of autoantigen-presentation by B cells for the development of systemic autoimmunity

A second aim of this study was to examine the influence of antigen-presentation by B cells on autoreactive T cells in a non-liver-related setting in CD19-iGP_Smarta mice. Also here, the first step was to determine whether the autoreactive T cells were deleted through the presentation of autoantigen by B cells. If Smarta T cells had not been deleted, it was planned to determine whether and what type of autoimmune disease would develop. Therefore, mice in a pre-clinical stage were examined, including T and B cell analysis as well as histological studies in central organs like liver, lung and kidney.

The mice were then followed for clinical and immune symptoms of disease. Disease severity was assessed with respect to survival, inflammation and tissue damage in liver, spleen, lung and kidney. T and B cell populations were studied, including Tregs and the B cell subpopulations germinal centre B cells, effector and memory B cells as well as plasma cells. Also, a comparison of male and female mice regarding disease severity was planned.

3 Material & Methods

3.1 Instruments

Table 1: Instruments

Instrument	Brand
BD LSR II Flow Cytometer	BD Bioscience, San Jose
BD LSRFortessa	BD Bioscience, San Jose
Centrifuge 5810R	Eppendorf AG, Hamburg
Centrifuge 5920R	Eppendorf AG, Hamburg
COBAS INTEGRA 400 plus	Roche Deutschland Holding GmbH, Grenzach-Wyhlen
Ismatec pump	Cole-Parmer GmbH, Wertheim
Microscope BH-2	Olympus Deutschland GmbH, Hamburg
Microscope BZ-9000 (Biorevo)	KEYENCE DEUTSCHLAND GmbH, Neu- Isenburg
Microtom Cut 5062	SLEE medical GmbH, Mainz
Microwave 216	Robert Bosch Hausgeräte GmbH, München
myFuge mini centrifuge	Benchmark Scientific, Inc., Edison
Neubauer improved counting chamber	Paul Marienfeld GmbH & Co.KG, Lauda Königshofen
Pipetboy 2	INTEGRA Biosciences GmbH, Biebertal
Pipettes	Eppendorf AG, Hamburg
Präzitherm PZ35	Harry Gestigkeit GmbH, Düsseldorf
Precision balance EMB 100-3	Kern & Sohn GmbH, Balingen

Preparation instruments	FST GmbH Filtrations-Separations-Technik, Essen
ScoutPro SPU6001	OHAUS Corporation, Parsippany
ThermoMixer C	Eppendorf AG, Hamburg
Tissue Cool Plate COP 20	MEDITE GmbH, Burgdorf
VortexGenie2 G560E	Scientific Industries, Inc., New York
Water bath GFL 1083	Gesellschaft für Labortechnik mbH, Burgwedel
Weight Sartorius analytic A2005	Sartorius AG, Göttingen

3.2 Material

Table 2: Chemicals

Chemical	Brand
Antibody Diluent	Zytomed Systems GmbH, Berlin
Aqua dest.	B. Braun Melsungen AG, Melsungen
Citrate buffer: Umasking Solution low pH (6.2) 250 ml	Vektor Laboratories, Inc., Burlingame
Dako Fluorescence mounting medium	Agilent technologies, Santa Clara
Entellan rapid mounting medium for microscopy	Merck KGaA, Darmstadt
Eosin-G solution, 0.5 % aqueous, for microscopy	Carl Roth GmbH&Co. KG, Karlsruhe
Ethanol absolute	Th. Geyer GmbH & Co. KG, Renningen
Ethanol, denatured, 99.8 % with about 1 % MEK ; 2.5 l	Carl Roth GmbH&Co. KG, Karlsruhe

Ethylendiaminetetraacetic acid (EDTA) solution pH 8.0 (0.5 M)	AppliChem GmbH, Darmstadt
Fixation/Permeabilization concentrate	Thermo Fisher Scientific Inc., Waltham
Fixation/Permeabilization diluent	Thermo Fisher Scientific Inc., Waltham
Haemalum-solution, sour after Mayer, for microscopy	Carl Roth GmbH&Co. KG, Karlsruhe
Hydrochloric acid (HCL) 37 %	Carl Roth GmbH&Co. KG, Karlsruhe
Nuclease-free water	Thermo Fisher Scientific Inc., Waltham
OneComp eBeads	Thermo Fisher Scientific Inc., Waltham
Optiprep density gradient medium	Merck KGaA, Darmstadt
Percoll	Merck KGaA, Darmstadt
Periodic acid	Merck KGaA, Darmstadt
Permeabilization buffer 10x	Thermo Fisher Scientific Inc., Waltham
Roti-Histofix, 2.5 l Paraformaldehyde (PFA) 4 %, buffered	Carl Roth GmbH&Co. KG, Karlsruhe
Schiff's reagent	Merck KGaA, Darmstadt
Tissue-Tek O.C.T. compound 125 ml	Sakura Finetek Europe B.V., Alphen aan den Rijn
Trypan blue 0,4 %	Thermo Fisher Scientific Inc., Waltham
Xylol z.A.; 2.5l, 96 %	Th. Geyer GmbH & Co. KG, Renningen

Table 3: Consumables

Consumable	Brand
Cell strainer 100 µm, yellow	Greiner Bio-One GmbH, Frickenhausen
Cell strainer 40 µm, green	Greiner Bio-One GmbH, Frickenhausen
Cellstar tube 15 ml	Greiner Bio-One GmbH, Frickenhausen
Cellstar tube 50 ml	Greiner Bio-One GmbH, Frickenhausen
Cover slip 24mm x 50mm	Carl Roth GmbH&Co. KG, Karlsruhe
Cover slip AutomatStar 24mm x 60 mm	Engelbrecht Medizin- und Labortechnik GmbH, Edermünde
CryoPure tube 1.6 ml, red	Sarstedt AG&Co, Nümbrecht
Dako pen	Agilent technologies, Santa Clara
Flow cytometry tubes	Sarstedt AG&Co, Nümbrecht
Hypodermic-needle (brown) 26G	Becton Dickinson GmbH, Heidelberg
Hypodermic-needle (green) 21G	B. Braun Melsungen AG, Melsungen
Injekt-F syringe 1 ml	B. Braun Melsungen AG, Melsungen
Micro tubes 0.5 ml	Sarstedt AG&Co, Nümbrecht
Micro tubes 1.5 ml	Sarstedt AG&Co, Nümbrecht
Micro tubes 1.5 ml SafeSeal	Sarstedt AG&Co, Nümbrecht
Micro tubes 5 ml SafeSeal	Sarstedt AG&Co, Nümbrecht
Pipette tips	Sarstedt AG&Co, Nümbrecht
Rotilabo-disposable weighing trays	Carl Roth GmbH&Co. KG, Karlsruhe
Sample cup for Cobas Bio, blue	Sarstedt AG&Co, Nümbrecht

Serological pipette	Sarstedt AG&Co, Nümbrecht
βTC-Plate 96 Well, Cell+, F	Sarstedt AG&Co, Nümbrecht
Tissue embedding cassettes	Kabe Labortechnik GmbH, Nümbrecht-Elsenroth

Table 4: Kits

Kit	Brand
IIFT mosaic basis profile 3	EUROIMMUN medizinische Labordiagnostika AG, Lübeck
Permanent AP Red Kit	Zytomed Systems GmbH, Berlin
POLAP-Kit: ZytoChem-Plus AP-Polymer-Kit	Zytomed Systems GmbH, Berlin

Table 5: Antibodies for histology

Antibody	Brand
Goat anti-Mouse IgG (H+L) Cross-Adsorbed Secondary Antibody, Alexa Fluor 488, 2 mg/ml	Thermo Fisher Scientific Inc., Waltham
Purified Anti-Hu/Mo CD45R (B220), 0.5 mg/ml, Clone: RA3-6B2	Thermo Fisher Scientific Inc., Waltham
Purified Anti-Mouse CD4, 0.5 mg/ml, Clone: 45M95	Thermo Fisher Scientific Inc., Waltham
Rabbit anti-Rat IgG (H+L) Secondary Antibody, Biotin, 1.5 mg/ml	Thermo Fisher Scientific Inc., Waltham

Table 6: Antibodies and Tetramer for flow cytometry

Antibody	Brand
AF700 anti-mouse CD45, 0.5 mg/ml, Clone: 30-F11	BioLegend, San Diego
APC anti-mouse CD19, Clone: 1D3/CD19	BioLegend, San Diego
APC/Cy7 anti-mouse CD38, 0.2 mg/ml, Clone: 90	BioLegend, San Diego
BV421 anti-mouse CD4, 0.2 mg/ml, Clone: GK 1.5	BioLegend, San Diego
BV421 mouse-anti-mouse I-A[b] (MHC-II), 0.2 mg/ml, Clone: AF6-120.1	BD Bioscience, San Jose
BV605 anti-mouse CD95 (Fas), 0.2 mg/ml, Clone: SA367H8	BioLegend, San Diego
BV650 anti-mouse CD138 (Syndecan-1), 0.2 mg/ml, Clone: 281-2	BioLegend, San Diego
BV711 rat-anti-mouse IgM, 0.2 mg/ml, Clone: R6-60.2	BD Bioscience, San Jose
BV785 anti-mouse CD69, 0.2 mg/ml, Clone: H1.2F3	BioLegend, San Diego
FITC Foxp3 monoclonal antibody, 0.5 mg/ml, Clone: FJK-16s	Thermo Fisher Scientific Inc., Waltham
PE rat-anti-mouse CD8a, 0.2 mg/ml, Clone: 53-6.7	BD Bioscience, San Jose
PE/Cy7 anti-mouse/human CD45R/B220, 0.2 mg/ml, Clone: RA3-6B2	BioLegend, San Diego
PE/Dazzle 594 goat-anti-mouse IgG, 0.2 mg/ml, Clone: Poly4053	BioLegend, San Diego
PerCP/Cy5.5. anti-mouse/human GL7 antigen, 0.2 mg/ml, Clone: GL7	BioLegend, San Diego

Tetramer LCMV GP 66-77 DIYKGVYQFKSV	NIH Tetramer Core Facility, Atlanta
--	-------------------------------------

3.3 Software

Table 7: Software

Software	Brand
BZ-II Analyzer	KEYENCE DEUTSCHLAND GmbH, Neu-Isenburg
BZ-II Viewer	KEYENCE DEUTSCHLAND GmbH, Neu-Isenburg
FACSDiva, version 8	BD Bioscience, San Jose
FlowJo, version 10	FLowJo, LLC, Ashland
GraphPad Prism, version 6	GraphPad Software, LLC, San Diego
Microsoft Office 365	Microsoft Corporation, Redmond
Windows 10	Microsoft Corporation, Redmond

3.4 Buffer and other solutions

Table 8: Buffer and other solutions

Solution	Components	Concentration	Brand
1x Ammonium-chloride-potassium (ACK) buffer	Ammonium chloride (NH ₄ Cl)	150 mmol	Merck KGaA, Darmstadt
	Potassium bicarbonate (KHCO ₃)	10 mmol	Merck KGaA, Darmstadt

	EDTA-Solution pH 8.0 (0.5 M)	100 mmol	AppliChem GmbH, Darmstadt
	Aqua dest.		B. Braun Melsungen AG, Melsungen
1x Phosphate buffered saline (PBS)	Potassium chloride (KCl)	2.7 mmol	Merck KGaA, Darmstadt
	Disodiumphosphate (Na ₂ HPO ₄)	6.5 mmol	Carl Roth GmbH&Co. KG, Karlsruhe
	Monopotassium phosphate (KH ₂ PO ₄)	1.5 mmol	Merck KGaA, Darmstadt
	Sodium chloride (NaCl)	137 mmol	Carl Roth GmbH&Co. KG, Karlsruhe
	Aqua dest.		B. Braun Melsungen AG, Melsungen
Digestion medium for kidney cell isolation	Collagenase NB 4G	0.4 mg/ml	SERVA Electrophoresis GmbH, Heidelberg
	Desoxyribonuclease (DNase)	1 %	Roche Diagnostics GmbH, Mannheim
	Fetal calf serum (FCS)	10 %	Thermo Fisher Scientific Inc., Waltham
	RPMI-1640 Medium		Merck KGaA, Darmstadt
Flow cytometry buffer	FCS	2 %	Thermo Fisher Scientific Inc., Waltham
	PBS		

Narcotic	Ketamin 10 %	12 mg/ml	Bela-pharm GmbH&Co.KG, Vechta
	Xylazin 2 %	1.6 mg/ml	Bayer Vital GmbH, Leverkusen
	PBS		
Pacific orange	Pacific Orange Succinimidyl Ester, Triethylammonium Salt	1 mg/ml	Thermo Fisher Scientific Inc., Waltham
	Dimethyl sulfoxide (DMSO)		SERVA Electrophoresis GmbH, Heidelberg

3.5 Laboratory animals

Heterozygous Alb-/CD19-iGP_Smarta, CD19-iGP_Smarta, Alb-iGP_Smarta, CD19-iGP_Smarta and C57BL/6 wild type mice were bred and kept in the animal facility of the University Medical Center Hamburg-Eppendorf under specific pathogen-free conditions. All animal experiments were approved by the “Behörde für Gesundheit und Verbraucherschutz, Fachbereich Veterinärwesen“ of the state of Hamburg, Germany. The mice were analysed at the age of 8 and 20 weeks, or when clinical disease symptoms occurred.

Table 9: Mouse Lines

Mouse Line	Background	Characteristic
CD19-iGP	C57BL/6J	Express GP peptide from LCMV in B cells
Alb-iGP	C57BL/6J	Express GP in hepatocytes
Smarta	C57BL/6J	Possess autoreactive CD4 Smarta T cells specific for the GP peptide from LCMV (antigen-specific)

CD19-iGP_Smarta	C57BL/6J	Express GP in B cells and possess antigen-specific Smarta T cells
Alb-iGP_Smarta	C57BL/6J	Express GP in Hepatocytes and possess antigen-specific Smarta T cells
Alb-/CD19-iGP_Smarta	C57BL/6J	Express GP in B cells and hepatocytes and possess antigen-specific Smarta T cells

3.6 Methods

3.6.1 Organ sampling

The mice were euthanised in deep anaesthesia with 15 ml/kg of ketamin (12 mg/ml)/ xylazine (1.6 mg/ml), injected intraperitoneally, by terminal collection of all blood from the vena cava inferior. The mice were weighed and one piece of tail was frozen at -80 °C for possibly required second genotyping. The liver was perfused with PBS, taken out, weighed and the gall bladder was removed. The bigger part of the middle lobe was put in 4 % PFA for histology. Three small pieces from the smaller part of the middle lobe were frozen in liquid nitrogen for messenger ribonucleic acid (mRNA) analysis, the rest was put in tissue-tek for cryostat sectioning. All other liver tissue was weighed again and kept in PBS for cell isolation. The thymus was taken out and kept in PBS on ice for cell isolation. The spleen was taken out and weighed. One third was put in 4 % PFA for histology, one third was cut in three small pieces and frozen in liquid nitrogen for mRNA analysis and the last third was weighed again and kept in PBS on ice for cell isolation. The right Lung was taken out, weighed and kept in PBS on ice for cell isolation. The left lung was taken out, three small pieces were frozen in liquid nitrogen for mRNA analysis and the rest was put in 4 % PFA for histology. The right kidney was taken out, weighed, the capsule was removed and the kidney was kept in PBS on ice for cell isolation. The left kidney was perfused, taken out, three small pieces were frozen in liquid nitrogen for mRNA analysis and the rest was put in 4 % PFA for histology.

3.6.2 Cell isolation

3.6.2.1 *Cell isolation from the spleen, thymus and lung*

Spleen, thymus or lung were mashed through a Ø 100 µm cell strainer and collected in a 50 ml cellstar tube. After washing (30 ml of PBS were added, and the cell suspension was centrifuged at 400 relative centrifugal force for 5 min), erythrocytes were lysed by resuspending the cell pellet in 1 ml of ACK buffer and incubation for 1 min. Lysis was stopped by adding another 30 ml of PBS and the suspension was then filtered through a Ø 40 µm cell strainer and washed. The cells were resuspended in 1 ml of PBS and a counting sample was pipetted in a Neubauer counting chamber (suspension was diluted either 1:10 or 1:100 in 0.04 % trypan blue). The living cells were counted in two opposing big squares of the counting chamber. The cell number was determined with the following formula:

Cell number = Counted number/number of counted squares x dilution factor x Volume in which cells were resuspended x chamber factor (10^4)

3.6.2.2 *Cell isolation from the liver*

The liver was also filtered through a Ø 100 µm cell strainer, collected in a 50 ml cellstar tube and filled up with PBS to 50 ml. To remove hepatocytes, the suspension was centrifuged at 40 relative centrifugal force (RCF) for 4 min for two times and one more time at 400 RCF for 7 min. After the last centrifugation, a density gradient was applied to isolate the nonparenchymal liver cells by resuspending the cell pellet in 4 ml PBS, transferring the suspension into a 15 ml cellstar tube, mixing it carefully with 2.5 ml optiprep density gradient medium, slowly adding 1 ml PBS on top and centrifuging at 400 RCF for 20 min, break 0. The ring of leukocytes and erythrocytes was carefully pipetted into a new 50 ml tube, filled up to 50 ml with PBS and centrifuged at 400 RCF for 7 min. The erythrocytes were lysed as described above, the cells were washed, resuspended in 1 ml PBS and counted in a Neubauer counting chamber (1:10 dilution).

3.6.2.3 *Cell isolation from the kidney*

The kidney was cut into small pieces and kept for 45 min in 5 ml RPMI medium with 10 % FCS, 1 % DNase and 2 mg collagenase in a water bath at 37 °C. Afterwards, the kidney was filtered through a Ø 100 µm cell strainer, collected in a 50 ml cellstar tube, filled up to 30-35 ml with PBS and centrifuged at 350 RCF for 7 min. A 37 % Percoll density gradient was applied by resuspending the cell pellet in 3150 µl PBS, mixing it carefully with 1850 µl Percoll in a 15 ml cellstar tube and centrifuging the suspension at 500 RCF for 15 min, break 0.

The cell pellet was resuspended in 1 ml PBS, transferred into a 50 ml cellstar tube and washed. The erythrocytes were lysed as explained above, the cells were washed, resuspended in 1 ml PBS and counted in a Neubauer counting chamber (1:10 dilution).

3.6.3 Flow cytometry

The cells were washed with 1 ml fluorescence-activated cell sorting (FACS) buffer and centrifuged at 400 RCF for 5 min. To stain antigen-specific T cells, 0.4 µl of the tetramer in 100 µl of FACS buffer were added per tube and incubated for 1.5 h at 37 °C. The cells were washed and stained for life-death distinction with 0.2 µl Pacific Orange in 200 µl PBS, with an incubation time of 20 min at 4 °C followed by another washing.

For cell surface marker staining, 1 µl of each antibody diluted in 100 µl FACS Buffer was added per tube and incubated for 10 min at 4 °C. Afterwards, the cells were washed again.

For intracellular staining, the cells were fixed and permeabilized. Afterwards, the cells were washed with 500 µl of permeabilization buffer diluted 1:10 in distilled water. 1 µl of antibody in 50 µl of permeabilization-buffer-dilution was added and incubated for 20 min at 4 °C. Then the cells were washed again in 500 µl permeabilization-buffer-dilution and diluted in 200 µl of FACS buffer. If no intracellular staining was necessary, the cells were diluted in 200 µl of FACS buffer if analysed the same day or fixed with 100 µl of 1 % PFA and analysed the next day.

As compensation control for each antibody, two drops of One Comp eBeads and 1 µl of the respective antibody were mixed in one flow cytometry tube; in addition, an unstained control of only One Comp eBeads without antibody was prepared. For Pacific Orange compensation control, a mixture of living and dead cells killed by cooking at 50 °C for 30 min in the ThermoMixer was stained as described above. All compensation controls were then incubated for 20 min at 4 °C with subsequent addition of 200 µl PBS respectively 100 µl of 4 % PFA for the Pacific Orange staining.

The cells were measured via flow cytometry on a BD LSR II or BD LSRFortessa Flow Cytometer with FACSDiva version 8, and were analysed with FlowJo version 10.

3.6.4 Histology

3.6.4.1 Haemalum and eosin (H&E)

2-4 µm thick formalin-fixed, paraffin-embedded liver sections were deparaffinised by sequential immersion for 4 min each into three staining jars of 96 % xylol, followed by a descending ethanol series of 100 %, 90 %, 70 % and 50 %, and finally distilled water.

The sections were then stained in haemalum for 10 min and blued in running tap water for 15 min. After 1 min in distilled water, the sections were stained in eosin for 1 min and dehydrated by sequential immersion into distilled water, an ascending ethanol series of 50 %, 70 % (30 sec), 90 % (1 min), 100 % (two times 2 min) and three jars of xylol (4 min each). The sections were then mounted by applying 1 drop of Entellan mounting medium on the tissue and carefully covering it with a coverslip.

3.6.4.2 *Periodic Acid Schiff (PAS)*

1 µm thick formalin-fixed, paraffin-embedded liver sections were deparaffinized as described above. Afterwards, they were stained for 5 min in periodic acid, washed in distilled water and stained for 15 min in Schiff's reagent. They were then washed in running tap water for 5 min, stained in haemalum for 90 sec and blued again in running tap water for 5 min. Finally, the slides were dehydrated as described above and covered with Entellan mounting medium and a coverslip.

3.6.5 Immunohistochemistry

The antibodies used for immunohistochemistry are listed in Table 5. 2-4 µm thick formalin-fixed, paraffin-embedded liver sections were deparaffinized in xylol, a descending ethanol series and distilled water (retention time in xylol was 5 min, in ethanol 4 min). Afterwards, antigen retrieval was performed by cooking the slides in a solution of 4.7 ml citrate buffer (pH 6.2) and 500 ml distilled water for 25 min. After antigen retrieval, the tissue on the slides was encircled with a hydrophobic pen and washed in PBS three times for 5 min. Then, 50-100 µl (depending on the amount of tissue) of blocking buffer were added and the slides were incubated for 10 min in a humid chamber at room temperature, followed by overnight incubation in the humid chamber at 4 °C with 100 µl of Rat-anti-hu/mo-CD45R (1:50) or rat-anti-ms-CD4 (1:100) diluted in antibody diluent.

On the next day, the sections were washed three times in PBS and incubated 30 min in the humid chamber at room temperature with 100 µl of Polyclonal-Rb-anti-rat-IgG-Biotin diluted 1:300 in antibody diluent. The sections were washed again and incubated with 50-100 µl Anti-rb-AP-complex 30 min in the humid chamber at room temperature. After washing with distilled water, the sections were incubated for 10 min in the humid chamber at room temperature with 100 µl permanent AP-Red chromogen diluted 1.6:100 in permanent AP-Red buffer. The slides were then rinsed in distilled water, stained in haemalum for 3 min, rinsed again and blued in running tap water for 5-10 min. The sections were kept for 5 sec in 0.1 % HCL (diluted from 37 % HCL), washed in distilled water and tap water and dehydrated in an ascending ethanol series of 50 %, 70 %, 90 % (30 sec), 100 % (two times

for 1 min) and three jars of xylol (for 3 min each). The sections were finally covered with Eukitt mounting medium and coverslip.

3.6.6 Indirect immunofluorescence staining of serum autoantibodies

Sera were diluted 1:40, 1:80, 1:160 and 1:320 in PBS-Tween with a final volume of 50 μ l each. 30 μ l of each solution as well as one control with only PBS-Tween but no serum were carefully filled onto a reaction field of the reagent plate. The object slide with the attached tissue was carefully set on top with the tissue facing downwards and incubated for 30 min at room temperature. Afterwards, the object slide was washed in PBS-Tween for 5 min. 30 μ l of AF 488 Goat-Anti-Mouse-IgG antibody diluted 1:500 in PBS-Tween were carefully loaded onto each reaction field of the reagent plate, covered with the object slide and incubated for 30 min at room temperature. The object slide was washed again in PBS-Tween for 5 min and covered with the fluorescence liquid mounting medium and a coverslip.

3.6.7 Measurement of transaminases

The transaminases alanine aminotransferase (ALT) and aspartate aminotransferase (AST) were measured from the serum diluted 1:4 in distilled water with the COBAS INTEGRA 400 plus.

3.6.8 Statistical analysis

The data was analysed in GraphPad Prism version 6 (GraphPad Software) using the parametric unpaired t-test or one-way ANOVA test, or log-rank (Mantel-cox) test for survival curve analyses. Significances were indicated by asterisks according to Table 10.

Table 10: Levels of significance

Symbol	Significance level
*	$p < 0.5$
**	$p < 0.01$
***	$p < 0.001$
****	$p < 0.0001$
ns	Non-significant

4 Results

The results of this work are structured in two parts: First, the results of the Alb-/CD19-iGP_Smarta mouse model analysis are shown, in which we examined the role of autoantigen presenting B cells in the Alb-iGP_Smarta mouse model for AIH (see 4.1). Second, the results of the CD19-iGP_Smarta mouse line analysis are shown, in which we characterized the consequences of autoantigen-presentation by B cells to autoreactive T cells (see 4.2).

4.1 The role of B cells in a mouse model for AIH: Alb-/CD19-iGP_Smarta mice

To examine the role of B cells in a mouse model for AIH, eight-week-old CD19-iGP_Smarta, Alb-iGP_Smarta and Alb-/CD19-iGP_Smarta mice were analysed. At this age the Alb-iGP_Smarta mice were in a preclinical stage, as clinical disease onset occurred only from the age of 20 weeks onward (see 2.4.2). As control lines, Smarta mice were used, which possess only the autoreactive antigen-specific Smarta T cells but do not present the cognate antigen, as well as CD19-iGP mice, which present the antigen on B cells but do not possess the Smarta T cells. The mouse lines were compared with respect to their B and T cell repertoires and liver pathology.

4.1.1 Autoantigen-presentation by B cells shapes the repertoire of autoreactive T cells

T cells isolated from liver, thymus or spleen were analysed by flow cytometry. The cells derived from the different mouse lines were stained for CD45, CD4, CD8, GP₆₆₋₇₇ tetramer and Foxp3.

4.1.1.1 Flow cytometry gating strategy for T cell analysis

First, non-lymphocyte cells, doublets, dead cells and CD45⁻ cells were excluded. The remaining CD45⁺ leucocytes were gated on CD4 and CD8 to differentiate CD4 T cells, CD8 T cells and non-T-cells. CD4⁺ CD8⁻ cells were gated for LCMV GP₆₆₋₇₇ tetramer positivity (Smartha T cells) as well as Foxp3 positivity. The tetramer⁺ population was again gated for Foxp3 positivity to determine the Treg frequency of the Smarta T cells (Figure 8).

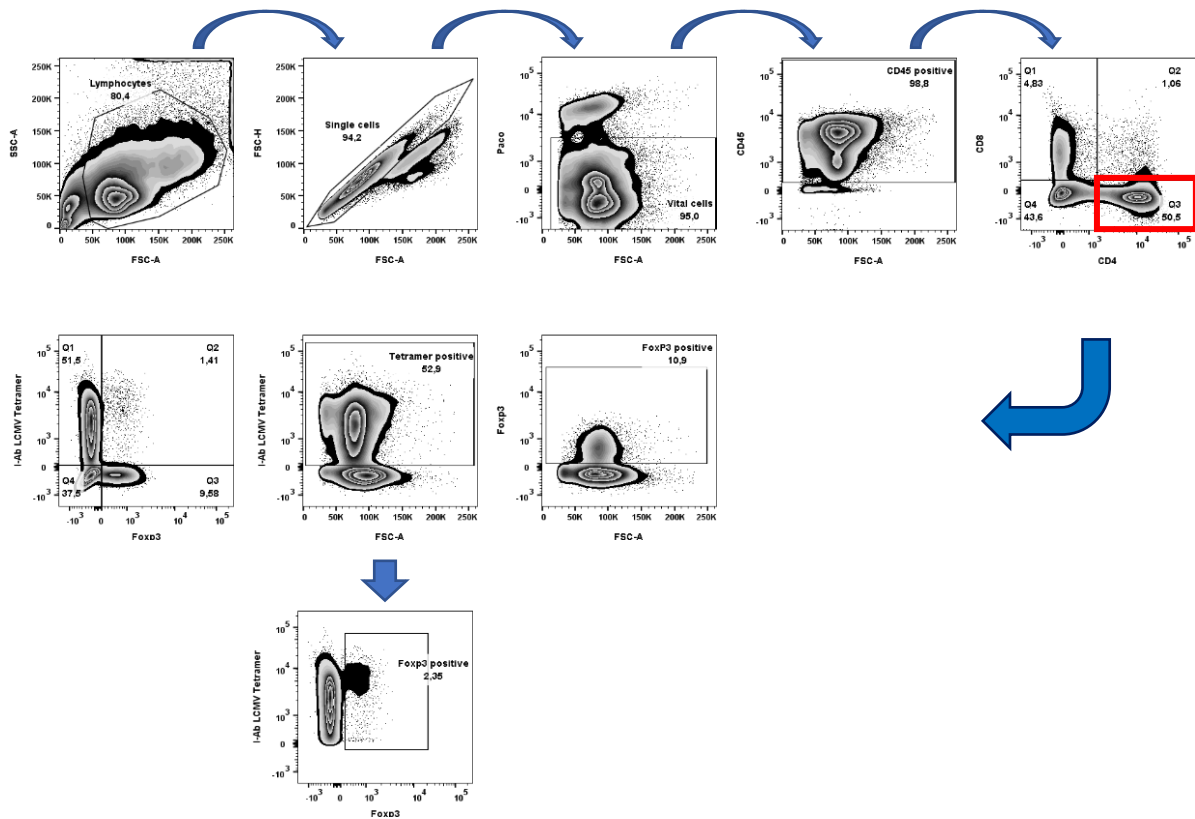


Figure 8: Gating strategy of the flow cytometry T cell panel used to stain for CD4 and CD8 T cells, antigen-specific Smarta T cells (tetramer⁺) and Tregs.

4.1.1.2 Antigen-specific Smarta T cells are not deleted when autoantigen is expressed in B cells or hepatocytes

Smarta control mice showed a high frequency of Smarta T cells in the CD4 T cell population (with a mean of 80.6 % in the thymus, 93.95 % in the spleen and 91.7 % in the liver, Figure 9). In contrast, as expected, CD19-iGP control mice had almost no tetramer⁺ cells (Figure 9). As has been previously shown by Max Preti, Alb-iGP_Smarta mice showed a high frequency of Smarta T cells, although their number was slightly reduced compared to the Smarta mice (representative dot plots are shown in Figure 9A). Also in CD19-iGP_Smarta and Alb-/CD19-iGP_Smarta mice, Smarta T cells were not fully deleted (Figure 9 A). The mean Smarta frequencies in the thymus were 85.77 % in CD19-iGP_Smarta mice, 89.27 % in Alb-iGP_Smarta mice and 89.27 % in Alb-/CD19-iGP_Smarta mice, which was comparable to Smarta control mice (80.6 %, ns, Figure 9 B). In the spleen however, the mean Smarta frequencies were reduced in CD19-iGP_Smarta mice (62.52 %, $p < 0.01$), Alb-iGP_Smarta mice (74.24 %, ns) and Alb-/CD19-iGP_Smarta mice (64.96 %, $p < 0.05$), as compared to the Smarta control line (93.95 %) (Figure 9 C).

Analysis of the absolute cell numbers confirmed significant reduction of Smarta cell numbers in CD19-iGP_Smarta spleens (6.3×10^6), Alb-iGP_Smarta spleens (5.12×10^6) and Alb-/CD19-iGP_Smarta spleens (4.62×10^6), as compared to the Smarta control spleens (15.82×10^6 , $p < 0.01$, Figure 9 C).

This finding indicated that the expression of antigen by B cells or hepatocytes led to partial deletion of autoreactive T cells in the periphery, but not in the thymus. In the liver, those lines expressing the autoantigen in hepatocytes, namely Alb-iGP_Smarta (64.88 %) and Alb-/CD19-iGP_Smarta (58.37 %), showed a higher frequency of antigen-specific Smarta T cells compared to the CD19-iGP_Smarta mice, which did not express the autoantigen in the liver (21.03 %, $p < 0.01$, Figure 9 D). This suggested that antigen-expression in the liver induced Smarta cell infiltration into the liver. Of note, Alb-iGP_Smarta mice had a higher absolute number of Smarta T cells in the liver (1.7×10^6) than Alb-/CD19-iGP_Smarta mice (0.27×10^6 , $p < 0.01$, Figure 9 D). Thus, expression of GP peptide in B cells concomitant to hepatocytes seemed to reduce liver infiltration of Smarta T cells.

Taken together, the observed presence of autoreactive T cells in the CD19-iGP_Smarta and Alb-/CD19-iGP_Smarta mice confirmed their suitability to study the role of B cells in our mouse model for AIH.

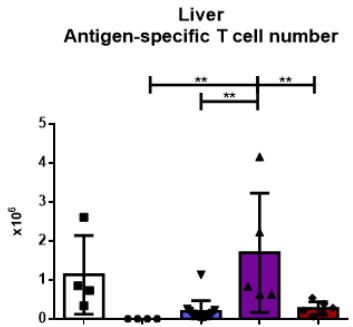
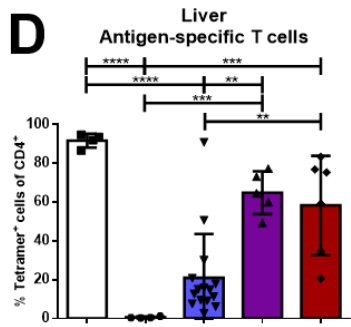
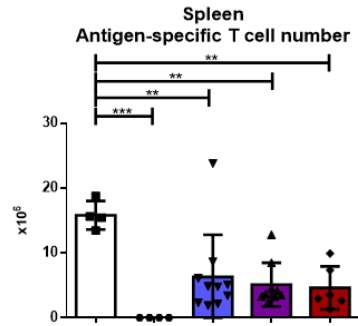
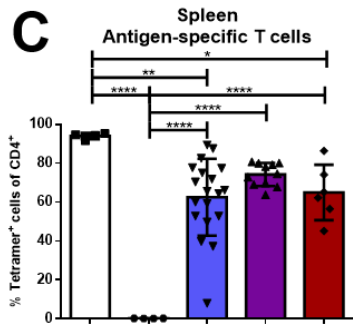
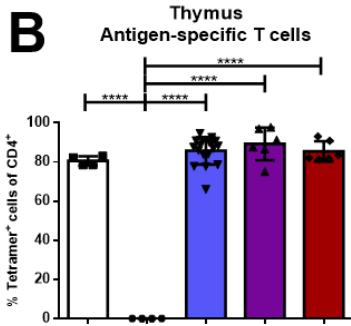
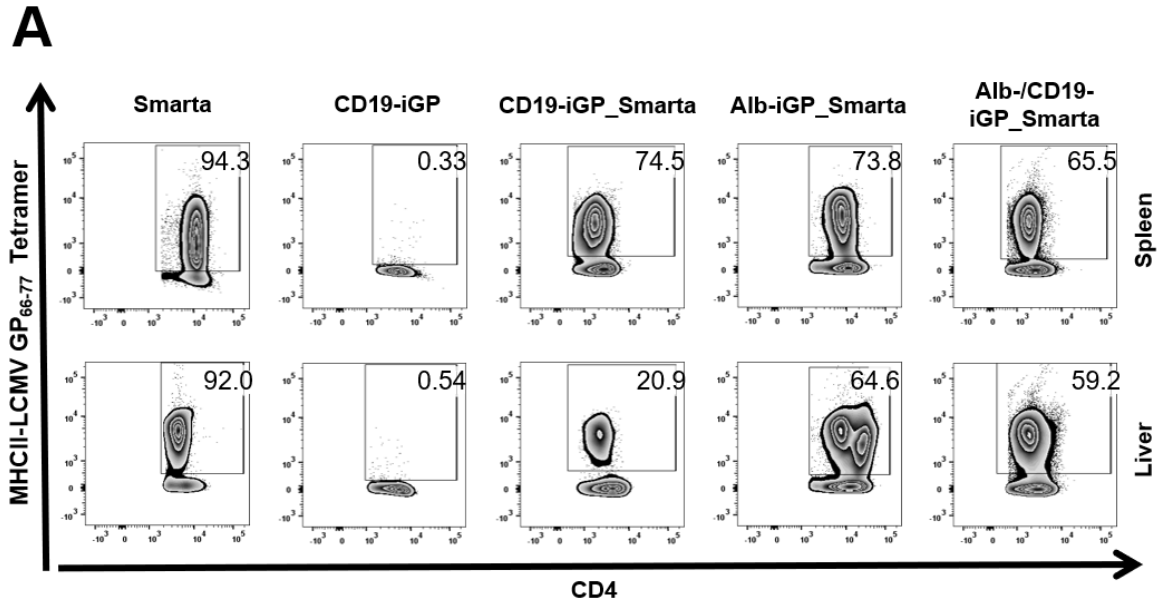


Figure 9: (A) Representative flow cytometry plots showing antigen-specific Smarta T cells (tetramer⁺) of CD4 T cells in spleen and liver of eight-week-old control mice (Smarta, CD19-iGP), CD19-iGP_Smarta, Alb-iGP_Smarta and Alb-/CD19-iGP_Smarta mice. Numbers beside gates indicate percent positive cells in each gate. (B) Percentages of antigen-specific Smarta T cells (tetramer⁺) in the thymus of eight-week-old control mice (Smarta, CD19-iGP), CD19-iGP_Smarta, Alb-iGP_Smarta and Alb-/CD19-iGP_Smarta. (C) Percentages as well as absolute numbers of antigen-specific Smarta T cells (tetramer⁺) in the spleen of eight-week-old control mice (Smarta, CD19-iGP), CD19-iGP_Smarta, Alb-iGP_Smarta and Alb-/CD19-iGP_Smarta. (D) Percentages as well as absolute numbers of antigen-specific Smarta T cells (tetramer⁺) in the liver of eight-week-old control mice (Smarta, CD19-iGP), CD19-iGP_Smarta, Alb-iGP_Smarta and Alb-/CD19-iGP_Smarta.

4.1.1.3 *Co-expression of autoantigen in B cells and hepatocytes does not alter the Foxp3⁺ Treg frequency in Alb-/CD19-iGP_Smarta mice*

Next, the frequency of Tregs was analysed, as these represent an important tolerance mechanism. Figure 10 A shows representative flow cytometry dot plots indicating tetramer- and Foxp3-staining of CD4 T cells from Smarta and CD19-iGP control mice, as compared to CD19-iGP_Smarta, Alb-iGP_Smarta and Alb-/CD19-iGP_Smarta mice.

All Smarta transgenic lines, i.e. Smarta (0.1 %), CD19-iGP_Smarta (0.12 %), Alb-iGP_Smarta (0.15 %) and Alb-/CD19-iGP_Smarta (0.14 %), showed a significantly reduced frequency of Foxp3⁺ Tregs in the thymus, as compared to the CD19-iGP control line (2.48 %, $p < 0.0001$, Figure 10 B). In the spleen, however, Alb-iGP_Smarta (6.18 %) and Alb-/CD19-iGP_Smarta mice (6.8 %) showed a Treg frequency that was similar to that of CD19-iGP control mice (10.69 %, ns, Figure 10 B). In contrast, CD19-iGP_Smarta (4.60 %) and Smarta control mice (1.67 %,) had reduced Treg frequencies in the spleen as compared to CD19-iGP control mice (10.69 %, $p < 0.01$, Figure 10 B). In the liver, Treg frequencies of CD19-iGP_Smarta (5.3 %), Alb-iGP_Smarta (3.37 %), Alb-/CD19-iGP_Smarta (5.43 %) and CD19-iGP control mice (3.26 %, ns, Figure 10 B) were in a similar range; only Smarta mice manifested low Treg frequencies (0.68 %; $p < 0.01$ and ns, Figure 10 B). These findings indicated that antigen-expression by B cells or hepatocytes had seemed to induce peripheral induction of Tregs. However, concomitant antigen-expression by both, B cells and hepatocytes, did not add to Treg induction.

We then analysed the frequencies of antigen-specific tetramer⁺ Foxp3⁺ Tregs, and found low frequencies in the thymus of Smarta control mice (0.06 %), Alb-iGP_Smarta mice (0.07 %) and Alb-/CD19-iGP_Smarta mice (0.07 %, ns, Figure 10 C). However, the tetramer⁺ Foxp3⁺ Treg frequencies were significantly elevated in spleen and liver of CD19-iGP_Smarta mice (1.97 % and 5.11 %, ns and $p < 0.01$, respectively), Alb-iGP_Smarta mice (4.55 % and 3.42 %, $p < 0.0001$ and ns, respectively) and Alb-/CD19-iGP_Smarta mice (2.98 % and 3.35 %, $p < 0.05$ and ns, respectively), as compared to Smarta controls (0.34 % and 0.31 %, Figure 10 C). CD19-iGP mice were not included in this analysis, as they possess (almost) no tetramer⁺ T cells.

Taken together, these findings confirmed antigen-specific Treg induction in the periphery, as a consequence of antigen expression in B cells or hepatocytes.

However, as we did not find significant differences in Treg numbers in Alb-iGP_Smarta vs. Alb-/CD19-iGP_Smarta mice, our results indicated that the autoantigen-presentation by B cells did not alter the frequency of Tregs in the Alb-iGP_Smarta model for AIH.

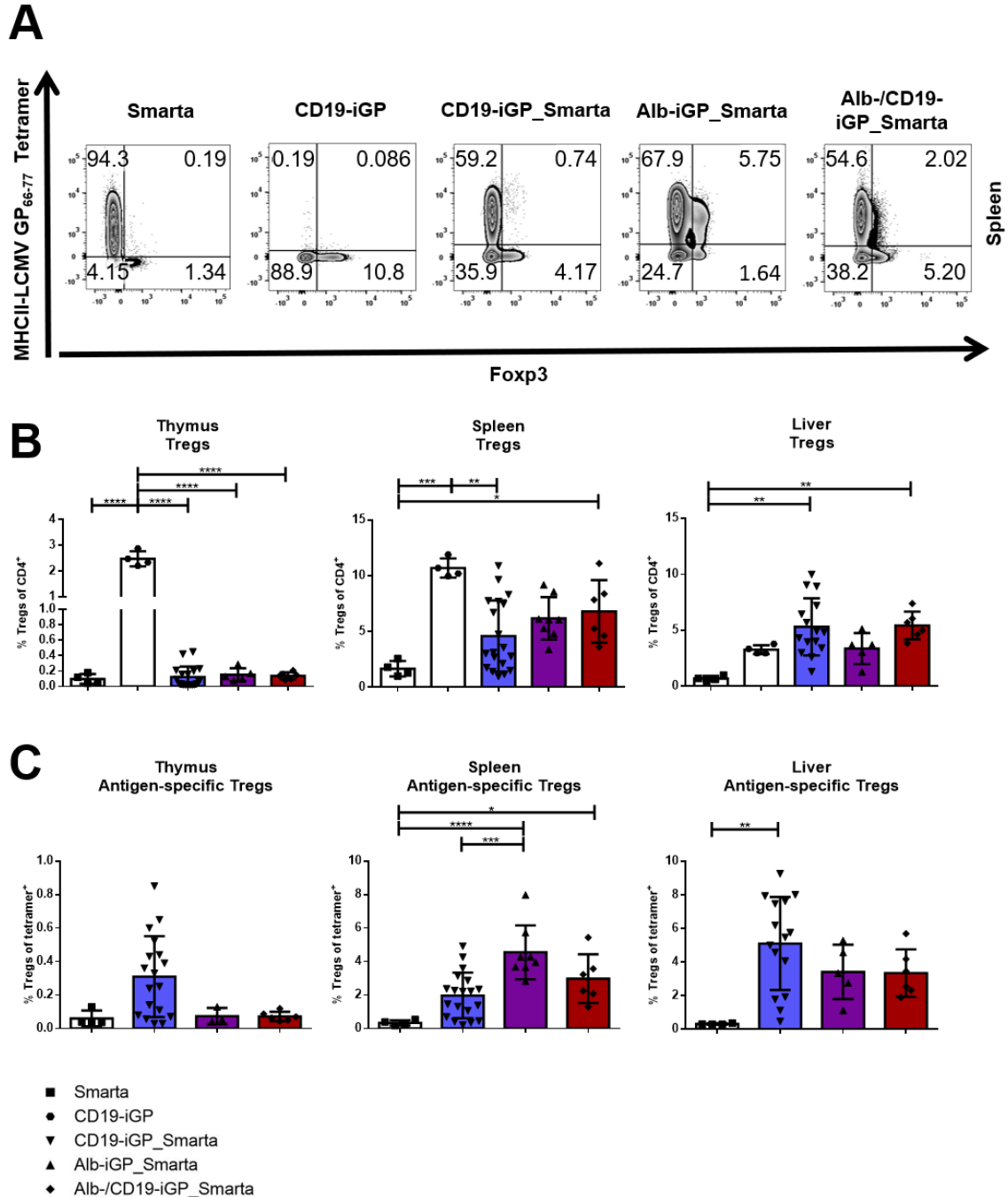


Figure 10: (A) Representative flow cytometry plots showing antigen-specific Smarta T cells (tetramer⁺) and Foxp3⁺ Tregs of CD4 T cells in the spleen of eight-week-old control mice (Smarta, CD19-iGP), CD19-iGP_Smarta, Alb-iGP_Smarta and Alb-/CD19-iGP_Smarta mice. Numbers in quadrants indicate percent positive cells in each of them. (B) Percentages of Tregs in thymus, spleen and liver of eight-week-old control mice (Smarta, CD19-iGP), CD19-iGP_Smarta, Alb-iGP_Smarta and Alb-/CD19-iGP_Smarta mice. (C) Percentages of antigen-specific Tregs (tetramer⁺) in thymus, spleen and liver of eight-week-old control mice (Smarta), CD19-iGP_Smarta, Alb-iGP_Smarta and Alb-/CD19-iGP_Smarta mice.

4.1.2 Autoantigen-presentation by B cells results in a diverse autoantibody production

After examining the consequences of autoantigen-presentation by B cells on the T cell population in our AIH model, we analysed whether autoantigen-presentation by B cells had an influence on the B cell population itself. Therefore, a flow cytometry panel was used to stain for CD19⁺ B220⁺ B cells.

4.1.2.1 Flow cytometry gating strategy for CD19⁺ B220⁺ B cells

First, non-lymphocyte cells, doublets, dead cells and CD45⁻ cells were excluded. The remaining CD45⁺ leucocytes were gated on CD19 and B220 to identify the CD19⁺ B220⁺ B cell population (Figure 11).

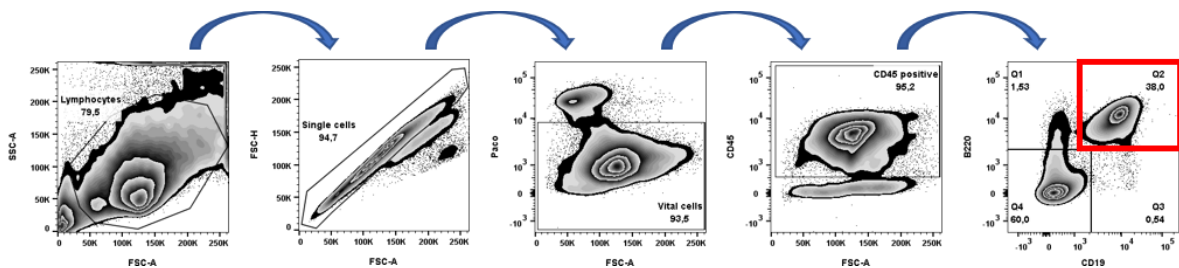


Figure 11: Gating strategy of the flow cytometry B cell panel used to stain for CD19⁺ B220⁺ B cells.

4.1.2.2 B cell numbers are not altered in mice co-expressing the autoantigen in B cells and hepatocytes

A comparison of the B cell percentages of all CD45⁺ cells in spleen and liver revealed, that there was no significant difference between the Alb-iGP_Smarta, Alb-/CD19-iGP_Smarta and the three control lines (wildtype, Smarta and CD19-iGP) (Figure 12). Because of strong variation of the liver data in Alb-iGP_Smarta and Alb-/CD19-iGP_Smarta lines, more data should be collected in order to verify this result. Nonetheless, the CD19-iGP_Smarta mice showed a significantly reduced B cell frequency in the liver compared to the wildtype and CD19-iGP control lines (4.4 % vs 25.16 % and 22.63 %, $p < 0.05$, Figure 12 B) as well as the Alb-iGP_Smarta and Alb-/CD19-iGP_Smarta lines (4.4 % vs 27.13 % and 24.87 %, $p < 0.01$, Figure 12 B). This observation will be addressed in more detail later in this work (see 4.2.1.2).

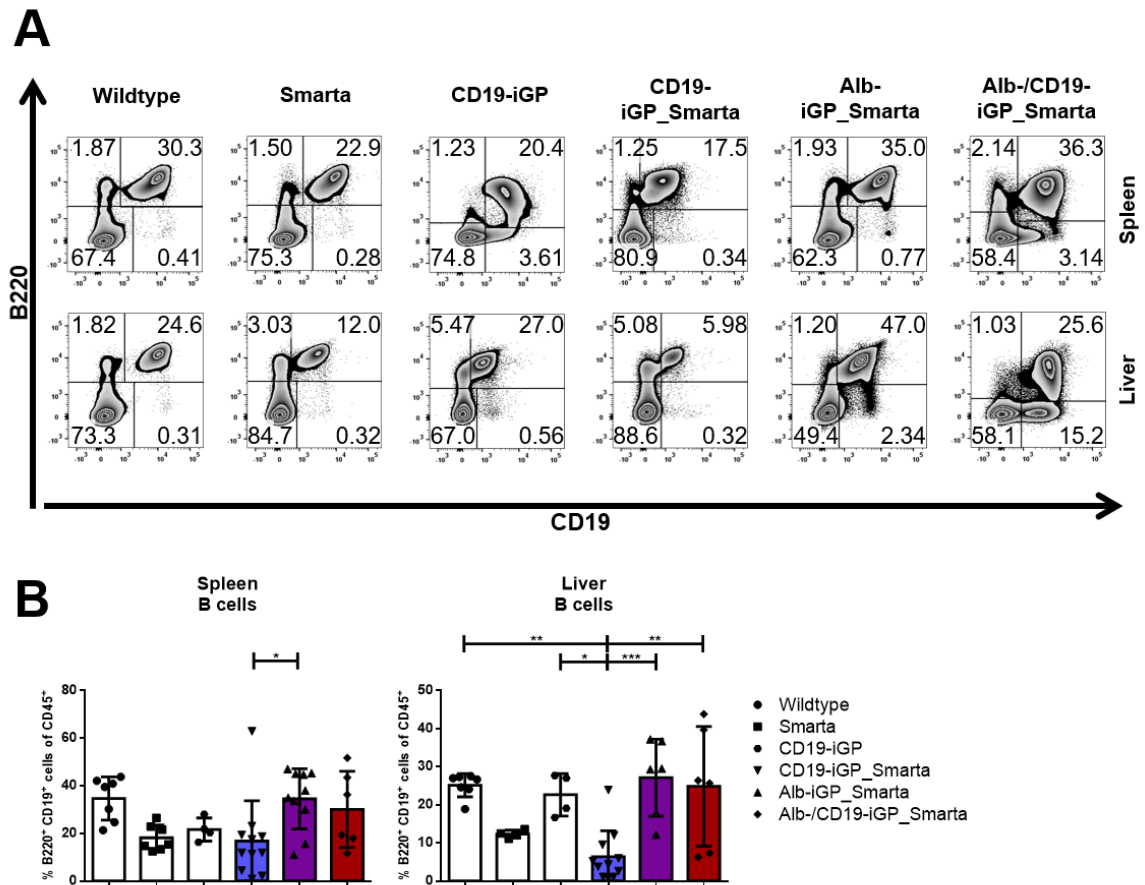


Figure 12: (A) Representative flow cytometry plots showing CD19⁺ B220⁺ B cells of CD45⁺ cells in spleen and liver of eight-week-old control mice (Smarta, CD19-iGP), CD19-iGP_Smarta, Alb-iGP_Smarta and Alb-/CD19-iGP_Smarta mice. Numbers in quadrants indicate percent positive cells in each of them. (B) Percentages of B cells in spleen and liver of eight-week-old control mice (wildtype, Smarta, CD19-iGP), CD19-iGP_Smarta, Alb-iGP_Smarta and Alb-/CD19-iGP_Smarta mice.

4.1.2.3 Autoantigen-presentation by B cells results in a diverse autoantibody pattern

Plasma cells in the liver and autoantibodies are a characteristic of AIH. Therefore, the autoantibodies found in the serum of the different mouse lines were characterized and a titre was determined.

Max Preti could show that the Alb-iGP_Smarta mice featured antinuclear antibodies already at the age of eight weeks, mostly at titres of 1:160 or 1:320 (Preti, 2019). As can be seen in Figure 13, the CD19-iGP and Alb-iGP control mice lacking autoreactive T cells did not show a positive immunofluorescence signal at that dilution but had a titre of 1:40 or lower. The CD19-iGP_Smarta mice also possessed autoantibodies with titres of 1:160 or 1:320, but the antibody pattern was more diverse, with not only antinuclear but also anti-cytoplasmic antibodies. The analysed Alb-/CD19-iGP_Smarta mice also showed this diverse pattern with a most frequent titre of 1:160. There was a large variation between the single animals of this line as well as the CD19-iGP_Smarta line in terms of the composition of the pattern. As can be seen in Figure 13 on the right, some mice mainly showed antinuclear antibodies (upper picture) and others showed different variations of an anti-cytoplasmic antibody pattern (lower picture). This suggested that autoantigen-presentation by B cells leads to the production of a more diverse and unspecific autoantibody pattern compared to the clear antinuclear pattern in the Alb-iGP_Smarta mice.

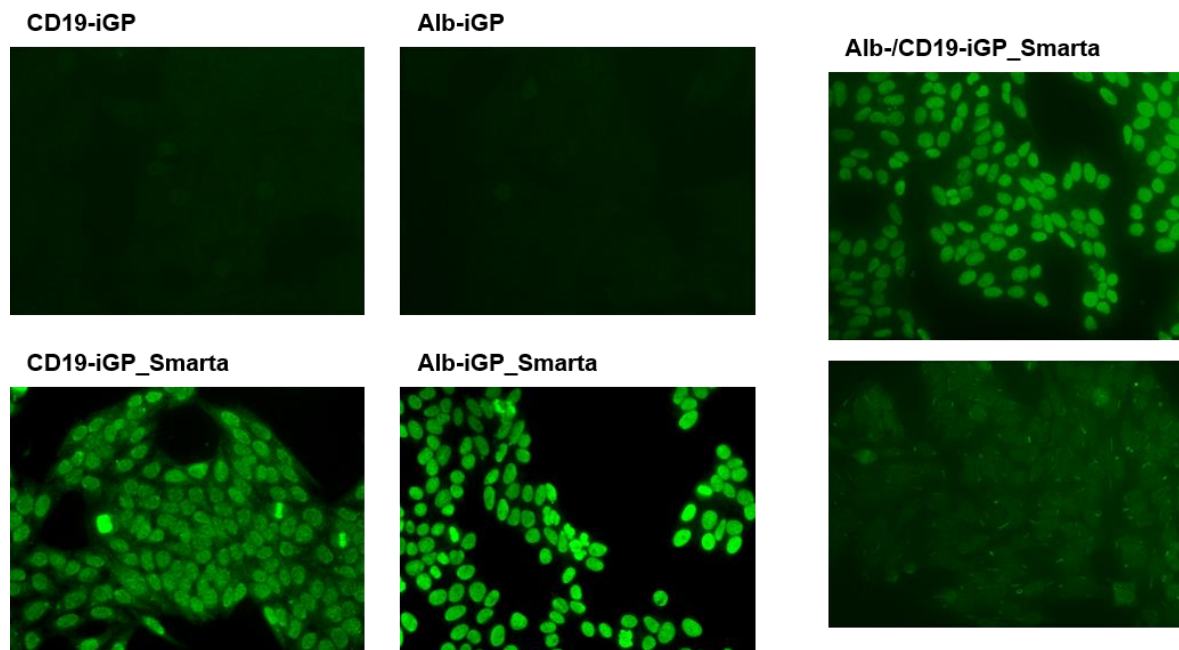


Figure 13: Indirect immunofluorescence staining of serum from control mice (CD19-iGP, Alb-iGP) as well as CD19-iGP_Smarta, Alb-iGP_Smarta and Alb-/CD19-iGP_Smarta mice on Hep2 cells at a dilution of 1:160. 400 fold magnification.

4.1.3 Co-expression of antigen in B cells and hepatocytes leads to the formation of ELT in the liver, but not to liver inflammation in young Alb-/CD19-iGP_Smarta mice

After the examination of the relevant immune cell populations regarding autoimmune disease development, namely B and T cells, an overview of the liver pathology should be gained via histological analysis and measurement of transaminases. In the Alb-iGP_Smarta mice, ELT could be observed in the liver at this age (see 2.4.2). The question was whether ELT could also be found in Alb-/CD19-iGP_Smarta mice.

4.1.3.1 ELT can be found in the liver of Alb-/CD19-iGP_Smarta mice

Liver tissue stained with H&E showed that ELT was detectable in the liver of 66.7 % of the Alb-/CD19-iGP_Smarta line; these ELT were of similar structure as those found in the Alb-iGP_Smarta mice (Figure 14). The Smarta and CD19-iGP control mice as well as the CD19-iGP_Smarta mice did not develop hepatic ELT.

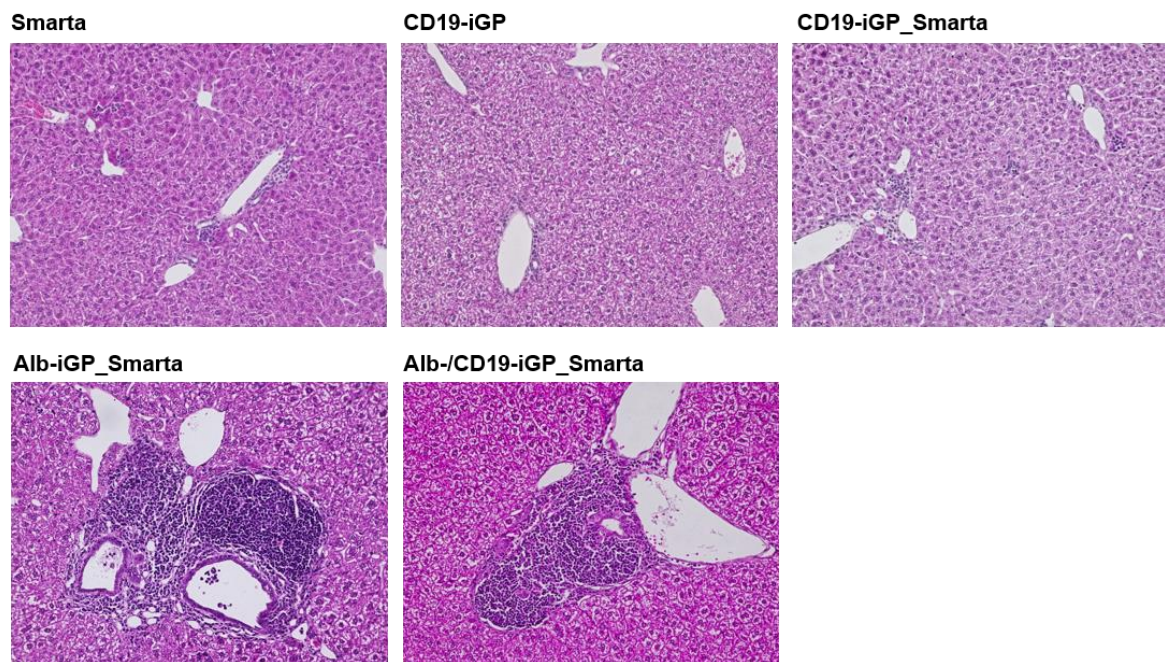


Figure 14: H&E staining of liver tissue from eight-week-old control mice (Smarta, CD19-iGP) as well as CD19-iGP_Smarta, Alb-iGP_Smarta and Alb-/CD19-iGP_Smarta mice. 200 fold magnification. Data of the Alb-iGP_Smarta mice was obtained from Max Preti (Preti, 2019).

Additional immunohistochemistry staining of consecutive liver sections for B220 as B cell marker and CD4 as CD4 T cell marker showed that the ELT in the Alb-/CD19-iGP_Smarta mice contained separate B and T cell zones (Figure 15). Also this is in accord with the findings in the Alb-iGP_Smarta mice (see 2.4.2).

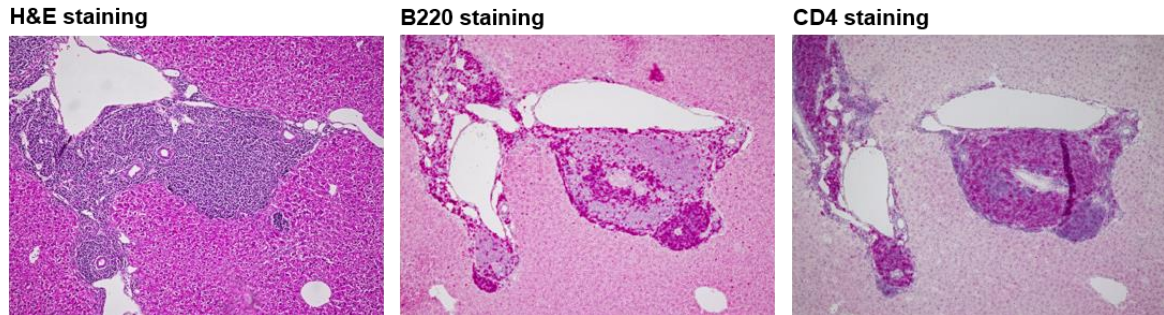


Figure 15: Histology of consecutive liver sections from eight-week-old Alb-/CD19-iGP_Smarta mice. H&E staining and immunohistochemistry staining for B220 (B cells stained in purple) and CD4 (CD4 T cells stained in purple). 100 fold magnification.

4.1.3.2 Alb-/CD19-iGP_Smarta mice show no exacerbated liver damage

To address whether the development of ELT was associated with liver damage, the transaminases ALT and AST were measured in the serum of the mice. A comparison of the groups showed that neither ALT nor AST were elevated in Alb-iGP_Smarta mice or Alb-/CD19-iGP_Smarta mice compared to the control lines and the CD19-iGP_Smarta mice that do not develop ELT (Figure 16).

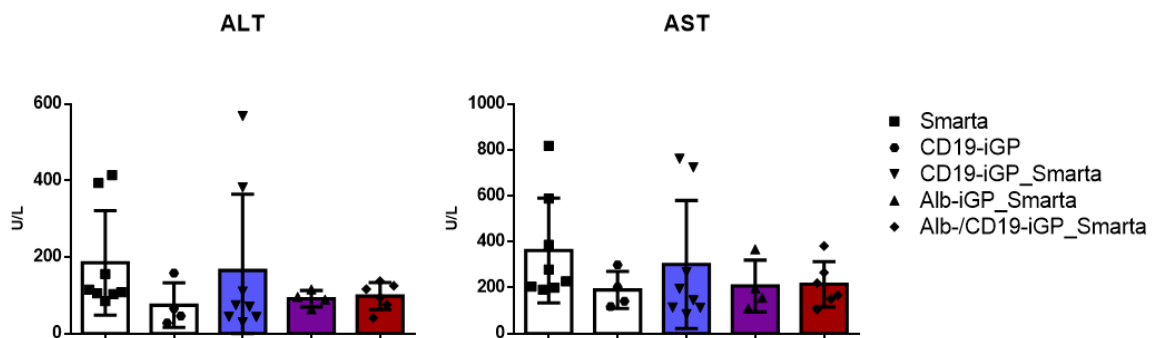


Figure 16: Measurement of ALT and AST as markers for liver damage in the serum of eight-week-old control mice (Smarta, CD19-iGP), CD19-iGP_Smarta, Alb-iGP_Smarta and Alb-/CD19-iGP_Smarta mice.

4.1.4 Lymphocyte composition in Alb-/CD19-iGP_Smarta mice is not sex-dependent

As human AIH is characterized by female preponderance (see 2.3.1), a comparison of male vs female Alb-/CD19-iGP_Smarta mice was performed with respect to the frequency of Smarta T cells, Tregs and B cells in spleen and liver. The comparison showed that there were no significant sex-related differences in any of the analysed cell populations, neither in the disease-causing Smarta cell or B cell populations, nor the tolerogenic Treg population (Figure 17).

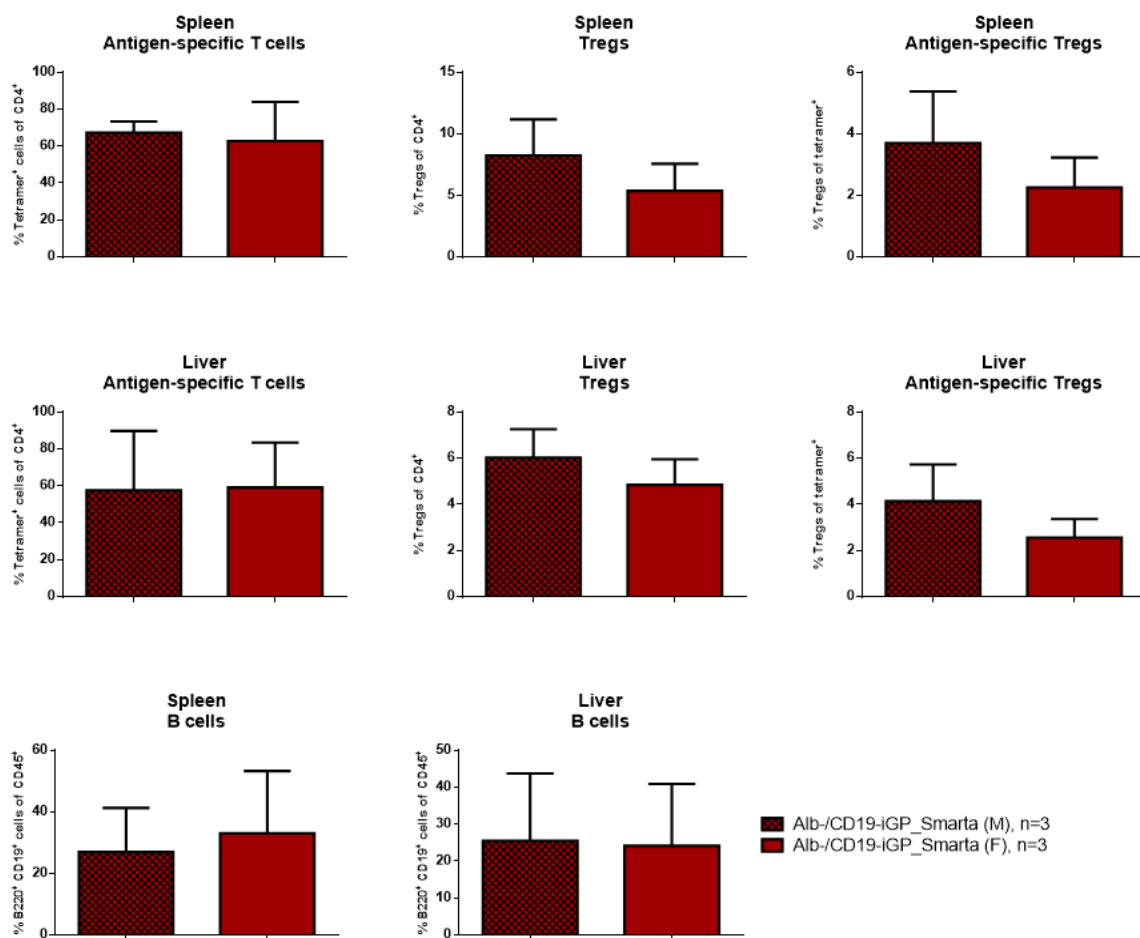


Figure 17: Comparison of flow cytometry data from male vs female Alb-/CD19-iGP_Smarta mice. Shown are percentages of antigen-specific Smarta T cells (tetramer⁺), Tregs, antigen-specific Tregs (tetramer⁺) and B cells in spleen and liver.

Thus, a more frequent development of autoimmune disease in female mice should not be expected. However, to confirm this notion, it will be necessary to monitor more and older Alb-/CD19-iGP_Smarta mice in future experiments.

4.2 Characterization of the CD19-iGP_Smarta mouse model of autoantigen-presentation by B cells

The analyses of the mouse lines presented in the previous section revealed that the CD19-iGP_Smarta mice, which we used as a control for the analysis of B cell function in AIH (see 4.1), were prone to spontaneously develop autoimmune disease. Therefore, these mice were further examined with respect to development of a systemic autoimmune disease.

The major findings in thymus, spleen and liver of eight-week-old mice, which have been shown in detail in the previous chapter, can be summarized as follows:

The Smarta T cells were not deleted in CD19-iGP_Smarta mice, but still present in high frequency (Figure 9). Yet, their proportion among the CD4 T cells was higher in the thymus than in the peripheral organs, indicating partial deletion in the periphery (see 4.1.1.2). Moreover, the frequency of Tregs in the thymus was lower than in the periphery, indicating peripheral induction of Tregs (see 4.1.1.3). Regarding the B cells, their proportion of all CD45⁺ cells in the spleen was similar to that of the control lines; however, their frequency was reduced in the liver (Figure 12). The CD19-iGP_Smarta mice most frequently showed autoantibodies at titres between 1:160 and 1:320, with diverse reactivities, including antinuclear and anti-cytoplasmic antibodies (see 4.1.2.3).

4.2.1 Development of immunological processes in eight-week-old CD19-iGP_Smarta mice

As shown above, in eight-week-old CD19-iGP_Smarta mice, liver damage was not detectable, despite liver infiltration with Smarta T cells. Lung and kidneys of 8- and 20-week-old mice were also examined in comparison to Smarta, CD19-iGP and wildtype control mice.

4.2.1.1 *Presence of antigen-specific Smarta T cells, reduction of Tregs and formation of ELT in the lungs of CD19-iGP_Smarta mice*

To receive an overview about possible processes taking place in the lung, it was assessed by histology and flow cytometry.

4.2.1.1.1 Formation of lymphatic structures in the lungs of CD19-iGP_Smarta mice

H&E staining of tissue sections from the lungs of CD19-iGP_Smarta mice revealed the formation of lymphatic structures, that could not be found in the Smarta and CD19-iGP control lines (Figure 18). The lymphatic structures were clearly distinguishable from the normal lung tissue and could be found in all parts of the lung, mainly between the alveoli with no association to bigger bronchi or vessels. It can be assumed that these structures were ELT similar to that found in the liver of Alb-iGP_Smarta and Alb-/CD19-iGP_Smarta mice (see Figure 14). The lung tissue from Alb-/CD19-iGP_Smarta mice also showed ELT, suggesting that the development of it was due to the antigen-presentation by B cells.

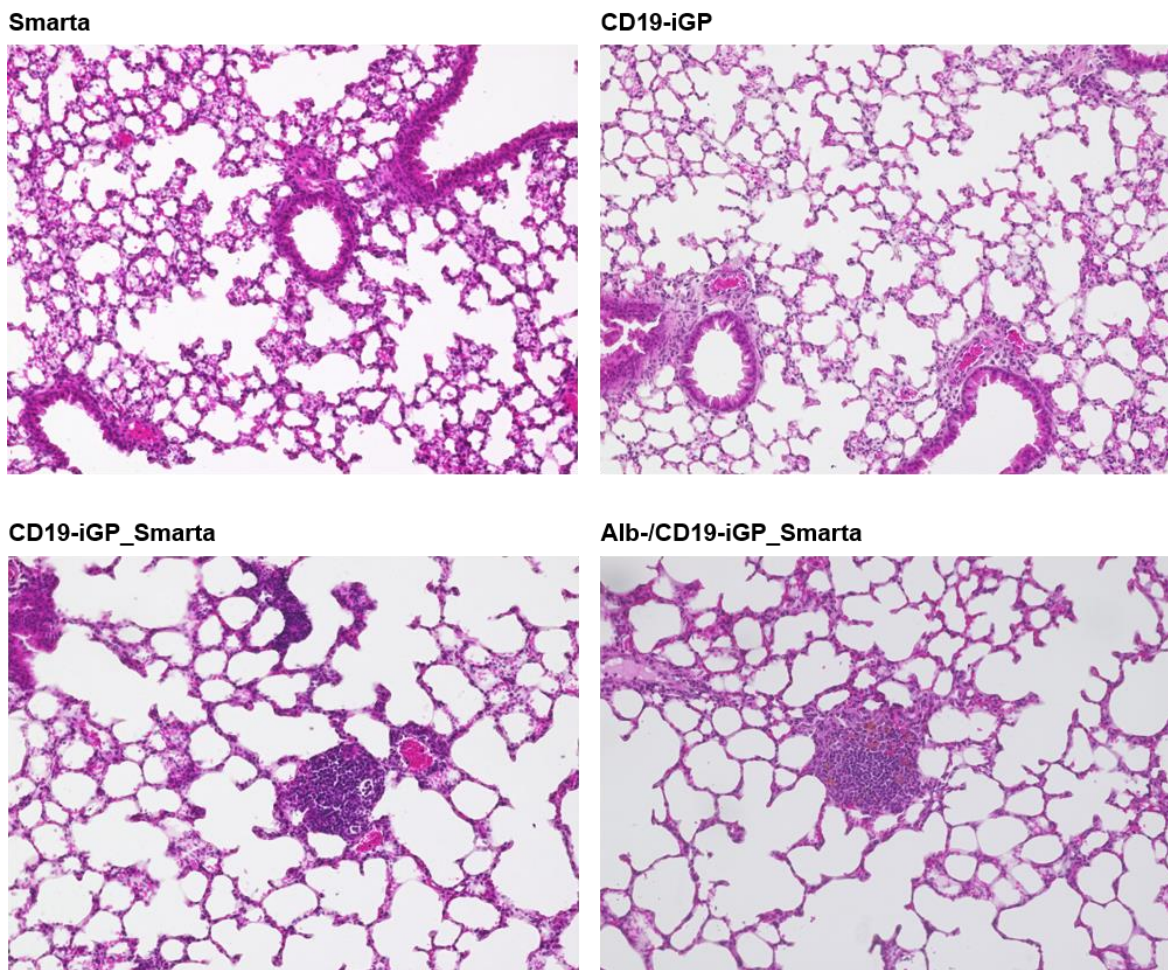


Figure 18: H&E staining of lung tissue from eight-week-old control mice (Smarta, CD19-iGP) as well as CD19-iGP_Smarta and Alb-/CD19-iGP Smarta mice. 200 fold magnification.

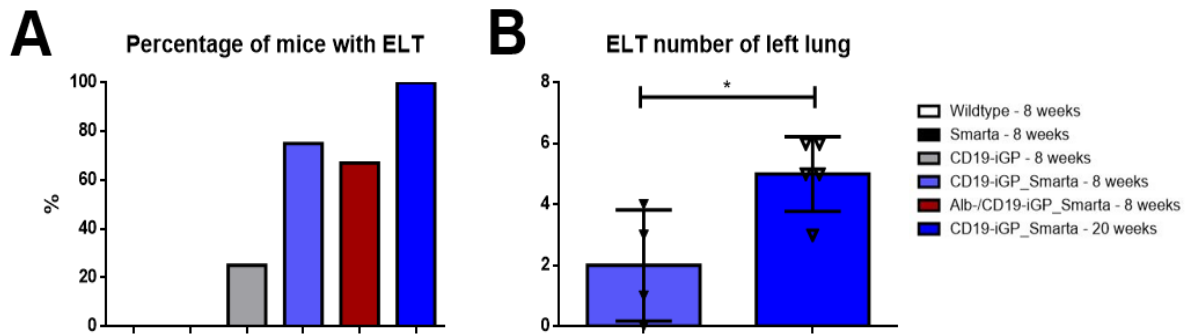


Figure 19: (A) Percentage of mice with ≥ 1 LS in one histological slide of the left lung from eight-week-old control mice (wildtype, Smarta, CD19-iGP) as well as eight-week-old CD19-iGP_Smarta and Alb-/CD19-iGP_Smarta mice and 20-week-old CD19-iGP_Smarta mice. (B) Number of ELT counted in one histological slide of the left lung from 8- and 20-week-old CD19-iGP_Smarta mice.

ELT could be found in the lungs of 75 % of the eight-week-old CD19-iGP_Smarta mice and of 67 % of the Alb-/CD19-iGP_Smarta mice. In 20-week-old CD19-iGP_Smarta mice, the occurrence rate was 100 %. In contrast, only 25 % of the CD19-iGP line and 0 % of all other control animals showed ELT in lungs (Figure 19 A). Moreover, the number of ELT structures per lung was higher in 20-week-old mice compared to eight-week-old, indicating that they become more frequent with increasing age (Figure 19 B). In addition, the average size of the ELT structures seemed to increase between 8-week-old and 20-week-old mice, as is illustrated in Figure 20.

To confirm that these structures were similar to the ELT found in the liver of Alb-iGP_Smarta and Alb-/CD19-iGP_Smarta mice, immunohistochemical staining for B and CD4 T cells of consecutive lung sections was performed. This staining demonstrated that the ELT in the

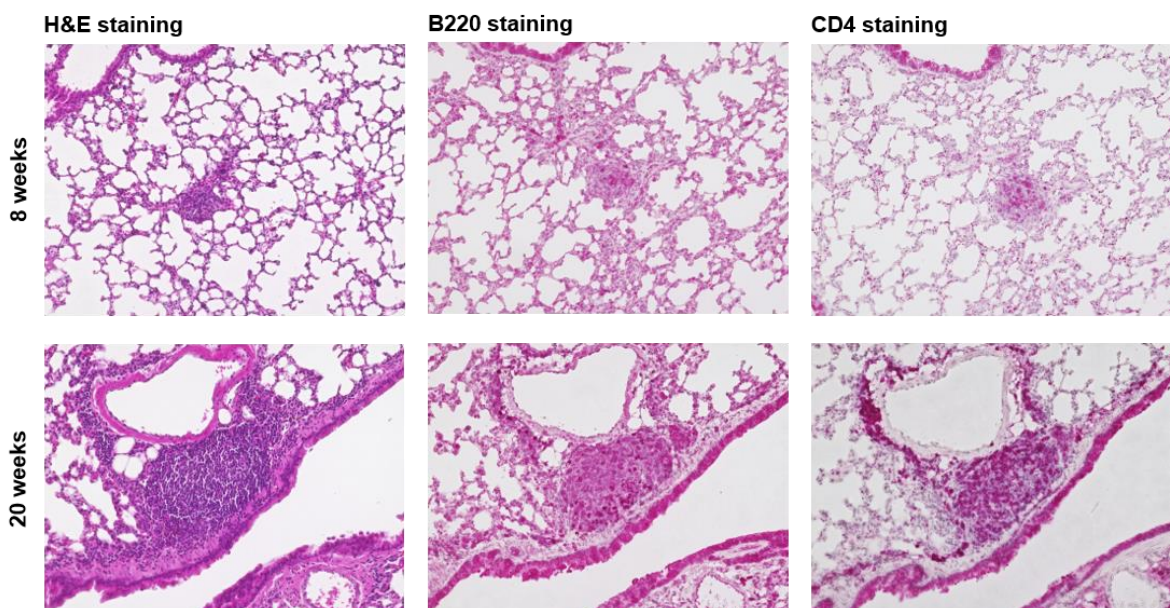


Figure 20: Histology of consecutive lung sections from 8- and 20-week-old CD19-iGP_Smarta mice. H&E staining and immunohistochemistry staining for B220 (B cells stained in purple) and CD4 (T cells stained in purple). 200 fold magnification.

lungs mainly consisted of B220⁺ B cells and CD4⁺ T cells. However, a clear zonation into separated B and T cell zones could not be seen (Figure 20). Thus, further examination of the structural and cellular composition of the ELT should be performed.

4.2.1.1.2 Autoantigen-presentation by B cells leads to presence of antigen-specific Smarta cells and a reduction of Tregs in the lungs of CD19-iGP_Smarta mice

The T cell population in the lung was characterized by flow cytometry. In the lungs of CD19-iGP_Smarta mice, 33.43 % of the CD4⁺ T cells were Smarta T cells, a frequency that was reduced compared to Smarta control mice (33.43 % vs 93.2 %, $p < 0.0001$, Figure 21). However, this reduction was also found in the liver of CD19-iGP_Smarta mice (21.03 % vs 91.7 %, $p < 0.0001$; see 4.1.1.2, Figure 9). Although the Smarta frequency was higher in the spleen (62.52 %), as compared to lung and liver, it was still reduced compared to Smarta control mice (93.95 %, $p < 0.01$; see 4.1.1.2, Figure 9). The higher frequency in the spleen might have been due to the increased frequency of antigen-presenting B cells (see 4.1.2.2 and 4.2.1.1.3), which may have led to increased accumulation of antigen-specific T cells.

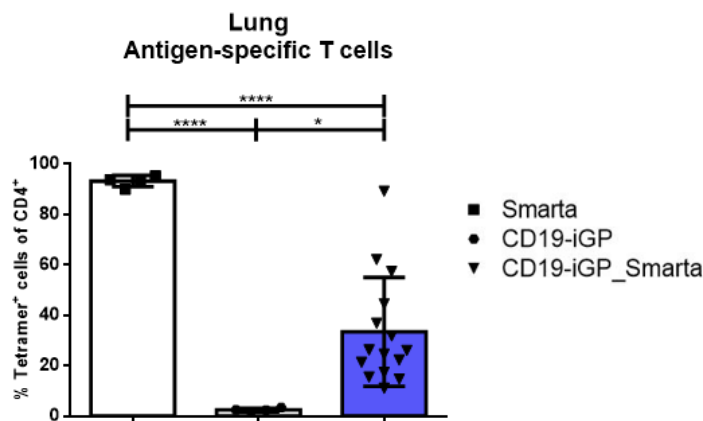


Figure 21: Percentages of antigen-specific Smarta T cells (tetramer⁺) in the lung of eight-week-old control mice (Smarta, CD19-iGP) and CD19-iGP_Smarta mice.

The overall frequency of Tregs in CD19-iGP_Smarta mice in the lung was lower compared to the CD19-iGP control line (3.2 % vs 8.68 %, $p < 0.001$, Figure 22). However, the frequency of all Tregs and of antigen-specific Tregs was higher compared to the Smarta control line (3.2 % vs 0.86 % and 2 % vs 0.35 %, respectively, ns, Figure 22). The reduction in Tregs compared to the normal Treg frequency in the CD19-iGP mice may be an explanation for the development of autoimmunity in the CD19-iGP_Smarta line. The reduced Treg frequency in Smarta mice was not associated with autoimmune disease, as these mice do not feature the cognate antigen of the Smarta T cells.

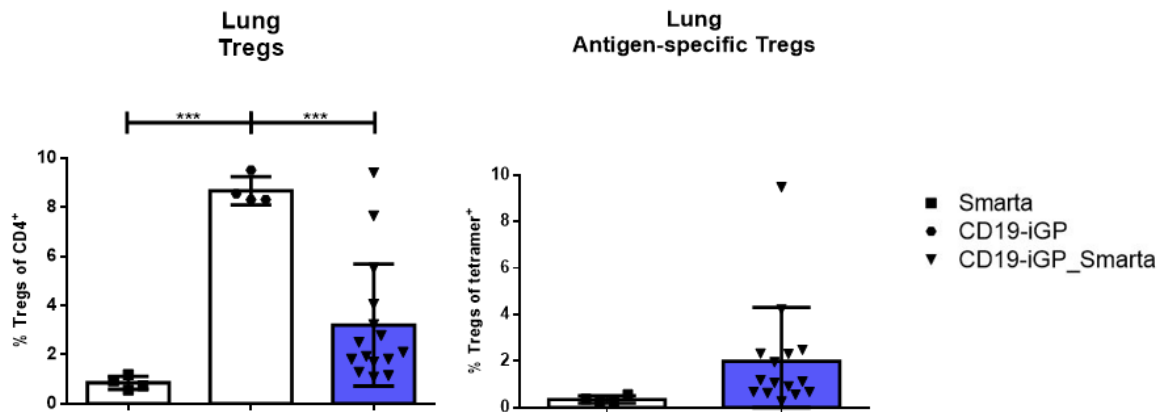


Figure 22: Percentages of Tregs and antigen-specific Tregs (tetramer⁺) in the lung of eight-week-old control mice (Smarta, CD19-iGP) and CD19-iGP_Smarta mice.

4.2.1.1.3 Autoantigen-presentation by B cells leads to reduced B cell frequencies in the lungs of CD19-iGP_Smarta mice

By flow cytometric analysis of lymphocytes isolated from the lung, we found that the proportion of B220⁺ CD19⁺ B cells of all CD45⁺ cells was significantly reduced in CD19-iGP_Smarta mice compared to all control lines (4.06 % vs 23.63 % in the wildtype mice, 17.8 % in the Smarta mice and 19.8 % in the CD19-iGP mice, $p < 0.01$, Figure 23). This was in accordance with the findings of the B cell analysis in the liver (see 4.1.2.2); however, this reduction could not be seen in the spleen at this age (see 4.1.2.2).

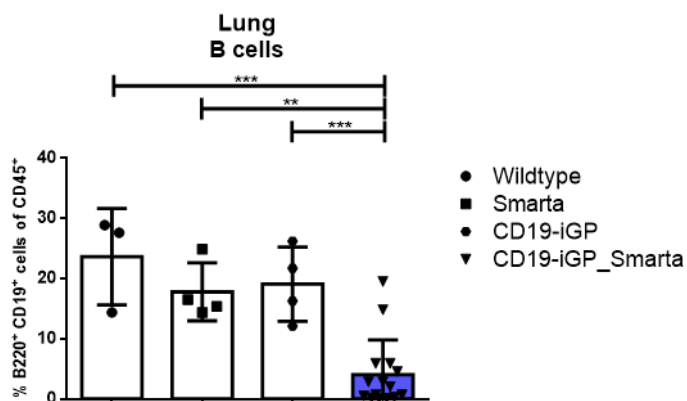


Figure 23: Percentages of B cells in the lung of eight-week-old control mice (wildtype, Smarta, CD19-iGP) and CD19-iGP_Smarta mice.

4.2.1.2 Reduced amount of B cells in the liver of CD19-iGP_Smarta mice

After examining the lung, we analysed livers of eight-week-old CD19-iGP_Smarta mice by immunohistochemical staining for B and CD4 T cells. As can be seen in Figure 24, the B220 staining for B cells showed a lower B cell number in the livers of CD19-iGP_Smarta mice compared to Smarta and CD19-iGP control mice. This was consistent with the results of the flow cytometric analysis described in 4.1.2.2. The CD4 staining for CD4 T cells showed no noticeable differences between the CD19-iGP_Smarta mice and the controls.

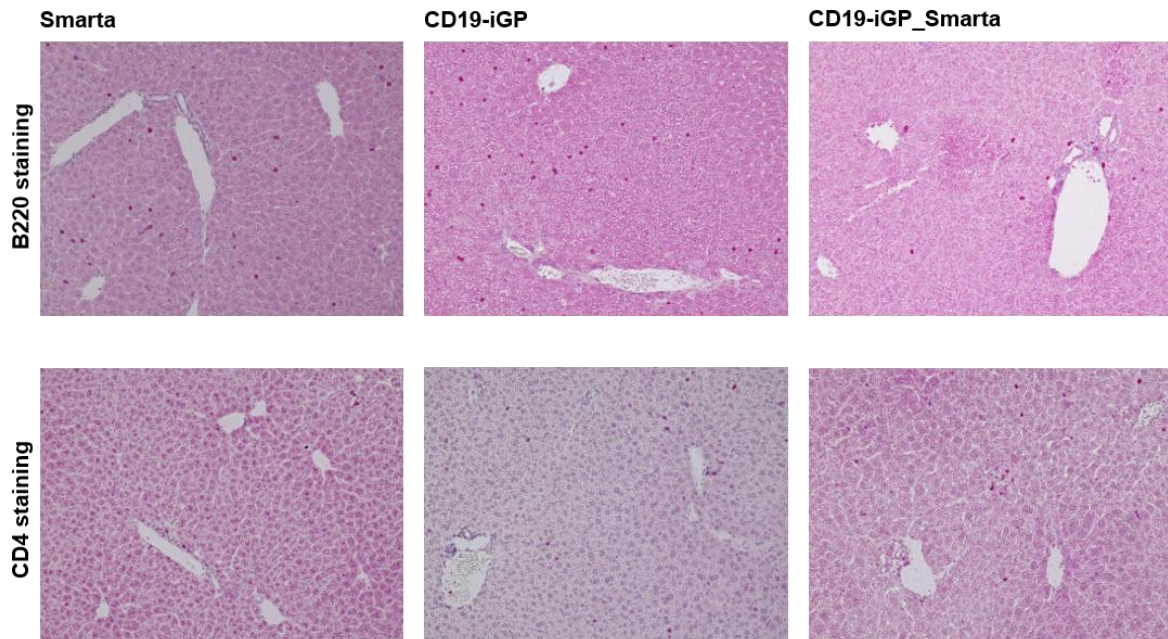


Figure 24: Immunohistochemistry staining of liver tissue from eight-week-old control mice (Smarta, CD19-iGP) and CD19-iGP_Smarta mice for B220 (B cells stained in purple) and CD4 (CD4 T cells stained in purple). 200 fold magnification.

4.2.1.3 Kidneys of CD19-iGP_Smarta mice show an age-related increase in intraglomerular cell number

To detect potential immune pathologies in the kidneys, PAS staining of tissue from 8- and 20-week-old control mice and CD19-iGP_Smarta mice was performed. The kidneys from CD19-iGP_Smarta mice showed no inflammation, like the control lines (Figure 25 A). However, quantification of the nuclei per glomerulus in 10 glomeruli of three to four mice per line revealed an increase of nuclei and therefore cell number in the 20-week-old CD19-iGP_Smarta mice compared to the eight-week-old mice of that line (36.73 vs 28.8, $p < 0.01$, Figure 25 B). In the control lines, no significant increase of cell number with age could be seen (data not shown). This finding suggested that further analysis of the cell types in the glomeruli could be of interest to show a possible infiltration of lymphocytes or other immune cells into the glomeruli.

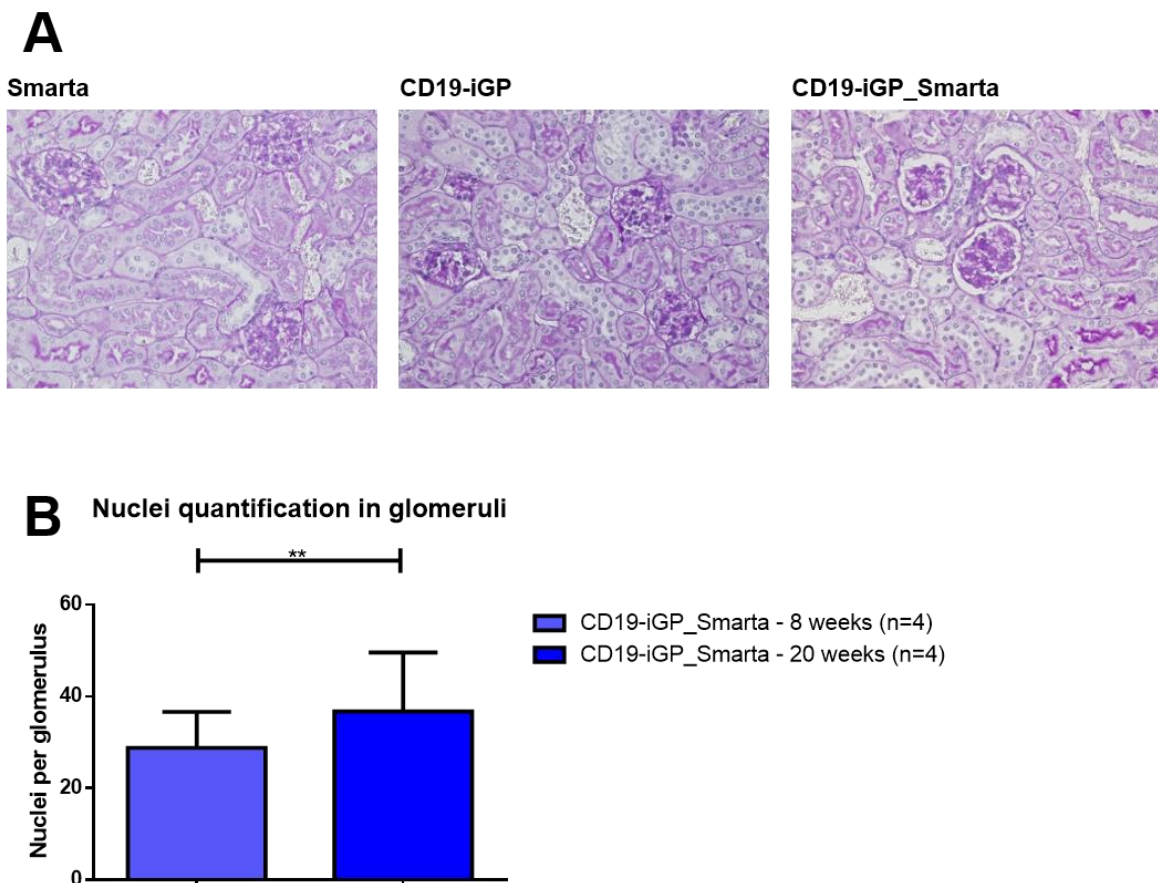


Figure 25: (A) PAS staining of kidney tissue from eight-week-old control mice (Smarta, CD19-iGP) and CD19-iGP_Smarta mice. 400 fold magnification. (B) Quantification of nuclei per glomerulus in 8- and 20-week-old CD19-iGP_Smarta mice. 10 glomeruli per mouse were quantified.

4.2.2 Systemic autoimmune disease in CD19-iGP_Smarta mice

As already mentioned in the beginning of this chapter, CD19-iGP_Smarta mice were found to develop systemic autoimmune disease, which develops from the age of 20 weeks on. Mice that showed signs of health impairment were sacrificed, analysed and compared to 20-week-old CD19-iGP_Smarta mice in a preclinical stage as well as 20-week-old wildtype, Smarta and CD19-iGP control mice.

4.2.2.1 Characterization of autoimmune pathology in CD19-iGP_Smarta mice

23 mice of the CD19-iGP_Smarta line and 8 mice of the CD19-iGP control line were closely monitored for and sacrificed upon development of disease symptoms, including an impaired general condition. The mice were monitored for 52 weeks and humane endpoints were applied accordingly (Figure 26). The CD19-iGP_Smarta mice showed a 50 % disease prevalence at the age of 35 weeks and only 8.7 % disease-free survival after one year, which is significantly less than the CD19-iGP control line in which all animals survived ($p < 0.01$).

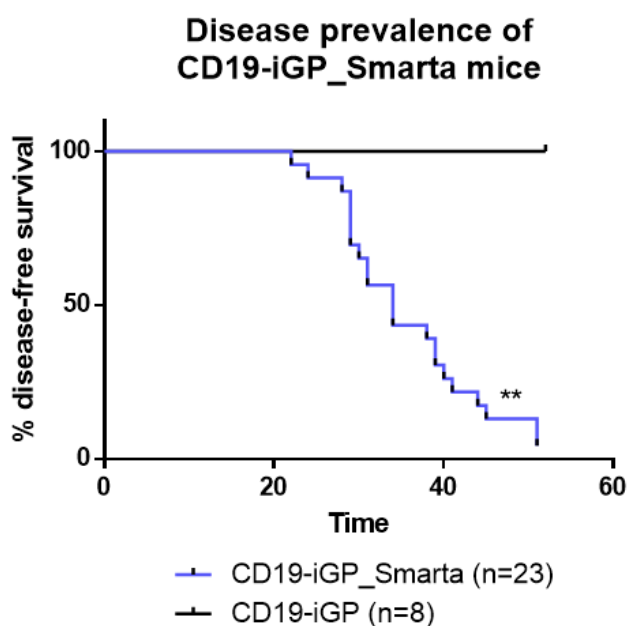


Figure 26: Disease prevalence of CD19-iGP_Smarta mice compared to CD19-iGP control mice.

Thirteen mice that had been sacrificed for impaired general condition were examined for pathologies. Of these 13 mice, 12 mice showed splenomegaly (spleen weight was 2 to 10 times higher than normal) and 10 mice showed a combined hepatosplenomegaly (Figure 27). 11 mice showed a massively enlarged thymus (Figure 27, right picture); seven mice showed additional enlargement of the submandibular, cervical, intrathoracic, intraabdominal and inguinal lymph nodes.

Six mice showed massively enlarged kidneys (2 to 10 times the normal weight, Figure 27, left picture). Two mice showed a reduced body weight and one mouse showed a paresis of the hind legs for which no macroscopic cause could be found. No macroscopic changes could be seen in the lungs.

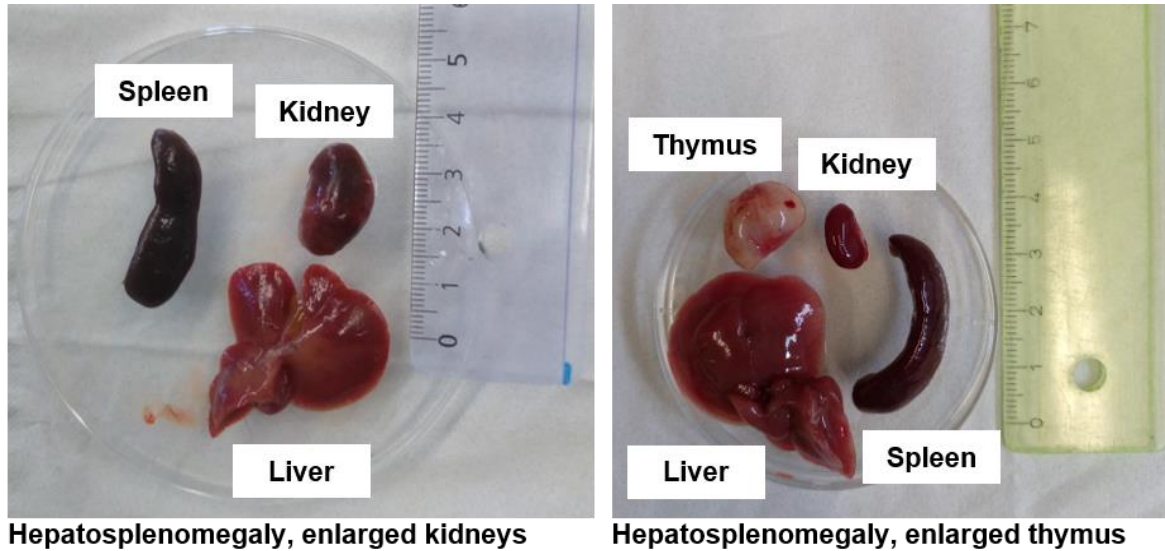
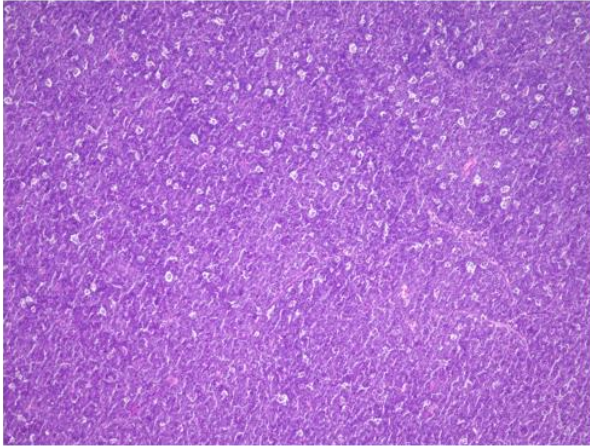


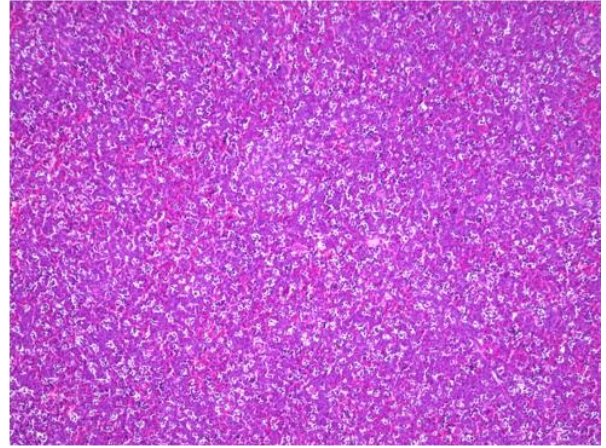
Figure 27: Photos of organs from CD19-iGP_Smarta mice displaying severe disease symptoms. (Left) Enlarged spleen, liver and kidney. (Right) Enlarged liver, thymus, normal sized kidney and enlarged spleen.

Based on these findings indicating systemic inflammation, histological analysis was concentrated on spleen, liver, thymus, kidney and lung of the diseased mice. H&E staining was performed on spleen, liver, thymus and lung tissue revealing extensive inflammation in all organs (Figure 28). Spleen and thymus were marked by unstructured, diffuse lymphocyte infiltration (Figure 28, top). In the liver, periportal inflammation as well as interface hepatitis could be seen, but in the most cases the inflammation was less severe than in the diseased Alb-iGP_Smarta mice, which express the autoantigen in hepatocytes instead of B cells (Figure 28, middle on the left, for comparison see Figure 5). In the lung, large partially confluent infiltrates, and also clearly delimited ELT were detected (Figure 28, bottom). A PAS staining of the kidney revealed extensive lymphatic infiltration into the renal parenchyma, mainly in the interstitial tissue (Figure 28, middle on the right). The glomeruli showed increased numbers of cells compared to healthy eight-week-old CD19-iGP_Smarta mice (data not shown).

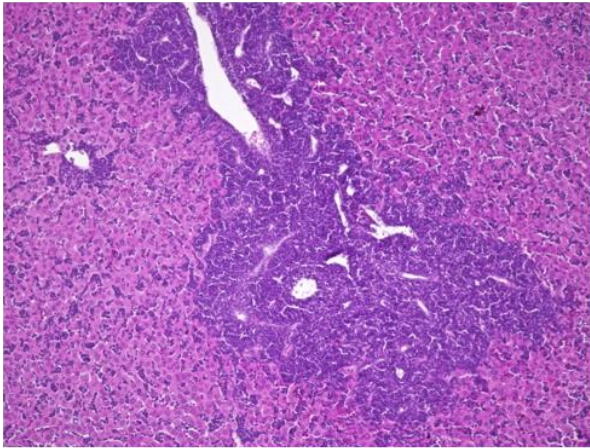
Thymus



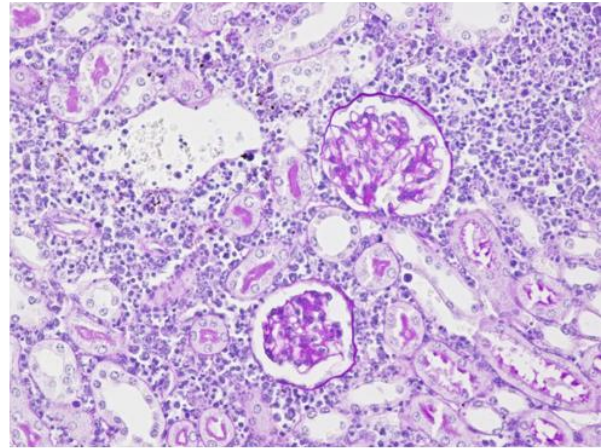
Spleen



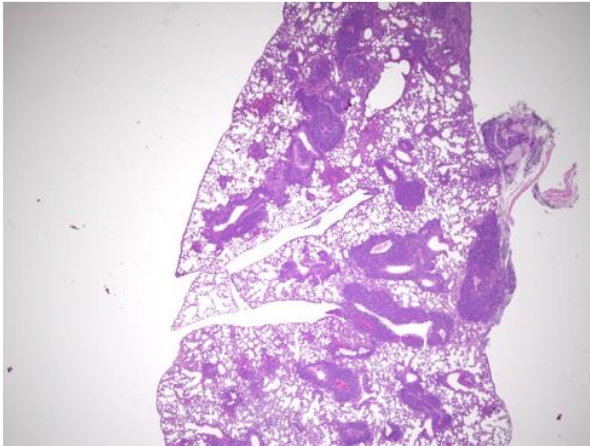
Liver



Kidney



Lung



Lung

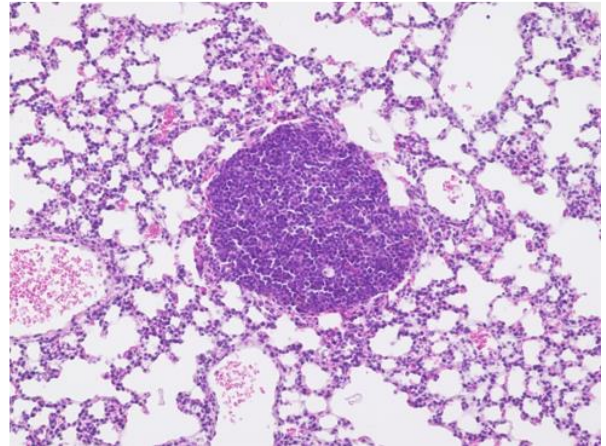


Figure 28: Histology of tissue from CD19-iGP_Smarta mice older than 20 weeks showing severe disease symptoms. (Up, from left to right) H&E staining of the thymus and spleen. 100 fold magnification. (Middle, from left to right) H&E staining of the liver. 100 fold magnification. PAS staining of the kidney. 400 fold magnification. (Down, from left to right) H&E staining of the lung. 20 and 200 fold magnification.

In conclusion, with age, CD19-iGP_Smarta mice developed a systemic autoimmune disease with extensive lymphoproliferation in lymphoid and non-lymphoid organs.

4.2.2.2 Increase of T cells with reduced frequency of Tregs in diseased CD19-iGP_Smarta mice

In order to understand the cellular mechanisms of the observed immunopathology, Smarta T cells and Tregs of diseased CD19-iGP_Smarta mice were analysed by flow cytometry.

4.2.2.2.1 Increase of T cells in diseased CD19-iGP_Smarta mice

Quantification of the overall splenocyte number as well as T cell number in spleen and liver revealed, that the splenocyte number in diseased CD19-iGP_Smarta mice was significantly increased compared to healthy CD19-iGP_Smarta mice (510.42×10^6 vs 63.9×10^6 , $p < 0.05$, Figure 29). This is in accordance with the splenomegaly in these animals. Also the number of T cells in the spleen of diseased CD19-iGP_Smarta mice (164.24×10^6 , $p < 0.05$) was significantly increased compared to healthy CD19-iGP_Smarta mice (13.45×10^6), Smarta mice (19.05×10^6), or CD19-iGP mice (16.03×10^6) (Figure 29). Likewise, the number of T cells in the liver of diseased CD19-iGP_Smarta mice (27.37×10^6 , $p < 0.05$) was significantly increased compared to healthy CD19-iGP_Smarta mice (1.67×10^6), Smarta mice (1.50×10^6) or CD19-iGP mice (0.28×10^6) (Figure 29). These findings indicated a strong proliferation of T cells associated with disease. In addition, the proportion of T cells among CD45⁺ cells was increased in the diseased animals (70.8 % vs 39.47 %, 45.13 % and 54.13 %, ns, Figure 29), however, due to the high standard deviation more mice should be analysed in order to confirm this result. Nonetheless, this finding suggested that also other cell populations seemed to proliferate upon disease manifestation.

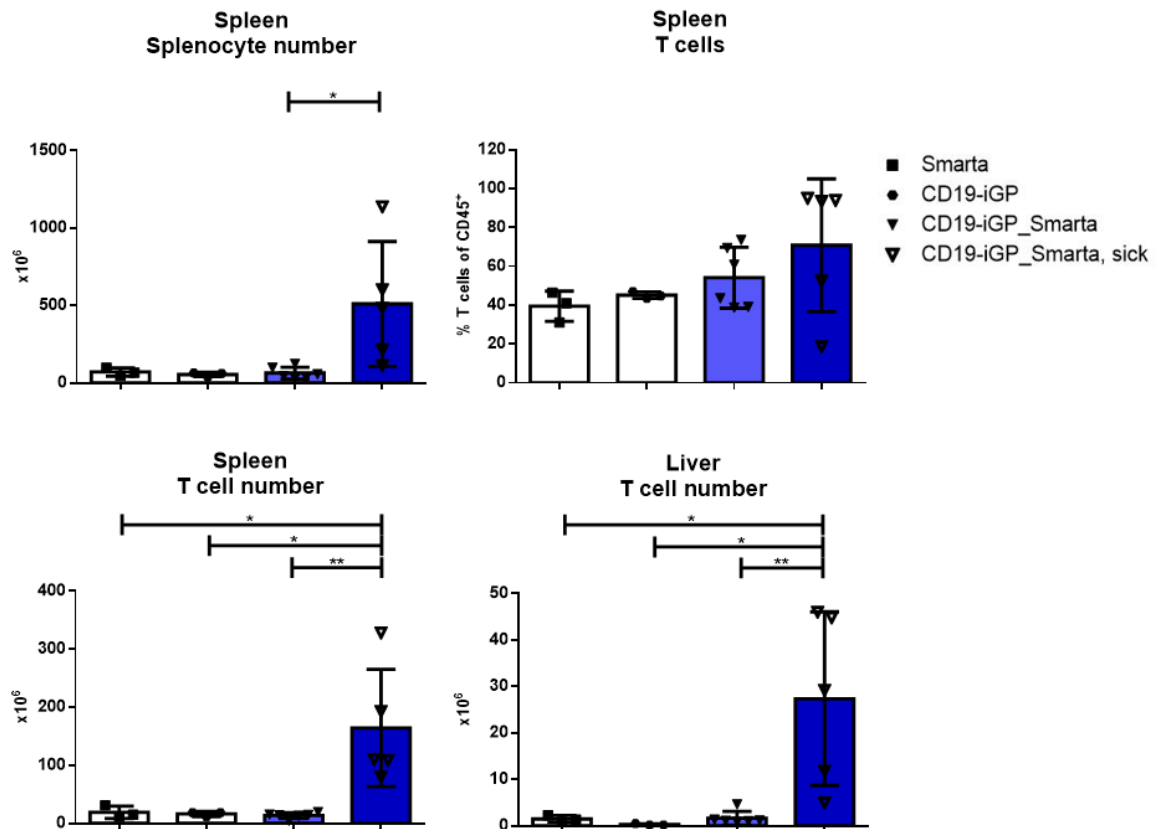


Figure 29: Splenocyte numbers, percentages as well as absolute numbers of T cells in the spleen and absolute numbers of T cells in the liver of 20-week-old control mice (Smarta, CD19-iGP) and CD19-iGP_Smarta mice as well as CD19-iGP_Smarta mice older than 20 weeks with clinical manifestation of disease.

Comparison of the Smarta T cell percentages of the CD4⁺ T cells in the spleen, liver, lung and kidney, however, showed a surprisingly low frequency of tetramer-binding Smarta T cells in diseased CD19-iGP_Smarta mice in spleen (14.64 % vs 82.93 %, $p < 0.0001$ %), liver (18.63 % vs 76.6 %, $p < 0.001$) and lung (15.7 % vs 73.73 %, $p < 0.0001$), as compared to Smarta control mice (Figure 30 A). This seemed to be inconsistent with the notion that disease development was associated with proliferation of Smarta T cells. However, tetramer staining of recently activated T cells is problematic, as T cell activation leads to alterations in cellular TCR distribution and diminishes cellular capacity to bind cognate tetramers (Drake et al., 2005). Thus, the seeming reduction of Smarta T cells in diseased mice was probably not due to their absence, but rather to their difficult detectability. The decreased tetramer staining capacity is illustrated in Figure 30, showing 20-week-old CD19-iGP_Smarta mice.

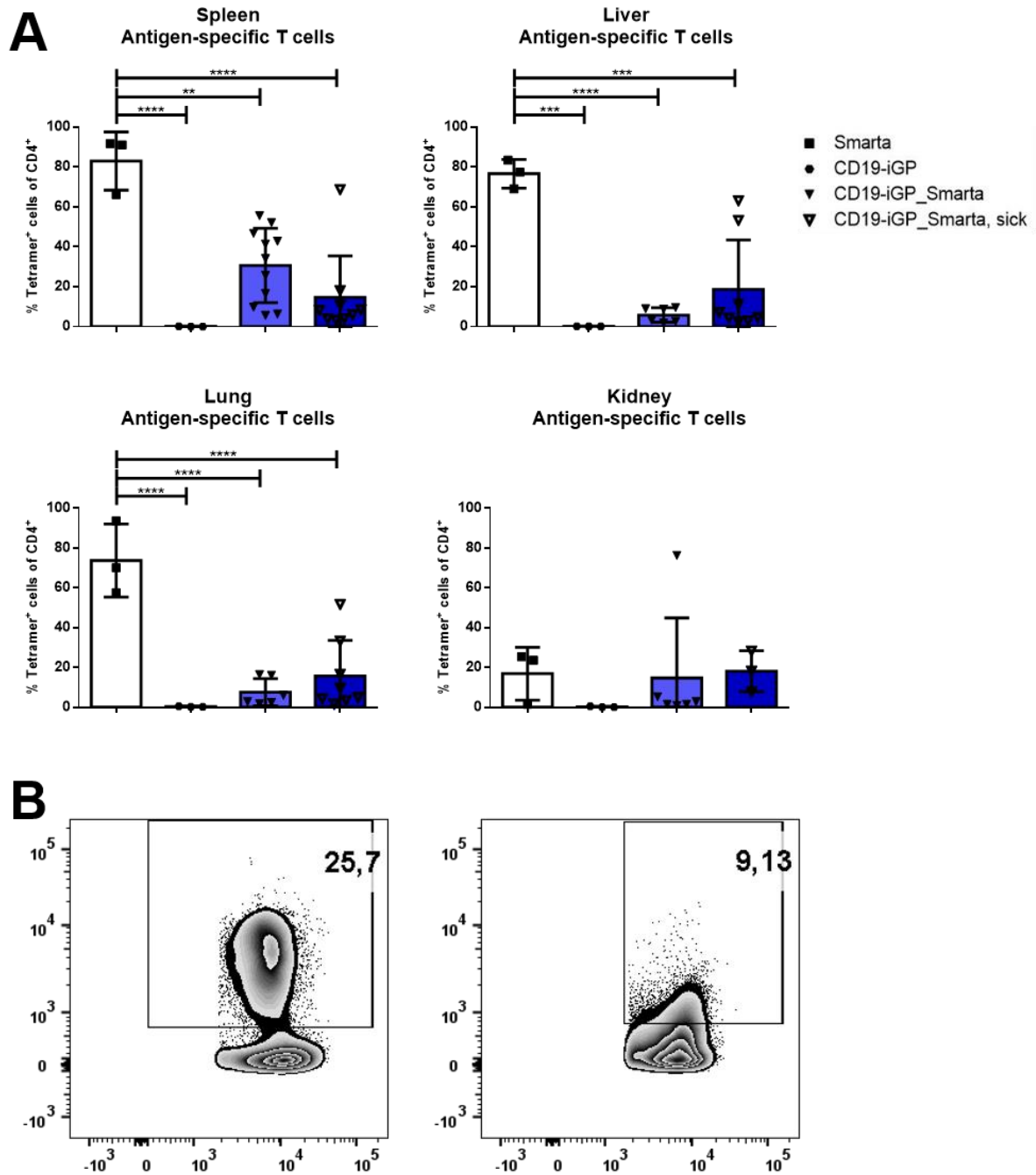


Figure 30: (A) Percentages of antigen-specific Smarta T cells (tetramer⁺) in spleen, liver, lung and kidney of 20-week-old control mice (Smarta, CD19-iGP) and CD19-iGP_Smarta as well as CD19-iGP_Smarta mice older than 20 weeks with clinical manifestation of disease.

(B) Representative flow cytometry plots showing antigen-specific Smarta T cells (tetramer⁺) of CD4 T cells in the spleen of 20-week-old CD19-iGP_Smarta mice and CD19-iGP_Smarta mice older than 20 weeks with clinical manifestation of disease.

4.2.2.2.2 Reduction of Tregs in diseased CD19-iGP_Smarta mice

The examination of the overall Treg population in spleen, liver, lung and kidney revealed that the frequency of Tregs in diseased CD19-iGP_Smarta mice was reduced compared to healthy 20-week-old mice of this line (1.08 % vs 7.71 % in the spleen, $p < 0.01$; 0.93 % vs 3.45 % in the liver, $p < 0.05$; 0.83 % vs 2.86 % in the lung, $p < 0.05$; and 0.56 % vs 4.95 % in the kidney, ns, Figure 31, top). The Treg frequencies of 8-week-old mice of this line was similar to healthy 20-week-old mice in spleen, liver and lung (see Figure 10 and Figure 22), indicating that the Treg reduction was disease-related. This decrease in the overall Treg pool might thus be a major cause for disease development in CD19-iGP_Smarta mice. Regarding the frequency of antigen-specific Tregs, we could not find significant differences between diseased and healthy CD19-iGP_Smarta mice in all analysed organs (Figure 31, bottom). However, due to the above described tetramer staining problems (see 4.2.2.2.1.), this finding should be interpreted with caution.

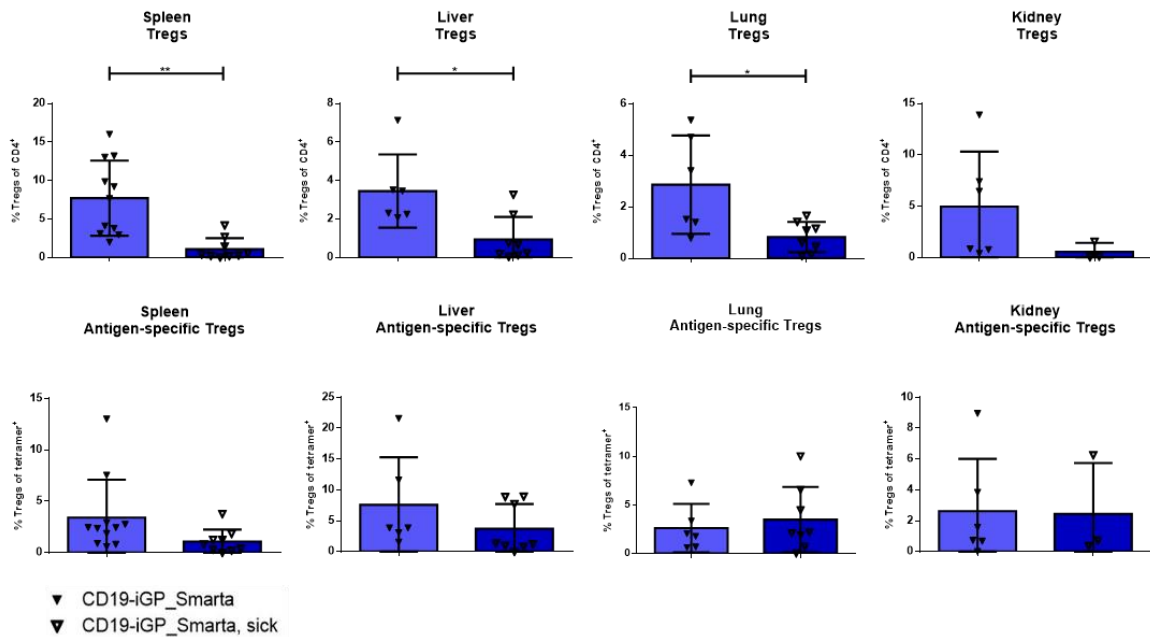


Figure 31: Percentages of Tregs and antigen-specific Tregs (tetramer⁺) in the spleen, liver, lung and kidney of 20-week-old CD19-iGP_Smarta mice as well as CD19-iGP_Smarta mice older than 20 weeks with clinical manifestation of disease.

4.2.2.3 Reduction of the overall B cell frequency but increase of the Plasma cell frequency in diseased CD19-iGP_Smarta mice

The B cell population of the diseased CD19-iGP_Smarta mice was examined with the flow cytometry panel introduced in section 4.1.2.1, extended by markers discriminating effector and memory B cells, germinal centre B cells and plasma cells, in accordance with Zhang et al., 2017.

4.2.2.3.1 Age-related reduction of B cells in CD19-iGP_Smarta mice

The frequency of CD19⁺ B220⁺ B cells in 20-week-old CD19-iGP_Smarta mice was reduced compared to 20-week-old Smarta or CD19-iGP control mice in spleen (8.87 % vs 20.53 % and 25.18 %, $p < 0.01$), liver (3.43 % vs 19.43 % and 27.48 %, $p < 0.0001$), lung (2.32 % vs 27 % and 26.55 %, $p < 0.001$) and kidney (0.42 % vs 17.87 % and 10.98 %, $p < 0.05$), (Figure 32). The B cell frequency of 20-week-old CD19-iGP_Smarta mice was also reduced compared to the frequency in 8-week-old mice of the same line in the spleen, liver and lung (8.87 % vs 16.74 % in the spleen, 3.43 % vs 6.4 % in the liver 2.32 % vs 4.06 % in the lung, Figure 32, Figure 12 and Figure 23). Quantification of the absolute B cell numbers in the spleens confirmed that diseased CD19-iGP_Smarta mice had not merely a reduced B cell proportion of all CD45⁺ cells, but truly a significantly reduced B cell number (1.21×10^6 in diseased mice vs 7.59×10^6 in Smarta mice and 4.46×10^6 in CD19-iGP mice, $p < 0.01$, Figure 32).

Taken together, these results showed a generally reduced frequency of B cells in CD19-iGP_Smarta mice compared to the control lines, as well as an age-dependent decline of B cells in the CD19-iGP_Smarta mice, which was most pronounced in disease.

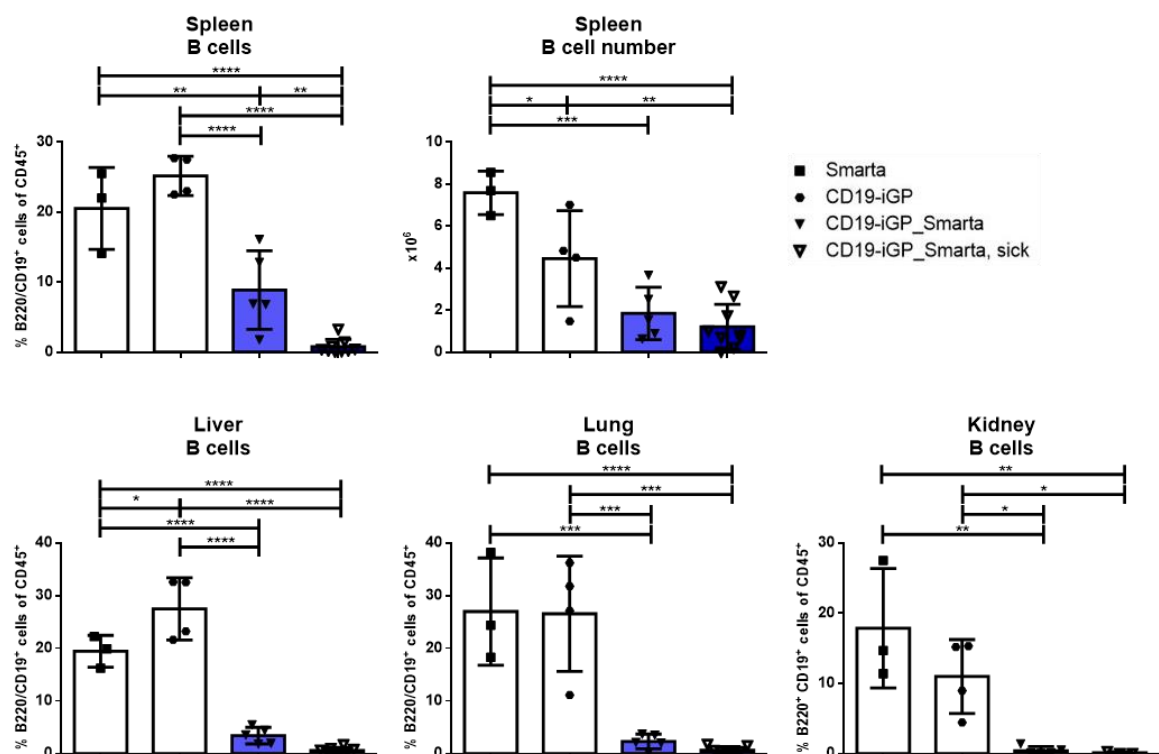


Figure 32: Percentages and absolute numbers of B cells in the spleen and percentages of B cells in the liver, lung and kidney of 20-week-old control mice (Smarta, CD19-iGP) and CD19-iGP_Smarta mice as well as CD19-iGP_Smarta mice older than 20 weeks with clinical manifestation of disease.

4.2.2.3.2 Higher frequency of Plasma cells in diseased CD19-iGP_Smarta mice

To gain a better understanding of the composition of the B cell population, the B cell subpopulations of diseased CD19-iGP_Smarta mice were analysed.

To analyse effector and memory B cells, CD45⁺ CD19⁺ B220⁺ cells were gated on CD38 and IgG. To properly set the gate, CD38 and IgG were also gated on all CD45⁺ cells, which show a clear separation between double negative and double positive populations (Figure 33, right plot).

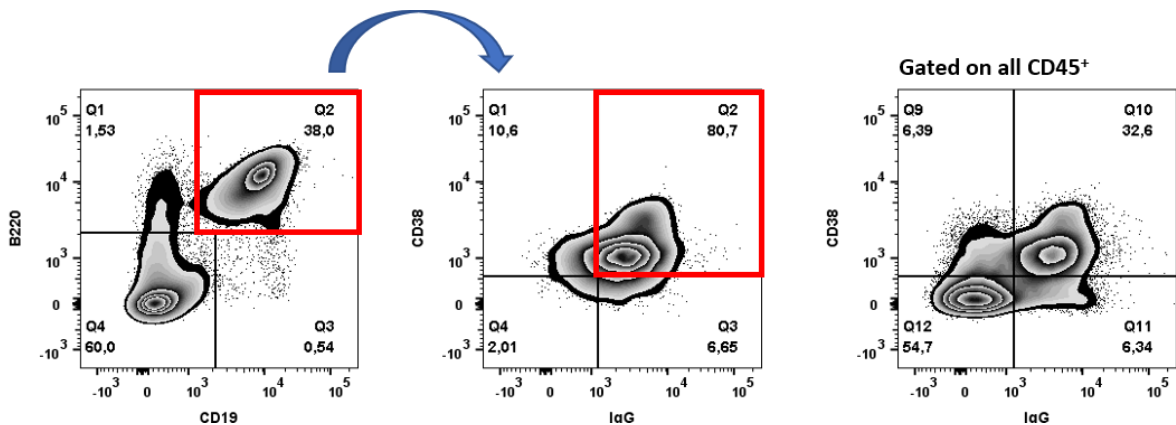


Figure 33: Gating strategy of the flow cytometry B cell panel for CD19⁺ B220⁺ IgG⁺ CD38⁺ effector and memory B cells isolated from the spleen.

The percentages of CD38⁺ IgG⁺ effector/memory B cells among all CD19⁺ B220⁺ B cells in spleen, liver, lung or kidney were similar in diseased or healthy CD19-iGP_Smarta mice, or Smarta and CD19-iGP control mice (Figure 34). Only in the kidneys of diseased mice, a reduced frequency of effector/memory B cells could be seen (39.97 % vs 89.17 % in Smarta mice, 77 % in CD19-iGP mice and 75 % in healthy CD19-iGP_Smarta mice, $p < 0.05$ and ns, Figure 34).

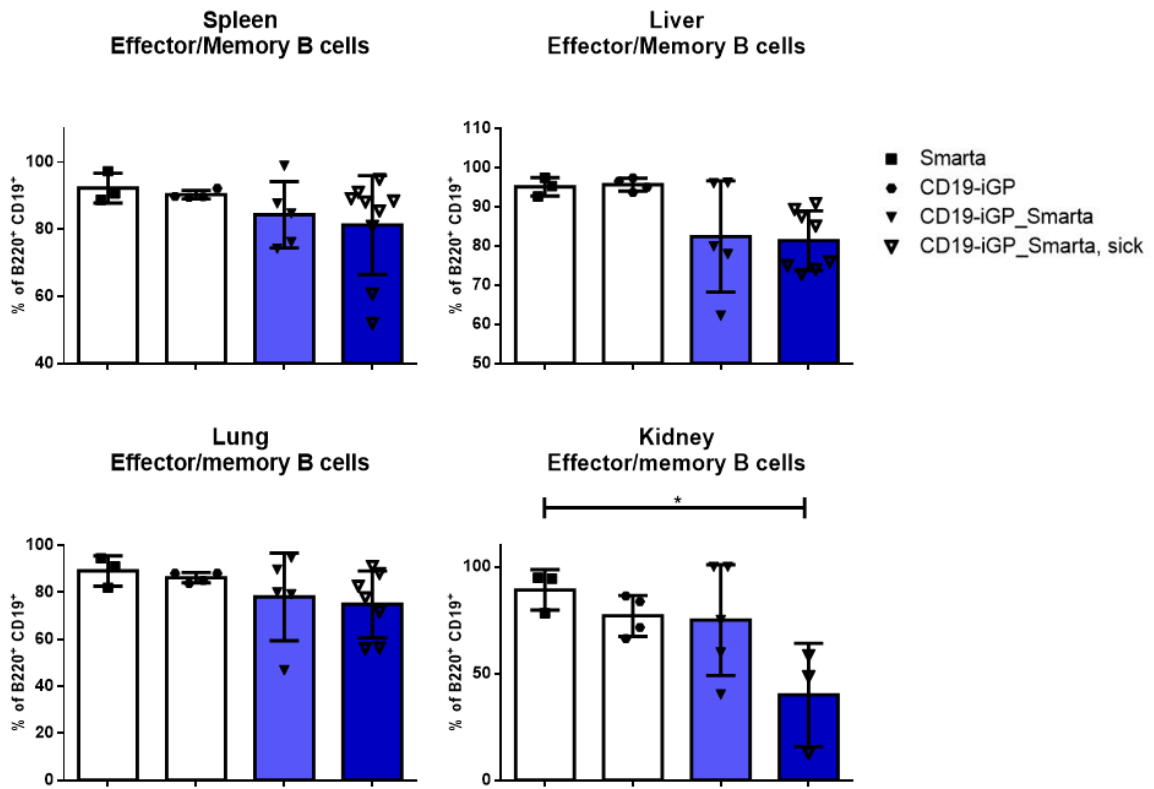


Figure 34: Percentages of effector and memory B cells in the spleen, liver, lung and kidney of 20-week-old control mice (Smarta, CD19-iGP) and CD19-iGP_Smarta as well as CD19-iGP_Smarta mice older than 20 weeks with clinical manifestation of disease.

To analyse the germinal centre B cells, CD45⁺ B220⁺ cells were gated on Fas (CD95) and Gl-7 (Figure 35).

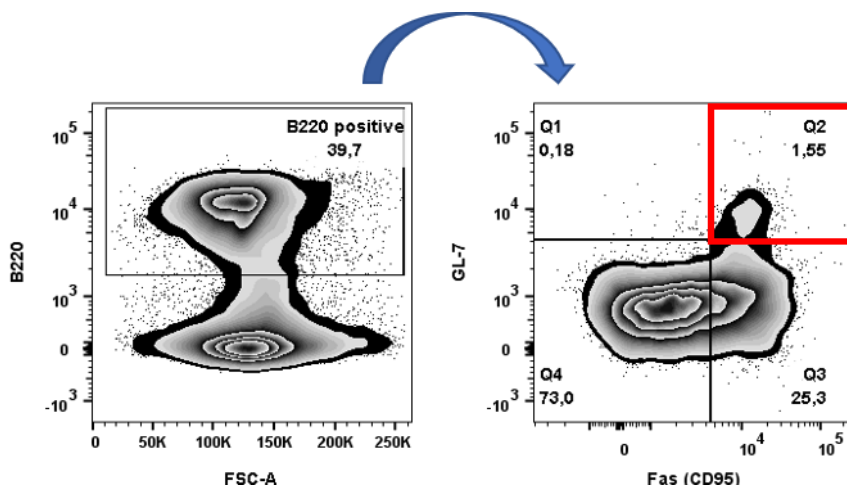


Figure 35: Gating strategy of the flow cytometry B cell panel for B220⁺ Fas (CD95)⁺ Gl-7⁺ germinal centre B cells isolated from the spleen.

The frequency of CD95⁺ Gl-7⁺ germinal centre B cells among B220⁺ cells was non-significantly higher in healthy CD19-iGP_Smarta mice compared to the CD19-iGP controls in spleen and liver (0.04 % vs 0.24 % respectively 3.97 % vs 0.83 %, ns, Figure 36). Also diseased CD19-iGP_Smarta mice had non-significantly higher germinal centre B cell frequencies compared to Smarta mice, CD19-iGP mice and healthy CD19-iGP_Smarta mice in lung and kidney (1.93 % vs 0.33 %, 0.06 % and 0.76 % respectively 1.75 % vs 0.58 %, 0.42 % and 0.71 %, ns, Figure 36). Analysis of larger sample numbers will be necessary to verify these tendencies. Elevated germinal centre B cell numbers could indicate the formation of secondary lymphoid follicles and germinal centres in the spleen as well as in non-lymphoid organs.

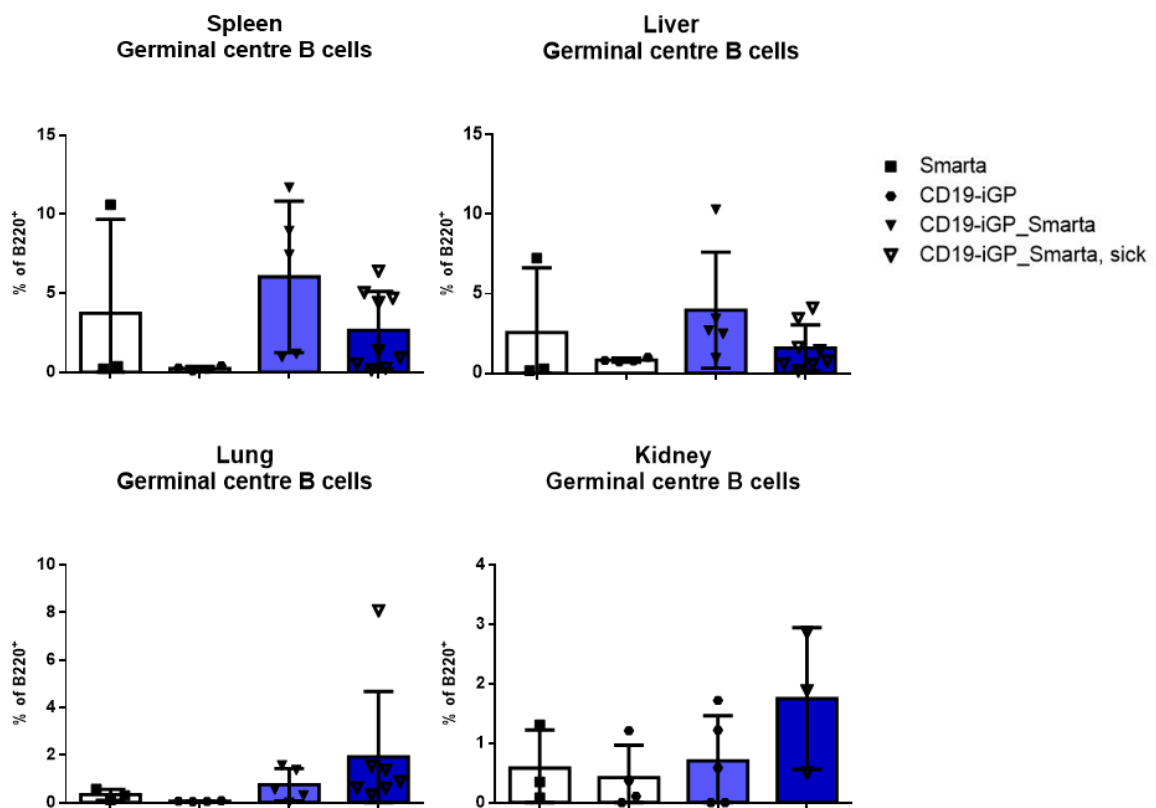


Figure 36: Percentages of germinal centre B cells in the spleen, liver, lung and kidney of 20-week-old control mice (Smarta, CD19-iGP) and CD19-iGP_Smarta mice as well as CD19-iGP_Smarta mice older than 20 weeks with clinical manifestation of disease.

To analyse the plasma cell population, CD45⁺ CD19⁺ cells were gated on CD138 positivity (Figure 37).

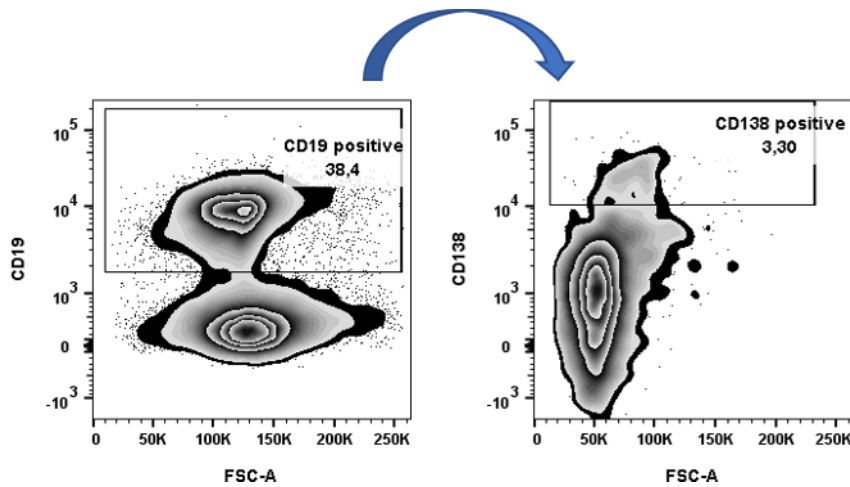


Figure 37: Gating strategy of the flow cytometry B cell panel for CD19⁺ CD138⁺ plasma cells isolated from the spleen.

The diseased CD19-iGP_Smarta mice showed a tendency towards higher CD138⁺ plasma cell frequencies within the CD19⁺ cell population in the spleen, liver and lung, as compared to the Smarta and CD19-iGP control lines (3.94 % vs 0.6 % and 0.86 % in the spleen, 1.12 % vs 0.3 % and 0.14 % in the liver and 1.65 % vs 0.16 % and 0.46 % in the lung, ns, Figure 38). Moreover, diseased CD19-iGP_Smarta mice seemed to have non-significantly more plasma cells than healthy CD19-iGP_Smarta mice in spleen and lung (3.94 % vs 1.32 % in the spleen and 1.65 % vs 0.78 % in the lung, ns, Figure 38). This might indicate a disease-associated elevation of the plasma cell frequency, but this needs to be confirmed with more mice. In the kidney, the plasma cell frequency of the CD19-iGP control line was considerably higher than that of all the other groups here (14.35 %, $p < 0.01$, Figure 38). This result lacks explanation, therefore, the experiment should be repeated in order to exclude a faulty measurement.

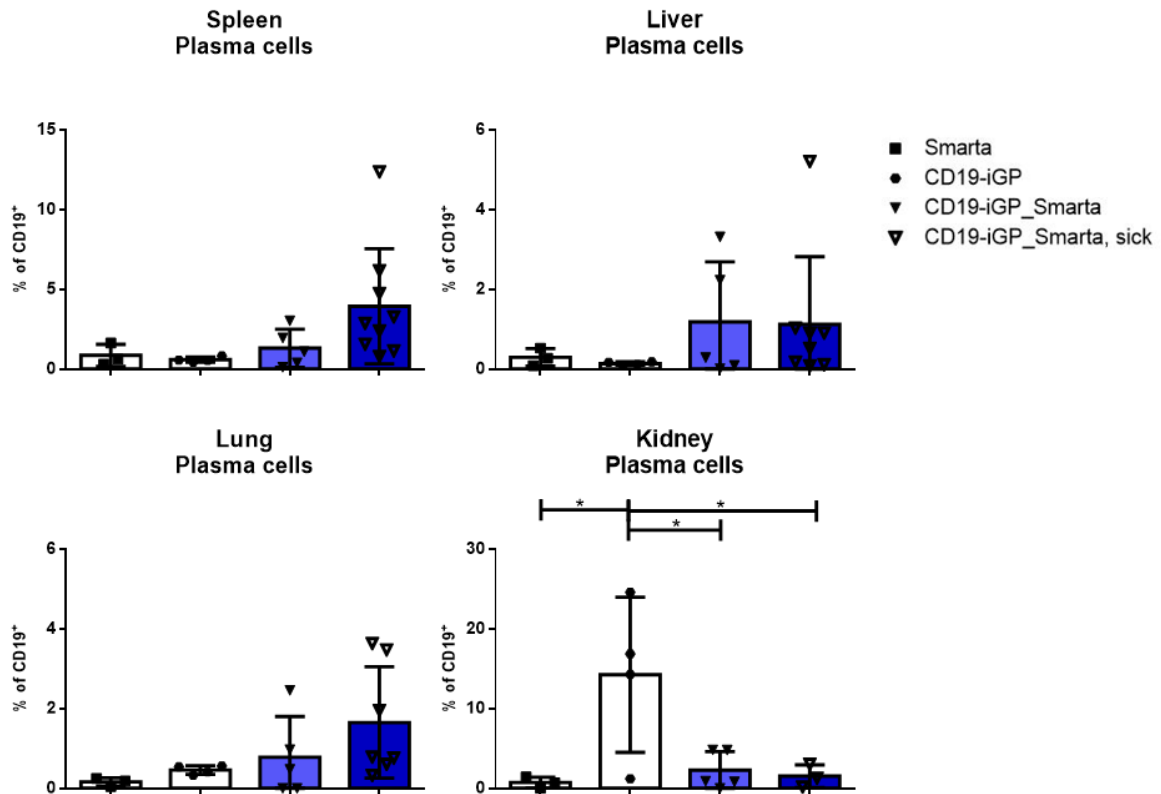


Figure 38: Percentages of plasma cells in the spleen, liver, lung and kidney of 20-week-old control mice (Smarta, CD19-iGP) and CD19-iGP_Smarta mice as well as CD19-iGP_Smarta mice older than 20 weeks with clinical manifestation of disease.

4.2.2.3.3 B cell activation marker expression is elevated in diseased CD19-iGP_Smarta mice

Finally, the activation status of the CD19⁺ B220⁺ B cells was analysed through the flow cytometric staining of the activation marker CD69 as well as MHC-II. The classical activation marker CD69 is temporally expressed by several activated cell populations, while MHC-II is also expressed by non-activated B cells, but the expression is increased upon activation. Through measuring the mean fluorescence intensity (MFI) of these markers it should be examined whether the diseased CD19-iGP_Smarta mice showed a higher B cell activation level compared to the controls.

As shown in Figure 39, the expression of MHC-II by CD19⁺ B220⁺ B cells in spleen and liver of diseased CD19-iGP_Smarta mice was significantly elevated compared to the CD19-iGP control (31988 vs 5489 respectively 23541 vs 4092, $p < 0.05$) and also elevated compared to the Smarta control (31988 vs 13650 respectively 23541 vs 10570, ns). Correspondingly, the expression of CD69 in diseased animals was higher in spleen and liver compared to the control lines (1062 vs 551 and 560, $p < 0.01$, respectively 934 vs 411 and 297, ns, Figure 39). These findings demonstrated that the B cell activation level in diseased CD19-iGP_Smarta mice was higher than in the healthy control lines. In addition, MHC-II and CD69 expression in 20-week-old CD19-iGP_Smarta mice were higher compared to the controls (19774 vs 13650 and 5489 in case of MHC-II and 758 vs 551 and 560 in case of CD69 in the spleen, respectively 12862 vs 10570 and 4092 in case of MHC-II and 821 vs 411 and 297 in case of CD69 in the liver, ns, Figure 39). This finding indicated that the B cells in 20-week-old CD19-iGP_Smarta mice were activated and participating in autoimmune disease development.

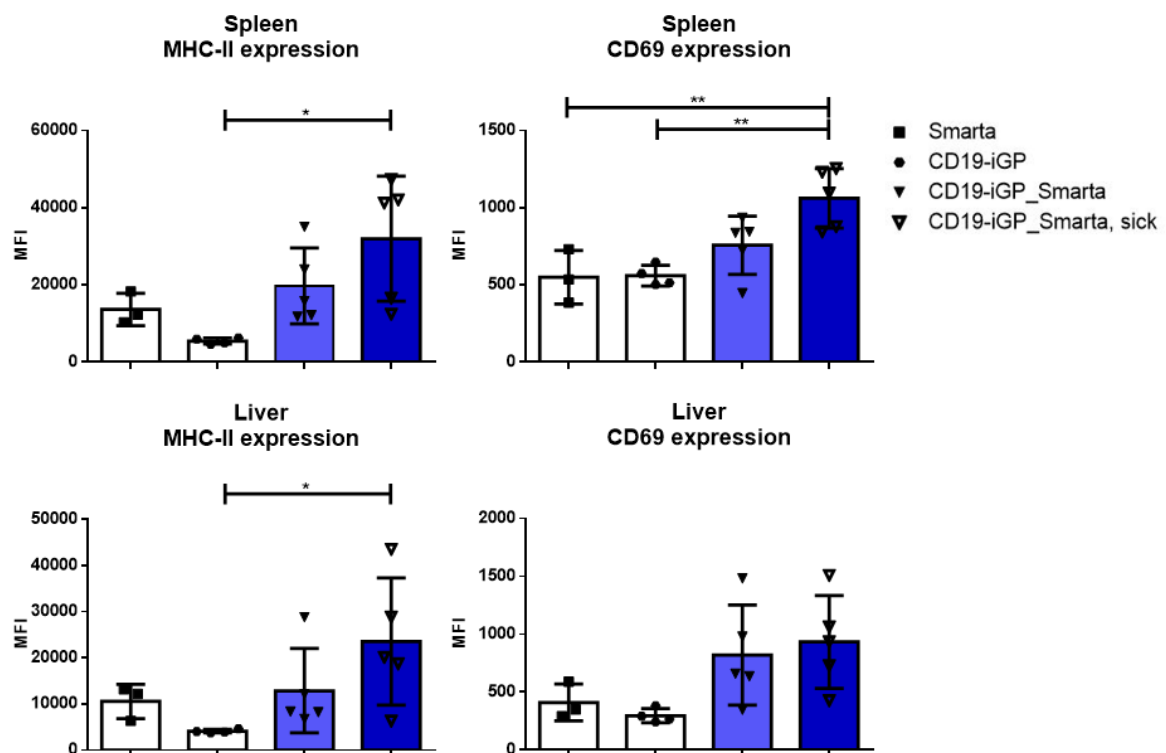


Figure 39: MFI as measure for the expression of the activation markers MHC-II and CD69 on CD19⁺ B220⁺ B cells in spleen and liver of 20-week-old control mice (S Warta, CD19-iGP) and CD19-iGP_Smarta as well as CD19-iGP_Smarta mice older than 20 weeks with clinical manifestation of disease.

4.2.3 Disease development and severity in CD19-iGP_Smarta mice is not sex-dependent

To detect whether there was sexual dimorphism with respect to disease development of CD19-iGP_Smarta mice, eight-week-old male and female mice were analysed for frequencies of antigen-specific Smarta T cells, Tregs and B cells, each in spleen, liver and lung. In none of these organs, significant differences could be found in the examined cell populations (Figure 40). This indicated that, similar to the Alb-/CD19-iGP_Smarta mice, male and female mice were equally susceptible to the development of autoimmune disease.

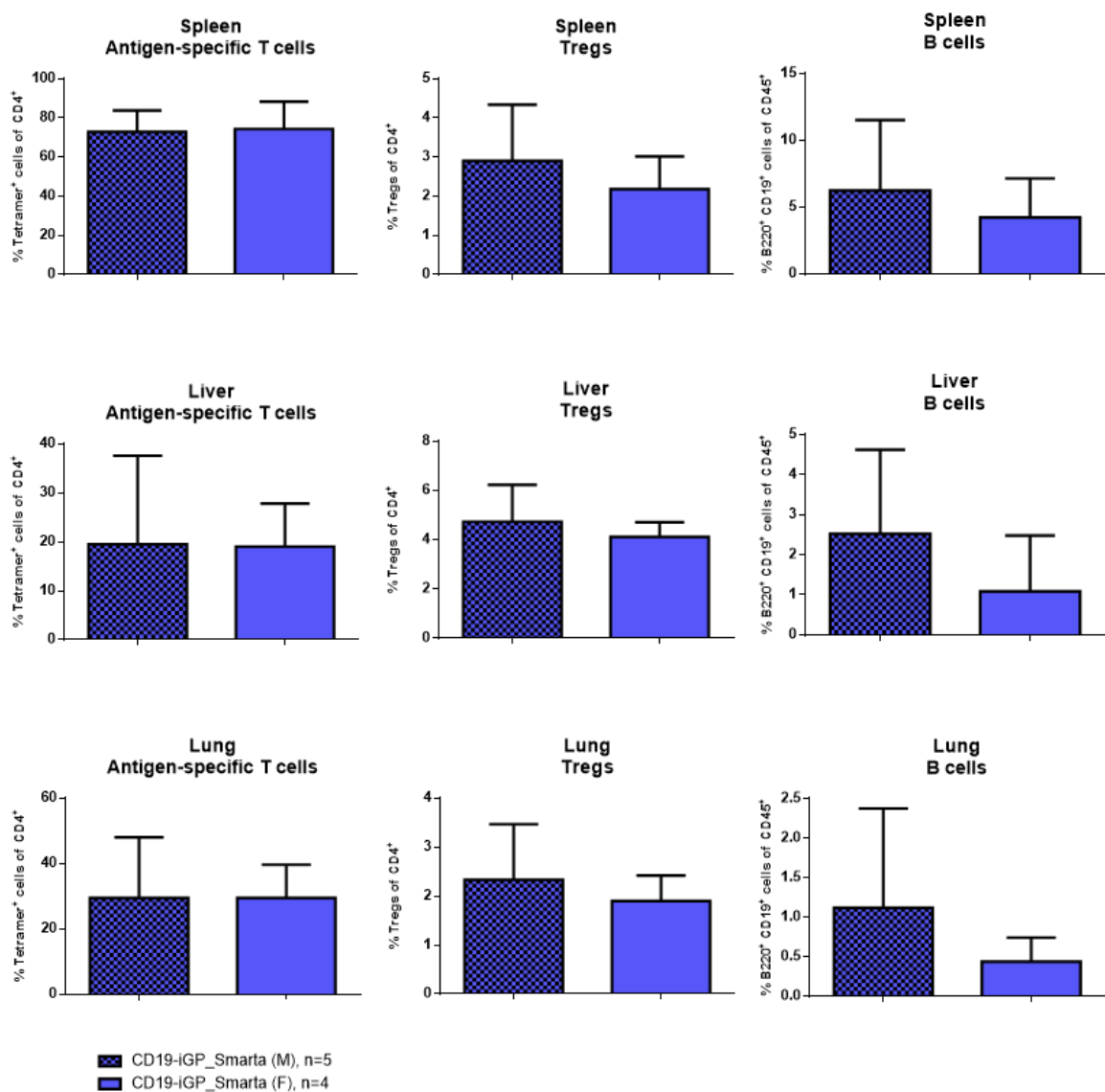


Figure 40: Comparison of flow cytometry data from male vs female CD19-iGP_Smarta mice. Shown are percentages of antigen-specific Smarta T cells (tetramer⁺) and B cells in spleen, liver and lung.

To confirm this notion, the disease prevalence in female and male CD19-iGP_Smarta mice were compared, showing no significant differences between the two groups (Figure 41). Thus, susceptibility of CD19-iGP_Smarta mice for systemic autoimmune disease was not sex-dependent.

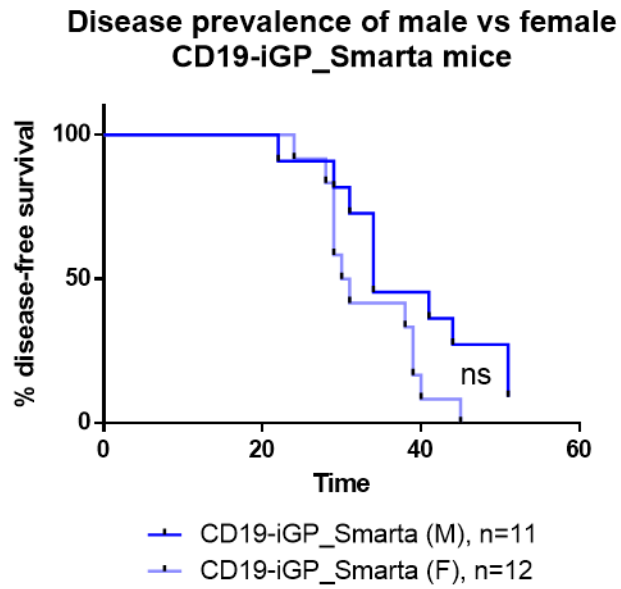


Figure 41: Disease prevalence of male vs female CD19-iGP_Smarta mice.

5 Discussion

The aim of this work was to examine the role of autoantigen-presenting B cells in a mouse model of AIH (Alb-/CD19-iGP_Smarta mice) as well as characterizing the systemic autoimmune disease observed in CD19-iGP_Smarta mice.

5.1 Autoantigen-presenting B cells in experimental AIH

The first observation in the Alb-/CD19-iGP_Smarta as well as the CD19-iGP_Smarta mice was that the antigen-presentation by B cells did not lead to a deletion of the antigen-specific Smarta T cells in the thymus (Figure 9B). However, the frequency of Smarta T cells in the spleen and liver was reduced compared to the Smarta control mice, in which the autoantigen is not present. This may be due to peripheral deletion of T cells, which, however, seemed to affect only a minority of the Smarta T cells. In effect, the majority of peripheral CD4 T cells was composed of GP-specific Smarta T cells (Figure 9). This was in contrast to the results of Frommer et al., who found that the presentation of a MOG-peptide on MHC-II by B cells led to central as well as peripheral tolerance against EAE (see 2.5.1) (Frommer et al., 2008, Frommer and Waisman, 2010). In their B^{MOG}/2D2 mouse model combining MOG-presenting B cells and MOG-specific T cells, which was similar to the CD19-iGP_Smarta mouse model used here, a drastic reduction of CD4 T cells in the thymus and lymph nodes could be seen. They drew the conclusion that this reduction was due to thymic deletion and that B cells play an important role in this tolerance mechanism (Frommer and Waisman, 2010). In our Alb-/CD19-iGP_Smarta and CD19-iGP_Smarta mice, however, the presentation of GP₆₁₋₈₀ by B cells did not affect the frequency of GP-specific T cells in thymus and only led to a partial reduction of these cells in the periphery. These contradictory results may be due to the different peptides used as autoantigens, as MOG is an endogenous protein that is also present in the central nervous system while the GP₆₁₋₈₀ peptide is a foreign antigen. Nevertheless, it poses the question under which circumstances antigen-presentation by B cells might lead to the central or peripheral deletion of antigen-specific T cells, a question that should be investigated more closely in the future.

Even though the Smarta T cells were present in the eight-week-old Alb-/CD19-iGP_Smarta and CD19-iGP_Smarta mice, no disease development could be observed at that age. This finding suggested that the Smarta T cells in these lines were in a state of ignorance, in which they did not react to their cognate antigen and therefore were not deleted (Nossal, 1994). The question then was why the Smarta T cells did not react to the antigen.

Antigen sequestration was unlikely, as both the antigen expressed by hepatocytes in the Alb-/CD19-iGP_Smarta mice as well as the antigen presented by B cells in the Alb-/CD19-iGP_Smarta and CD19-iGP_Smarta mice was accessible for mature Smarta T cells. In fact, a higher frequency of Smarta T cells could be observed in the liver, when the cognate antigen was presented there (i.e. in Alb-iGP_Smarta and Alb-/CD19-iGP_Smarta mice). This leads to the conclusion that the GP antigen was recognized by antigen-specific T cells, resulting in T cell accumulation or proliferation in the liver. Another possible explanation for the absence of pathology in young mice could be that T cell activation occurred in the absence of inflammatory co-stimulation. However, given the high frequency of Smarta T cells it was conceivable that at least some Smarta T cells were activated accidentally in the presence of inflammatory signals, leading to an autoaggressive response. Such activation seemed to occur in ELT, which had formed in eight week old mice (Figure 14), but at that age still remained subclinical. With increasing age, the likelihood for autoaggressive T cell activation, and the probability to develop autoimmune disease also increased. It will be of interest to further examine which environmental factors might expedite the pathogenic activation of Smarta T cells and the resulting clinical disease.

Analysis of the Treg population revealed that the Alb-/CD19-iGP_Smarta mice as well as the CD19-iGP_Smarta mice had a higher Treg frequency in the periphery than in the thymus (Figure 10). In the literature, the normal Treg frequency in wildtype mice is given with 5 % in the thymus and 10 - 15 % in the periphery (Fontenot et al., 2005, Sakaguchi et al., 2008). Compared to these numbers, the frequency of Tregs in the Alb-/CD19-iGP_Smarta and CD19-iGP_Smarta mice was reduced (0.14 % and 0.12 % in the thymus, 5.43 % and 5.3 % in the liver, Figure 10). However, the difference in the thymus was markedly higher than in the liver. The higher Treg frequencies in the periphery might have been due to the peripheral induction of Tregs. This induction usually takes place when a T cell recognizes its specific antigen in a non-inflammatory environment (Sakaguchi et al., 2008). This was likely to take place in young Alb-/CD19-iGP_Smarta and CD19-iGP_Smarta mice, which did not exhibit overt inflammation. A higher frequency in the periphery compared to the thymus could also be found in the antigen-specific Tregs (Figure 10 C), however it was not becoming clear whether this increase was proportional to the overall Treg population. Be that as it may, the Treg presence in the liver might be one explanation for the ability of the mice to hold the autoreactive T cells in check for at least several weeks without overt AIH.

Antigen-presentation by B cells did not alter the B cell frequency in the Alb-/CD19-iGP_Smarta mice, indicating that no augmented proliferation or deletion of B cells was taking place. In the CD19-iGP_Smarta mice, however, the B cell frequency was reduced, which will be discussed in 5.2.

The autoantibody pattern found in the serum of Alb-/CD19-iGP_Smarta and CD19-iGP_Smarta mice was diverse, ranging from antinuclear to anti-cytoplasmic autoantibodies. This was in contrast to the clear antinuclear autoantibody-pattern in Alb-iGP_Smarta mice. Nonetheless, this was not surprising, as all B cells in the Alb-/CD19-iGP_Smarta and CD19-iGP_Smarta mice present the GP₆₁₋₈₀ on MHC-II independent of their BCR-specificity. Therefore, TCR-MHC-II-interaction has led to the activation and antibody-production of B cells independent of their BCR-specificity.

In Alb-/CD19-iGP_Smarta and Alb-iGP_Smarta mice, development of ELT in the liver could be observed. Thus, hepatic ELTs seemed to be associated with expression of the autoantigen in hepatocytes. The presence of these structures might drive the development of autoimmune disease in the older Alb-iGP_Smarta mice (Preti, 2019). The occurrence of these structures also in the Alb-/CD19-iGP_Smarta mice was a strong indicator that these mice develop autoimmune liver disease as well. That some mice of this line showed larger ELTs than those found in the Alb-iGP_Smarta mice with eight weeks of age might indicate a faster disease progression, due to additional antigen-presentation by B cells. However, the normal levels of transaminases observed in the eight-week-old Alb-/CD19-iGP_Smarta mice show that no liver damage had taken place so far. Therefore, the aggravation of the liver disease through antigen-presentation by B cells can only be assessed by long-term monitoring of Alb-/CD19-iGP_Smarta mice for disease development.

A comparison of the T cell, Treg and B cell frequencies of male and female Alb-/CD19-iGP_Smarta mice showed no sex-related differences. It remains to be seen whether this observation might indicate equal affection of both sexes with respect to development of AIH in older mice. Human AIH, like many other autoimmune diseases, affects women more frequently than men (Moritoki et al., 2006, Manns et al., 2015). Thus far, it is unclear why the Alb-iGP_Smarta model (Preti, 2019), like several other mouse models of AIH (Jaeckel et al., 2011, Christen and Hintermann, 2015) do not reflect the female predominance seen in human AIH.

In conclusion, antigen-presentation by B cells in the Alb-/CD19-iGP_Smarta mice did not induce complete deletional tolerance to the GP₆₁₋₈₀ peptide. However, an aggravation or acceleration of AIH development could not be observed in this model yet. Whether B cells, in general, play a disease-aggravating or pro-tolerogenic role in AIH is controversially discussed without a clear answer being found so far. In a mouse model of type 2 AIH induced by xenoinmunization to human liver antigens, it could be shown that B cells were disease-driving as they secreted more proinflammatory and less anti-inflammatory cytokines (Beland et al., 2015).

Treatment with anti-CD20-antibody at the peak of disease severity led to a significant reduction of liver inflammation, and treatment before disease manifestation even prevented AIH-development. Treatment efficacy was explained by abrogation of the communication between B cells and T_{eff} cells without affecting the Treg or other regulatory populations (Beland et al., 2015). In addition, some studies described a successful anti-CD20-therapy with Rituximab in patients with AIH refractory to conventional therapy (Burak et al., 2013, D'Agostino et al., 2013, Al-Busafi et al., 2013). These results clearly suggest a disease-driving role of B cells in AIH. However, in a study of murine experimental AIH (EAH) induced by immunisation to liver extract, B cell deficient or B cell depleted mice developed a more severe disease than B cell replete mice. This finding was explained by the regulatory functions of CD11b⁺ B cells secreting IL-10, suggesting a pro-tolerogenic role of B cells in AIH (Liu et al., 2015).

At the current stage of investigation, the role of B cells in the model studied here could not be definitely settled. Our preliminary results rather indicate that antigen-presentation by B cells did not seem to affect AIH development at all, neither accelerating nor retarding it. Nonetheless, it should be noted that this does not indicate that B cells do not play a role in the pathogenesis of AIH, as B cells can have diverse functions beyond autoantigen presentation. However, the antigen-presenting function of B cells did not seem to be a key mechanism involved in the pathogenesis of AIH.

In the future, the disease development in Alb-/CD19-iGP_Smarta mice will have to be monitored and compared to the Alb-iGP_Smarta mice to clarify whether the presentation of autoantigens by B cells is really not affecting the severity of AIH. This could be done by assessing the disease prevalence over time, the grade of liver inflammation and liver damage in sick mice, as well as the grade of affection of other organs like spleen, lung and kidney. Moreover, the T and B cell populations of 20-week-old and sick mice will have to be analysed, including Tregs and the B cell subpopulations of germinal centre B cells, effector and memory B cells as well as plasma cells. In addition, a cytokine analysis for the characteristic cytokines of different T helper cell subtypes as well as B cell subtypes will have to be performed in diseased and control mice. Thus, the type of immune response and the potential involvement of certain B cell subpopulations in disease development may be determined.

To examine the functions of B cells in the onset and perpetuation of AIH more closely, it will be useful to perform in-vitro-stimulation-assays with B and T cells of Alb-/CD19-iGP_Smarta, Alb-iGP_Smarta and control mice with measurement of autoantibody and cytokine secretion.

In addition, B cell transfer experiments from CD19-iGP, CD19-iGP_Smarta and wildtype mice to Alb-iGP_Smarta mice should be performed, indicating whether the transfer of autoantigen-presenting B cells has any effect on disease development. Finally, to address the question whether B cells in our mouse model have a role beyond the presentation of the GP₆₁₋₈₀ peptide, B-cell-depletion will have to be performed in Alb-/CD19-iGP_Smarta and Alb-iGP_Smarta mice. The effect of this depletion might definitely clarify whether B cells play a disease-driving or tolerance-inducing role in the Alb-iGP_Smarta mouse model of AIH.

5.2 Systemic autoimmune disease induction by autoantigen-presenting B cells

The CD19-iGP_Smarta mice expressing the GP₆₁₋₈₀ antigen in B cells and possessing antigen-specific Smarta T cells developed a systemic autoimmune disease that was characterized in this study. Therefore, young mice of this line were analysed to identify the preconditions later leading to the development of autoimmunity. In addition, diseased mice were examined to analyse the underlying processes that caused disease manifestation and progression.

In the lungs of CD19-iGP_Smarta mice, the development of ELT could be observed. The ELT was also present in the Alb-/CD19-iGP_Smarta mouse line, but no other monitored line, indicating that its development was due to the autoantigen-presentation by B cells. The ELT mainly consisted of B and T cells, even though no separate B and T cell zones were found. The formation of such ELT in the lung indicated ongoing immune processes there, which might have been the nucleus for lung inflammation that could be seen in diseased mice of the CD19-iGP_Smarta line. The ELT structures found in eight-week-old mice were rather small in size and number and clearly distinguishable from the normal lung tissue. In line with that, the mice did not show any symptoms of lung destruction at that age. In 20-week-old mice, ELT structures were increased in number and size, yet they were clearly limited and made up only a small part of the lung tissue. In the diseased mice, however, the lymphatic infiltrations in the lungs were diffuse and expansive, so that no clear distinction between healthy tissue and infiltrate was possible. It is most likely that these infiltrates, along with similar infiltrates in other organs, were causative for the observed sickness symptoms of the mice. Be that as it may, the age-related increase in lung inflammation, mainly with B and T cells, in CD19-iGP_Smarta mice was reminiscent of the development of liver inflammation in Alb-iGP_Smarta mice (Preti, 2019). Thus, ELT seemed to drive inflammation both in liver and lung.

Secondary lymphoid tissue in the lungs is called bronchus-associated lymphatic tissue (BALT) and is not constitutively present in mice as well as humans (Sminia et al., 1989, Pabst, 1992, Pabst and Gehrke, 1990). In response to microbial stimulation or inflammation, however, the formation of ELT in the lungs can be induced, which is then called inducible BALT (iBALT) (Tschernig and Pabst, 2000, Moyron-Quiroz et al., 2004). Opposed to the classical BALT which is located in the airway walls along major bronchial airways, this iBALT can be located throughout the lung, even in the alveolar space (Moyron-Quiroz et al., 2006, Pabst, 2007). It is therefore quite possible that the structures found in the CD19-iGP_Smarta and Alb-/CD19-iGP_Smarta mice were iBALT. To differentiate iBALT from unstructured pulmonary lymphoid clusters, they should at least contain a B cell follicular structure including FDCs. Furthermore, BALT as well as iBALT usually contain a stroma cell network, separate B and T cell areas and high endothelial venules (HEVs) as well as lymphatics in the T cell zones (Pabst, 2007). The fact that the structures in the lungs of CD19-iGP_Smarta mice showed no B and T cell zonation in the B220- and CD4-staining argued against the hypothesis that these were iBALT. To get a clearer picture, however, it will be necessary to perform a staining for FDCs and HEVs. It may also be helpful to stain for CD8 T cells to differentiate unstructured lymphoid clusters from iBALT with B cell follicles, as the latter usually do not contain CD8 T cells (Woodland and Randall, 2004).

The inflamed lungs of CD19-iGP_Smarta mice showed the presence of Smarta T cells (Figure 21). This is in line with the findings in the liver that were already discussed in 5.1. It can be assumed that the Smarta T cells were present in all peripheral organs not protected by specific anatomical barriers from immune cell invasion. However, it was noticeable that the frequency of Smarta T cells in the spleen as a secondary lymphoid organ was higher compared to the target tissues (62.52 % vs. 21.03 % in the liver and 33.43 % in the lung, see 4.2.1.1.2). A possible explanation for this finding might be that the frequency of APCs, including GP₆₁₋₈₀ presenting B cells, was higher in the spleen than in non-lymphoid organs, leading to accumulation of antigen-specific T cells. Analysis of the B cell populations in different organs of CD19-iGP_Smarta mice confirmed that their frequency was highest in the spleen. Moreover, the proportion of Tregs in the lungs of CD19-iGP_Smarta mice was reduced compared to CD19-iGP control mice (Figure 22) as well as to the normal peripheral Treg frequency of wildtype mice (10 – 15 %, see 5.1). A lower Treg frequency compared to CD19-iGP control mice could also be seen in the spleen of the CD19-iGP_Smarta mice (Figure 10). This low Treg frequency may indicate a beginning collapse of the tolerance mechanisms and could be one explanation for the development of autoimmune disease.

Histological analysis of the kidneys of 8- and 20-week-old CD19-iGP_Smarta mice showed no visible inflammation, but a quantification of the nuclei per glomerulus revealed an age-related increase of the cell number here. This could be an indicator for the development of proliferative glomerulonephritis, as an increase in cell number within the glomeruli is one characteristic sign for this disease, both in patients and mice (Vijayakumar, 2002, Zubair and Frieri, 2013, Richard and Gilkeson, 2018). Since autoimmune glomerulonephritis, as found in SLE patients, is caused by immune-complex-deposition (Frieri, 2002, de Zubiria Salgado and Herrera-Diaz, 2012) it would be of interest to perform a staining for immune complexes in the kidneys of CD19-iGP_Smarta mice.

The examination of CD19-iGP_Smarta mice older than 20 weeks showed that they developed a systemic inflammatory disease with inflammatory infiltrates in several organs with a 50 % prevalence at the age of 35 weeks. Mostly affected were the kidneys, lungs, spleen and thymus. This inflammation most likely occurred due to the reaction of autoreactive Smarta T cells to autoantigen presented by B cells; the disease could then be classified as systemic autoimmune disease (Murphy and Weaver, 2016). All analysed organs of CD19-iGP_Smarta mice with disease symptoms showed lymphatic infiltrates with lymphoproliferation. Interestingly, the kidneys showed expansive interstitial infiltrates, but also a higher intraglomerular cell number compared to eight-week-old mice of the same line, indicating a development of interstitial as well as glomerulonephritis.

The frequency and number of CD45⁺ lymphocytes and especially T cells was highly increased in diseased CD19-iGP_Smarta mice, which matched the histological picture of the expanding lymphocytic infiltrates and showed that mostly T cells were proliferating. However, the staining of Smarta T cells showed no increase of this population. It seems most likely that this finding was due to impaired tetramer binding in the diseased mice, as the TCR is downregulated on highly activated T cells. This problem has been described in literature before (Liu et al., 2000). Nonetheless, it could also be possible that due to collateral damage in inflamed organs, epitope spreading had occurred activating also other non-GP-specific T and B cells as well as innate immune cells (Powell and Black, 2001). Thus, these immune cell populations might also have proliferated to some degree in diseased mice. However, as the Smarta T cells were the cell population that initially caused the disease, could be stimulated by virtually all B cells through MHC-II-TCR contact and constitutes the major part of the T cell pool, it can be assumed that this cell population had extensively proliferated during disease manifestation.

The Treg frequency in all analysed organs of diseased CD19-iGP_Smarta mice was reduced compared to healthy mice of the same line. This showed that although in young mice Tregs were present in peripheral organs, they were not able to keep the autoreactive T cells in check in the long run. Yet, the lower Treg frequency in sick mice must not necessarily have been caused by actual reduction of absolute Treg numbers but could have also been due to proliferation of T_{eff} cells, which had outcompeted Tregs. As a result in both cases, T_{eff} cells were predominating over Tregs, which might explain the manifestation of autoimmune disease.

The examination of the B cell population in diseased CD19-iGP_Smarta mice showed a reduced B cell frequency in these mice. This reduction was already apparent in eight-week-old mice in liver and lung, as detected by flow cytometry (Figure 12 and Figure 23) as well as immunohistochemistry staining for B cell markers in the liver (Figure 24). B cell frequency further decreased with age and especially upon disease manifestation (Figure 32). This finding was unexpected, as mutual stimulation of Smarta T cells and GP-presenting B cells were assumed to result in B cell proliferation. The finding of autoantibodies already in young mice as well as the elevated B cell activation markers in diseased mice show that B cell activation actually occurred. One might speculate that the reduced B cell frequency was due to some tolerance mechanism impeding autoimmune disease development, as a reduced B cell frequency implied less GP-presentation and thus reduced activation of the Smarta T cells. Nonetheless, a reduction of B cells through clonal deletion was unlikely, as this mechanism depends on BCR signals and BCR-specificity (Nemazee and Hogquist, 2003, Hartley et al., 1993, Fields and Erikson, 2003), which were independent of GP-presentation on MHC-II in CD19-iGP_Smarta mice. It was possible, however, that a larger proportion of B cells had become anergic through contact with the Smarta T cells in the periphery, as this contact occurs in a non-inflammatory environment in young mice. Anergic B cells show a reduced lifespan (Fulcher and Basten, 1994, Nossal, 1994), which could possibly explain the observed reduction of B cell numbers. Nevertheless, this does not fully explain the reduction in B cell frequency with age and upon disease manifestation. It should be considered that the pro-inflammatory conditions at that stage might have expedited B cell differentiation towards plasma cells, which do not express B220 and were therefore not included in the $CD19^+ B220^+$ B cell pool (see 2.2.2.2). Indeed, as discussed in the following, plasma cells were predominant at that stage.

Analysis of the B cell subpopulations revealed a tendency towards higher frequencies of germinal centre B cells in 20-week-old and diseased CD19-iGP_Smarta mice (Figure 36), which was probably related to the formation of germinal centres in these animals.

Together with a tendency towards higher frequencies of plasma cells in diseased mice (Figure 38), this finding suggests an increased rate of B cell activation. This is consistent with the occurrence of autoantibodies in CD19-iGP_Smart mice, as these are produced by plasma cells, which are derived from activated B cells in germinal centres (see 2.2.2.2). The high frequency of effector/memory B cells in all analysed lines, however, should be taken with caution, as the effector B cell frequency in mice reported by Zhang et al. in 2017 using a similar panel was much lower (0.5 – 3 % in lymph nodes, compared to 81 – 92 % in the spleen of our mice lines, Figure 34). In addition to the shown staining of effector/memory B cells, germinal centre B cells and plasma cells, another staining for class-switched B cells using IgM and IgG as markers was performed. This data could unfortunately not be used, as the staining with the IgM antibody showed unreliable results with almost no IgM positive cells. However, the staining with the IgG antibody that was also used to identify the effector/memory B cells, seemed to work quite well, as clearly distinguishable positive and negative populations were found. Nonetheless, additional specificity tests for the IgG antibody should be performed, in order to exclude non-specific binding of this antibody to other B cell markers as a possible cause for the obtained high effector/memory B cell frequency.

Since CD19-iGP_Smart mice developed a systemic autoimmune disease with major involvement of the kidneys, these mice might serve as a mouse model for SLE. It is already known that mouse models with genetic changes in B cells most commonly develop lupus-like diseases (Guo et al., 2013). These genetic changes lead to break of B cell tolerance enabling B cell activation and survival independent of the BCR specificity (Pao et al., 2007, Maxwell et al., 2011). They also lead to autoantibody-production, including ANAs (Tsubata, 2017). Both these features were also present in our model, as GP₆₁₋₈₀ presentation on MHC-II to the autoreactive T cells enabled B cell stimulation and activation without involvement of the BCR. In addition, a diverse autoantibody-pattern could be found already in young mice, and diseased mice showed a higher plasma cell frequency. There are many existing SLE mouse models of different kinds. Most of them show autoantibody production and development of immunocomplex glomerulonephritis. The latter is the most common feature in the SLE models, in many models it is even the only lupus component represented (Du et al., 2015). From this it can already be deduced that none of the previous mouse models for SLE is completely representative, each only represents part of the disease features (Nadeau, 1989, Mestas and Hughes, 2004). Therefore, the development of new lupus models with a more comprehensive picture of the disease or the mapping of new disease aspects could lead to a better understanding of SLE.

The CD19-iGP_Smarta mice developed interstitial nephritis. Yet, a higher intraglomerular cell number seemed to indicate additional glomerulonephritis, however, based on the performed PAS staining, a clear pathology could not be found there. As already mentioned above, it would be necessary to perform additional staining for immune complexes deposition in the glomeruli.

Based on disease development, the previous SLE mouse models can be categorized into spontaneous, inducible, or transgenic and knockout mouse models. It is noticeable here that only some of the models show a female preponderance as in the human disease, while in many models male and female animals are affected equally, or disease development is even limited to male mice (Richard and Gilkeson, 2018). In CD19-iGP_Smarta mice and Alb-/CD19-iGP_Smarta mice, no sex-related differences regarding B and T cell frequencies or disease prevalence were found (Figure 40 and Figure 41). Thus, CD19-iGP_Smarta mice did not represent the sex difference of human SLE.

Besides the already mentioned glomerulonephritis and autoantibody production, some of the spontaneous SLE models also show other features of the disease like arthritis, cerebritis or skin rash (Richard and Gilkeson, 2018). From macroscopic examination, these features were not present in CD19-iGP_Smarta mice. However, microscopic analysis of joints, brain and skin should be performed to determine potential affection of other organs.

However, CD19-iGP_Smarta mice also showed features that are rarely observed in classical SLE, such as liver inflammation or thymus enlargement. Thus, it remains to be seen whether CD19-iGP_Smarta mice might serve as a meaningful lupus model. However, thus far, there is no transgenic mouse model with spontaneous lupus development based on enhanced communication between T and B cells.

In the future, in-depth analysis of young and diseased CD19-iGP_Smarta mice should be carried out in order to further characterize the systemic autoimmune disease and its development. This should include immunohistochemical staining of the ELT in the lungs for FDCs, HEVs and CD8 T cells. In addition, flow cytometry staining for T and B cell populations in the kidneys of young mice should be performed to see whether renal cell composition differs from that in other organs. The B cell panel should be modified by adding a suitable IgM antibody and possibly a different IgG antibody in order to include class-switched B cells in the analysis of all organs. Furthermore, an IgG ELISA with serum samples should be performed to determine whether the mice showed hypergammaglobulinemia as another classical feature of autoimmune diseases.

An immunocomplex staining of the glomeruli of young and diseased mice should be performed, as well as staining for B cells, T cells and innate cells including macrophages in order to confirm the occurrence of glomerulonephritis. Proteinuria should also be examined in diseased mice. The histological analysis should be expanded to joints, brain, skin and intestinal tract, to define more clearly all the organs affected by the autoimmune disease. Taken together, this should provide a comprehensive picture of the systemic autoimmune disease in CD19-iGP_Smarta mice.

6 Summary

This study investigated the role of autoantigen-presentation by B cells in the development of autoimmune diseases. To that end, we modified an established mouse model of autoimmune hepatitis (AIH), Alb-iGP_Smarta mice in which hepatocytes present a peptide autoantigen that specifically activates Smarta CD4 T cells and drives AIH. The role of B cells was studied in Alb/CD19-iGP_Smarta mice in which autoreactive Smarta T cells can be activated also by autoantigen-presenting B cells in addition to hepatocytes. Moreover, CD19-iGP_Smarta mice were studied to learn whether exclusive antigen-presentation by B cells leads to systemic autoimmunity.

Analysis of Alb/CD19-iGP_Smarta mice revealed that antigen-presentation by B cells did not substantially influence the development of hepatocyte-driven AIH. Histological liver inflammation was also not influenced by antigen-presenting B cells. Moreover, antigen-presentation by B cells did not influence the presence or frequencies of Smarta T cells in the periphery, including the liver. Furthermore, the peripheral induction of Tregs was not influenced by antigen-presenting B cells. However, antigen presentation by B cells induced a more diverse pattern of autoantibodies, indicating a non-specific activation of B cells as a consequence of T and B cell cooperation.

Analysis of CD19-iGP_Smarta mice revealed that autoantigen-presentation exclusively by B cells induced spontaneous sickness and systemic autoimmune disease. Autoreactive Smarta T cells were present in the periphery in high frequencies, whereas Tregs and B cells were present in reduced frequencies. In the lungs, lymphoid aggregates were found that increased in size with age. In the kidney, interstitial nephritis and an increase of cells per glomerulus could be seen. Upon spontaneous sickness manifestation, the mice showed extensive inflammation in all analysed organs, with highly increased T cell numbers, reduced Treg frequencies and even lower B cell number than in young mice. Analysis of the B cell subpopulations revealed a tendency for a higher frequency of plasma cells in diseased mice.

In conclusion, antigen-presentation by B cells did not seem to influence spontaneous development of autoimmune hepatitis that was driven by autoantigen-presenting hepatocytes. Yet a different autoantibody pattern was found, indicating B cell activation. Thus, autoantibody-producing B cells may be an epiphenomenon in AIH, but do not seem to drive AIH pathology. However, exclusive antigen-presentation by B cells in cooperation with cognate CD4 T cells can result in systemic autoimmune disease, affecting various organs in a rather non-specific way.

7 Zusammenfassung

In dieser Arbeit wurde die Rolle der Präsentation von Autoantigenen durch B-Zellen bei der Entstehung von Autoimmunerkrankungen untersucht. Zu diesem Zweck modifizierten wir ein etabliertes Mausmodell der Autoimmunhepatitis (AIH), Alb-iGP_Smarta-Mäuse, in denen Hepatozyten ein Peptid-Autoantigen präsentieren, das spezifisch Smarta-CD4-T-Zellen aktiviert und AIH antreibt. Die Rolle der B-Zellen wurde in Alb-/CD19-iGP_Smarta-Mäusen untersucht, in denen autoreaktive Smarta-T-Zellen zusätzlich zu den Hepatozyten auch durch Autoantigen-präsentierende B-Zellen aktiviert werden können. Darüber hinaus wurden CD19-iGP_Smarta-Mäuse untersucht, um zu erfahren, ob die ausschließliche Antigenpräsentation durch B-Zellen zu einer systemischen Autoimmunität führt.

Die Analyse der Alb/CD19-iGP_Smarta-Mäuse ergab, dass die Antigenpräsentation durch B-Zellen keinen wesentlichen Einfluss auf die Entwicklung einer durch Hepatozyten getriebenen AIH hat. Auch die histologische Leberentzündung wurde durch Antigen-präsentierende B-Zellen nicht beeinflusst. Darüber hinaus hatte die Antigenpräsentation durch B-Zellen keinen Einfluss auf das Vorhandensein oder die Häufigkeit von Smarta-T-Zellen in der Peripherie, einschließlich der Leber. Des Weiteren wurde die periphere Induktion von regulatorischen T-Zellen nicht durch Antigen-präsentierende B-Zellen beeinflusst. Allerdings induzierte die Antigenpräsentation durch B-Zellen ein vielfältigeres Muster von Autoantikörpern, was auf eine unspezifische Aktivierung von B-Zellen als Folge der Kooperation zwischen T- und B-Zellen hinweist.

Die Analyse von CD19-iGP_Smarta-Mäusen ergab, dass die Autoantigen-Präsentation ausschließlich durch B-Zellen das spontane Entstehen einer systemischen Autoimmunerkrankung auslöste. Autoreaktive Smarta-T-Zellen bildeten in der Peripherie einen hohen Anteil der Lymphozyten, während der Anteil an regulatorischen Z-Zellen und B-Zellen reduziert war. In der Lunge wurden lymphoide Aggregate gefunden, die mit zunehmendem Alter der Mäuse an Größe zunahmen. In der Niere konnten eine interstitielle Nephritis sowie eine Zunahme der Zellen pro Glomerulus festgestellt werden. Bei Krankheitsmanifestation zeigten die Mäuse eine ausgedehnte Entzündung in allen untersuchten Organen, mit stark erhöhten T-Zellzahlen, reduzierten Anteile an regulatorischen T-Zellen und sogar niedrigeren B-Zellzahlen als bei jungen Mäusen. Die Analyse der B-Zell-Subpopulationen zeigte eine Tendenz zu einem höheren Anteil an Plasmazellen in erkrankten Mäusen.

Zusammenfassend lässt sich sagen, dass die Antigenpräsentation durch B-Zellen keinen Einfluss auf die spontane Entwicklung einer durch Autoantigen-präsentierende Hepatozyten angetriebenen Autoimmunhepatitis zu haben schien. Dennoch wurde ein verändertes Autoantikörpermuster gefunden, was auf eine B-Zell-Aktivierung hinweist. Autoantikörper-produzierende B-Zellen können also ein Epiphänomen bei AIH sein, scheinen aber nicht die Pathologie der AIH zu bestimmen. Allerdings kann die Antigenpräsentation ausschließlich durch B-Zellen in Kooperation mit korrespondierenden CD4-T-Zellen zu einer systemischen Autoimmunerkrankung führen, die verschiedenste Organe auf unspezifische Weise betrifft.

8 Bibliography

- AL-BUSAFI, S. A., MICHEL, R. P. & DESCHENES, M. 2013. Rituximab for refractory autoimmune hepatitis: a case report. *Arab J Gastroenterol*, 14, 135-8.
- ALVAREZ, F. 2006. Autoimmune hepatitis and primary sclerosing cholangitis. *Clin Liver Dis*, 10, 89-107, vi.
- ANDERSON, M. S. & SU, M. A. 2016. AIRE expands: new roles in immune tolerance and beyond. *Nat Rev Immunol*, 16, 247-58.
- BECCASTRINI, E., D'ELIOS, M. M., EMMI, G., SILVESTRI, E., SQUATRITO, D., PRISCO, D. & EMMI, L. 2013. Systemic lupus erythematosus: immunopathogenesis and novel therapeutic targets. *Int J Immunopathol Pharmacol*, 26, 585-96.
- BELAND, K., MARCEAU, G., LABARDY, A., BOURBONNAIS, S. & ALVAREZ, F. 2015. Depletion of B cells induces remission of autoimmune hepatitis in mice through reduced antigen presentation and help to T cells. *Hepatology*, 62, 1511-23.
- BELKAID, Y., PICCIRILLO, C. A., MENDEZ, S., SHEVACH, E. M. & SACKS, D. L. 2002. CD4+CD25+ regulatory T cells control Leishmania major persistence and immunity. *Nature*, 420, 502-7.
- BENSCHOP, R. J., AVISZUS, K., ZHANG, X., MANSER, T., CAMBIER, J. C. & WYSOCKI, L. J. 2001. Activation and anergy in bone marrow B cells of a novel immunoglobulin transgenic mouse that is both hapten specific and autoreactive. *Immunity*, 14, 33-43.
- BURAK, K. W., SWAIN, M. G., SANTODOMINGO-GARZON, T., LEE, S. S., URBANSKI, S. J., ASPINALL, A. I., COFFIN, C. S. & MYERS, R. P. 2013. Rituximab for the treatment of patients with autoimmune hepatitis who are refractory or intolerant to standard therapy. *Can J Gastroenterol*, 27, 273-80.
- CAMERON, J. S. 1999. Lupus nephritis. *J Am Soc Nephrol*, 10, 413-24.
- CHRISTEN, U. & HINTERMANN, E. 2015. An Update on Animal Models of Autoimmune Hepatitis: Are we There Yet? *Curr Pharm Des*, 21, 2391-400.
- CHU, V. T., ENGHARD, P., SCHURER, S., STEINHAUSER, G., RUDOLPH, B., RIEMEKASTEN, G. & BEREK, C. 2009. Systemic activation of the immune system induces aberrant BAFF and APRIL expression in B cells in patients with systemic lupus erythematosus. *Arthritis Rheum*, 60, 2083-93.
- COSMI, L., MAGGI, L., SANTARLASCI, V., LIOTTA, F. & ANNUNZIATO, F. 2014. T helper cells plasticity in inflammation. *Cytometry A*, 85, 36-42.
- CZAJA, A. J. 2005. Diverse manifestations and evolving treatments of autoimmune hepatitis. *Minerva Gastroenterol Dietol*, 51, 313-33.
- CZAJA, A. J. 2008. Safety issues in the management of autoimmune hepatitis. *Expert Opin Drug Saf*, 7, 319-33.
- D'AGOSTINO, D., COSTAGUTA, A. & ALVAREZ, F. 2013. Successful treatment of refractory autoimmune hepatitis with rituximab. *Pediatrics*, 132, e526-30.
- DE ZUBIRIA SALGADO, A. & HERRERA-DIAZ, C. 2012. Lupus nephritis: an overview of recent findings. *Autoimmune Dis*, 2012, 849684.
- DILILLO, D. J., HORIKAWA, M. & TEDDER, T. F. 2011. B-lymphocyte effector functions in health and disease. *Immunol Res*, 49, 281-92.

- DRAKE, D. R., 3RD, REAM, R. M., LAWRENCE, C. W. & BRACIALE, T. J. 2005. Transient loss of MHC class I tetramer binding after CD8+ T cell activation reflects altered T cell effector function. *J Immunol*, 175, 1507-15.
- DU, Y., SANAM, S., KATE, K. & MOHAN, C. 2015. Animal models of lupus and lupus nephritis. *Curr Pharm Des*, 21, 2320-49.
- FELD, J. J., DINH, H., ARENOVICH, T., MARCUS, V. A., WANLESS, I. R. & HEATHCOTE, E. J. 2005. Autoimmune hepatitis: effect of symptoms and cirrhosis on natural history and outcome. *Hepatology*, 42, 53-62.
- FIELDS, M. L. & ERIKSON, J. 2003. The regulation of lupus-associated autoantibodies: immunoglobulin transgenic models. *Curr Opin Immunol*, 15, 709-17.
- FONTENOT, J. D., RASMUSSEN, J. P., GAVIN, M. A. & RUDENSKY, A. Y. 2005. A function for interleukin 2 in Foxp3-expressing regulatory T cells. *Nat Immunol*, 6, 1142-51.
- FRIERI, M. 2002. Complement-related diseases. *Allergy Asthma Proc*, 23, 319-24.
- FRIERI, M. 2013. Mechanisms of disease for the clinician: systemic lupus erythematosus. *Ann Allergy Asthma Immunol*, 110, 228-32.
- FROMMER, F., HEINEN, T. J., WUNDERLICH, F. T., YOGEV, N., BUCH, T., ROERS, A., BETTELLI, E., MULLER, W., ANDERTON, S. M. & WAISMAN, A. 2008. Tolerance without clonal expansion: self-antigen-expressing B cells program self-reactive T cells for future deletion. *J Immunol*, 181, 5748-59.
- FROMMER, F. & WAISMAN, A. 2010. B cells participate in thymic negative selection of murine auto-reactive CD4+ T cells. *PLoS One*, 5, e15372.
- FUJINAMI, R. S., OLDSTONE, M. B., WROBLEWSKA, Z., FRANKEL, M. E. & KOPROWSKI, H. 1983. Molecular mimicry in virus infection: crossreaction of measles virus phosphoprotein or of herpes simplex virus protein with human intermediate filaments. *Proc Natl Acad Sci U S A*, 80, 2346-50.
- FULCHER, D. A. & BASTEN, A. 1994. Reduced life span of anergic self-reactive B cells in a double-transgenic model. *J Exp Med*, 179, 125-34.
- GOODNOW, C. C., BRINK, R. & ADAMS, E. 1991. Breakdown of self-tolerance in anergic B lymphocytes. *Nature*, 352, 532-6.
- GOODNOW, C. C., SPRENT, J., FAZEKAS DE ST GROTH, B. & VINUESA, C. G. 2005. Cellular and genetic mechanisms of self tolerance and autoimmunity. *Nature*, 435, 590-7.
- GUO, Y., ORME, J. & MOHAN, C. 2013. A genopedia of lupus genes - lessons from gene knockouts. *Curr Rheumatol Rev*, 9, 90-9.
- HARRIS, D. P., HAYNES, L., SAYLES, P. C., DUSO, D. K., EATON, S. M., LEPAK, N. M., JOHNSON, L. L., SWAIN, S. L. & LUND, F. E. 2000. Reciprocal regulation of polarized cytokine production by effector B and T cells. *Nat Immunol*, 1, 475-82.
- HARTLEY, S. B., COOKE, M. P., FULCHER, D. A., HARRIS, A. W., CORY, S., BASTEN, A. & GOODNOW, C. C. 1993. Elimination of self-reactive B lymphocytes proceeds in two stages: arrested development and cell death. *Cell*, 72, 325-35.
- IGNATOWICZ, L., KAPPLER, J. & MARRACK, P. 1996. The repertoire of T cells shaped by a single MHC/peptide ligand. *Cell*, 84, 521-9.
- ITOH, M., TAKAHASHI, T., SAKAGUCHI, N., KUNYASU, Y., SHIMIZU, J., OTSUKA, F. & SAKAGUCHI, S. 1999. Thymus and autoimmunity: production of CD25+CD4+ naturally anergic and suppressive T cells as a key function of the thymus in maintaining immunologic self-tolerance. *J Immunol*, 162, 5317-26.

- JACOB, N. & STOHL, W. 2011. Cytokine disturbances in systemic lupus erythematosus. *Arthritis Res Ther*, 13, 228.
- JAECKEL, E., HARDTKE-WOLENSKI, M. & FISCHER, K. 2011. The benefit of animal models for autoimmune hepatitis. *Best Pract Res Clin Gastroenterol*, 25, 643-51.
- JANKOVIC, M., CASELLAS, R., YANNOUTSOS, N., WARDEMANN, H. & NUSSENZWEIG, M. C. 2004. RAGs and regulation of autoantibodies. *Annu Rev Immunol*, 22, 485-501.
- KESSEL, A., ROSNER, I. & TOUBI, E. 2008. Rituximab: beyond simple B cell depletion. *Clin Rev Allergy Immunol*, 34, 74-9.
- KESSLER, W. R., CUMMINGS, O. W., ECKERT, G., CHALASANI, N., LUMENG, L. & KWO, P. Y. 2004. Fulminant hepatic failure as the initial presentation of acute autoimmune hepatitis. *Clin Gastroenterol Hepatol*, 2, 625-31.
- KOGAN, J., SAFADI, R., ASHUR, Y., SHOUVAL, D. & ILAN, Y. 2002. Prognosis of symptomatic versus asymptomatic autoimmune hepatitis: a study of 68 patients. *J Clin Gastroenterol*, 35, 75-81.
- KRAWITT, E. L. 2006. Autoimmune hepatitis. *N Engl J Med*, 354, 54-66.
- LARSEN, F. S. 2008. Treatment of patients with severe autoimmune hepatitis. *Minerva Gastroenterol Dietol*, 54, 57-63.
- LAUFER, T. M., DEKONING, J., MARKOWITZ, J. S., LO, D. & GLIMCHER, L. H. 1996. Unopposed positive selection and autoreactivity in mice expressing class II MHC only on thymic cortex. *Nature*, 383, 81-5.
- LAURENCE, A., TATO, C. M., DAVIDSON, T. S., KANNO, Y., CHEN, Z., YAO, Z., BLANK, R. B., MEYLAN, F., SIEGEL, R., HENNIGHAUSEN, L., SHEVACH, E. M. & O'SHEA J, J. 2007. Interleukin-2 signaling via STAT5 constrains T helper 17 cell generation. *Immunity*, 26, 371-81.
- LIU, H., RHODES, M., WIEST, D. L. & VIGNALI, D. A. 2000. On the dynamics of TCR:CD3 complex cell surface expression and downmodulation. *Immunity*, 13, 665-75.
- LIU, X., JIANG, X., LIU, R., WANG, L., QIAN, T., ZHENG, Y., DENG, Y., HUANG, E., XU, F., WANG, J. Y. & CHU, Y. 2015. B cells expressing CD11b effectively inhibit CD4+ T-cell responses and ameliorate experimental autoimmune hepatitis in mice. *Hepatology*, 62, 1563-75.
- LO, M. S. & TSOKOS, G. C. 2018. Recent developments in systemic lupus erythematosus pathogenesis and applications for therapy. *Curr Opin Rheumatol*, 30, 222-228.
- LUND, F. E., GARVY, B. A., RANDALL, T. D. & HARRIS, D. P. 2005. Regulatory roles for cytokine-producing B cells in infection and autoimmune disease. *Curr Dir Autoimmun*, 8, 25-54.
- LUXON, B. A. 2008. Diagnosis and treatment of autoimmune hepatitis. *Gastroenterol Clin North Am*, 37, 461-78, vii-viii.
- MACKAY, F., SCHNEIDER, P., RENNERT, P. & BROWNING, J. 2003. BAFF AND APRIL: a tutorial on B cell survival. *Annu Rev Immunol*, 21, 231-64.
- MAMULA, M. J., FATENEJAD, S. & CRAFT, J. 1994. B cells process and present lupus autoantigens that initiate autoimmune T cell responses. *J Immunol*, 152, 1453-61.
- MANNS, M. P., CZAJA, A. J., GORHAM, J. D., KRAWITT, E. L., MIELI-VERGANI, G., VERGANI, D., VIERLING, J. M. & AMERICAN ASSOCIATION FOR THE STUDY OF LIVER, D. 2010. Diagnosis and management of autoimmune hepatitis. *Hepatology*, 51, 2193-213.

- MANNS, M. P., LOHSE, A. W. & VERGANI, D. 2015. Autoimmune hepatitis--Update 2015. *J Hepatol*, 62, S100-11.
- MANZI, S. 2001. Epidemiology of systemic lupus erythematosus. *Am J Manag Care*, 7, S474-9.
- MAXWELL, M. J., DUAN, M., ARMES, J. E., ANDERSON, G. P., TARLINTON, D. M. & HIBBS, M. L. 2011. Genetic segregation of inflammatory lung disease and autoimmune disease severity in SHIP-1^{-/-} mice. *J Immunol*, 186, 7164-75.
- MESTAS, J. & HUGHES, C. C. 2004. Of mice and not men: differences between mouse and human immunology. *J Immunol*, 172, 2731-8.
- METCALF, E. S. & KLINMAN, N. R. 1977. In vitro tolerance induction of bone marrow cells: a marker for B cell maturation. *J Immunol*, 118, 2111-6.
- MIZOGUCHI, A. & BHAN, A. K. 2006. A case for regulatory B cells. *J Immunol*, 176, 705-10.
- MORITOKI, Y., LIAN, Z. X., OHSUGI, Y., UENO, Y. & GERSHWIN, M. E. 2006. B cells and autoimmune liver diseases. *Autoimmun Rev*, 5, 449-57.
- MOYRON-QUIROZ, J. E., RANGEL-MORENO, J., HARTSON, L., KUSSER, K., TIGHE, M. P., KLONOWSKI, K. D., LEFRANCOIS, L., CAULEY, L. S., HARMSSEN, A. G., LUND, F. E. & RANDALL, T. D. 2006. Persistence and responsiveness of immunologic memory in the absence of secondary lymphoid organs. *Immunity*, 25, 643-54.
- MOYRON-QUIROZ, J. E., RANGEL-MORENO, J., KUSSER, K., HARTSON, L., SPRAGUE, F., GOODRICH, S., WOODLAND, D. L., LUND, F. E. & RANDALL, T. D. 2004. Role of inducible bronchus associated lymphoid tissue (iBALT) in respiratory immunity. *Nat Med*, 10, 927-34.
- MURPHY, K. & WEAVER, C. 2016. *Janeway's Immunobiology*, New York, Garland Science.
- NADEAU, J. H. 1989. Maps of linkage and synteny homologies between mouse and man. *Trends Genet*, 5, 82-6.
- NEMAZEE, D. & HOGQUIST, K. A. 2003. Antigen receptor selection by editing or downregulation of V(D)J recombination. *Curr Opin Immunol*, 15, 182-9.
- NOSSAL, G. J. 1994. Negative selection of lymphocytes. *Cell*, 76, 229-39.
- NOSSAL, G. J. & PIKE, B. L. 1975. Evidence for the clonal abortion theory of B-lymphocyte tolerance. 1975. *J Immunol*, 179, 5619-32.
- OXENIUS, A., BACHMANN, M. F., ZINKERNAGEL, R. M. & HENGARTNER, H. 1998. Virus-specific MHC-class II-restricted TCR-transgenic mice: effects on humoral and cellular immune responses after viral infection. *Eur J Immunol*, 28, 390-400.
- PABST, R. 1992. Is BALT a major component of the human lung immune system? *Immunol Today*, 13, 119-22.
- PABST, R. 2007. Plasticity and heterogeneity of lymphoid organs. What are the criteria to call a lymphoid organ primary, secondary or tertiary? *Immunol Lett*, 112, 1-8.
- PABST, R. & GEHRKE, I. 1990. Is the bronchus-associated lymphoid tissue (BALT) an integral structure of the lung in normal mammals, including humans? *Am J Respir Cell Mol Biol*, 3, 131-5.
- PALMER, E. 2003. Negative selection--clearing out the bad apples from the T-cell repertoire. *Nat Rev Immunol*, 3, 383-91.
- PAO, L. I., LAM, K. P., HENDERSON, J. M., KUTOK, J. L., ALIMZHANOV, M., NITSCHKE, L., THOMAS, M. L., NEEL, B. G. & RAJEWSKY, K. 2007. B cell-specific deletion of

- protein-tyrosine phosphatase Shp1 promotes B-1a cell development and causes systemic autoimmunity. *Immunity*, 27, 35-48.
- PETRI, M. 2002. Epidemiology of systemic lupus erythematosus. *Best Pract Res Clin Rheumatol*, 16, 847-58.
- PONS-ESTEL, G. J., ALARCON, G. S., SCOFIELD, L., REINLIB, L. & COOPER, G. S. 2010. Understanding the epidemiology and progression of systemic lupus erythematosus. *Semin Arthritis Rheum*, 39, 257-68.
- POWELL, A. M. & BLACK, M. M. 2001. Epitope spreading: protection from pathogens, but propagation of autoimmunity? *Clin Exp Dermatol*, 26, 427-33.
- PRETI, M. 2019. *Immune mechanisms in the pathogenesis of experimental autoimmune hepatitis*. PhD, University of Hamburg.
- RIBATTI, D. 2017. The discovery of plasma cells: An historical note. *Immunol Lett*, 188, 64-67.
- RICHARD, M. L. & GILKESON, G. 2018. Mouse models of lupus: what they tell us and what they don't. *Lupus Sci Med*, 5, e000199.
- SAKAGUCHI, S., TAKAHASHI, T. & NISHIZUKA, Y. 1982. Study on cellular events in post-thymectomy autoimmune oophoritis in mice. II. Requirement of Lyt-1 cells in normal female mice for the prevention of oophoritis. *J Exp Med*, 156, 1577-86.
- SAKAGUCHI, S., YAMAGUCHI, T., NOMURA, T. & ONO, M. 2008. Regulatory T cells and immune tolerance. *Cell*, 133, 775-87.
- SAMY, E. T., PARKER, L. A., SHARP, C. P. & TUNG, K. S. 2005. Continuous control of autoimmune disease by antigen-dependent polyclonal CD4+CD25+ regulatory T cells in the regional lymph node. *J Exp Med*, 202, 771-81.
- SHEVACH, E. M., DIPAOLO, R. A., ANDERSSON, J., ZHAO, D. M., STEPHENS, G. L. & THORNTON, A. M. 2006. The lifestyle of naturally occurring CD4+ CD25+ Foxp3+ regulatory T cells. *Immunol Rev*, 212, 60-73.
- SMINIA, T., VAN DER BRUGGE-GAMELKOORN, G. J. & JEURISSEN, S. H. 1989. Structure and function of bronchus-associated lymphoid tissue (BALT). *Crit Rev Immunol*, 9, 119-50.
- STRASSER, A. & BOUILLET, P. 2003. The control of apoptosis in lymphocyte selection. *Immunol Rev*, 193, 82-92.
- SUMMERSKILL, W. H., KORMAN, M. G., AMMON, H. V. & BAGGENSTOSS, A. H. 1975. Prednisone for chronic active liver disease: dose titration, standard dose, and combination with azathioprine compared. *Gut*, 16, 876-83.
- TAKAHASHI, T., KUNIYASU, Y., TODA, M., SAKAGUCHI, N., ITOH, M., IWATA, M., SHIMIZU, J. & SAKAGUCHI, S. 1998. Immunologic self-tolerance maintained by CD25+CD4+ naturally anergic and suppressive T cells: induction of autoimmune disease by breaking their anergic/suppressive state. *Int Immunol*, 10, 1969-80.
- TIEGS, S. L., RUSSELL, D. M. & NEMAZEE, D. 1993. Receptor editing in self-reactive bone marrow B cells. *J Exp Med*, 177, 1009-20.
- TSCHERNIG, T. & PABST, R. 2000. Bronchus-associated lymphoid tissue (BALT) is not present in the normal adult lung but in different diseases. *Pathobiology*, 68, 1-8.
- TSUBATA, T. 2017. B-cell tolerance and autoimmunity. *F1000Res*, 6, 391.
- URIBE, M., GO, V. L. & KLUGE, D. 1984. Prednisone for chronic active hepatitis: pharmacokinetics and serum binding in patients with chronic active hepatitis and steroid major side effects. *J Clin Gastroenterol*, 6, 331-5.

- VAN SANTEN, H. M., BENOIST, C. & MATHIS, D. 2004. Number of T reg cells that differentiate does not increase upon encounter of agonist ligand on thymic epithelial cells. *J Exp Med*, 200, 1221-30.
- VIJAYAKUMAR, M. 2002. Acute and crescentic glomerulonephritis. *Indian J Pediatr*, 69, 1071-5.
- WARDEMANN, H., YURASOV, S., SCHAEFER, A., YOUNG, J. W., MEFFRE, E. & NUSSENZWEIG, M. C. 2003. Predominant autoantibody production by early human B cell precursors. *Science*, 301, 1374-7.
- WOODLAND, D. L. & RANDALL, T. D. 2004. Anatomical features of anti-viral immunity in the respiratory tract. *Semin Immunol*, 16, 163-70.
- YILDIRIM-TORUNER, C. & DIAMOND, B. 2011. Current and novel therapeutics in the treatment of systemic lupus erythematosus. *J Allergy Clin Immunol*, 127, 303-12; quiz 313-4.
- YU, C., GERSHWIN, M. E. & CHANG, C. 2014. Diagnostic criteria for systemic lupus erythematosus: a critical review. *J Autoimmun*, 48-49, 10-3.
- ZERRAHN, J., HELD, W. & RAULET, D. H. 1997. The MHC reactivity of the T cell repertoire prior to positive and negative selection. *Cell*, 88, 627-36.
- ZHANG, R., SAGE, P. T., FINN, K., HUYNH, A., BLAZAR, B. R., MARANGONI, F., MEMPEL, T. R., SHARPE, A. H. & TURKA, L. A. 2017. B Cells Drive Autoimmunity in Mice with CD28-Deficient Regulatory T Cells. *J Immunol*, 199, 3972-3980.
- ZUBAIR, A. & FRIERI, M. 2013. Lupus nephritis: review of the literature. *Curr Allergy Asthma Rep*, 13, 580-6.

9 List of figures

Figure 1: Creation of the mutated iGP gene: The CLIP sequence of the class II-associated invariant chain gene was replaced by the GP ₆₁₋₈₀ peptide sequence. In addition, the gene was inserted into the ROSA26 gene with a floxed stop codon put in front.....	21
Figure 2: Mouse model of autoimmune hepatitis: Alb-iGP_Smarta mice expressing the GP ₆₁₋₈₀ peptide from LCMV in hepatocytes and possessing autoreactive CD4 Smarta T cells specific for this peptide.	22
Figure 3: (Left) Serum levels of alanine aminotransferase (ALT) from Alb-iGP_Smarta mice older than 20 weeks with clinical manifestation of the disease compared to 20-week-old Alb-iGP mice. (Right) Disease prevalence of Alb-iGP_Smarta mice compared to Alb-iGP mice. Data obtained from Max Preti (Preti, 2019).	23
Figure 4: Histology of consecutive liver sections from eight-week-old Alb-iGP_Smarta mice. Haemalaun and eosin (H&E) staining and immunohistochemistry staining for B220 (B cells stained in purple) and CD4 (T cells stained in purple). 200 fold magnification. Data obtained from Max Preti (Preti, 2019).	23
Figure 5: Histology of liver tissue from Alb-iGP_Smarta mice older than 20 weeks with clinical manifestation of the disease. H&E staining and immunohistochemistry staining for B220 (B cells stained in purple). 100 fold magnification. Data obtained from Max Preti (Preti, 2019).	24
Figure 6: CD19-iGP_Smarta mice expressing the GP ₆₁₋₈₀ peptide in B cells and possessing autoreactive CD4 Smarta T cells specific for this peptide.....	25
Figure 7: Mouse model to study the role of B cells in autoimmune hepatitis: Alb-/CD19-iGP_Smarta mice expressing the the GP ₆₁₋₈₀ peptide in hepatocytes and B cells and possessing autoreactive CD4 Smarta T cells specific for this peptide.	26
Figure 8: Gating strategy of the flow cytometry T cell panel used to stain for CD4 and CD8 T cells, antigen-specific Smarta T cells (tetramer ⁺) and Tregs.....	43
Figure 9: (A) Representative flow cytometry plots showing antigen-specific Smarta T cells (tetramer ⁺) of CD4 T cells in spleen and liver of eight-week-old control mice (Smarta, CD19-iGP), CD19-iGP_Smarta, Alb-iGP_Smarta and Alb-/CD19-iGP_Smarta mice. Numbers beside gates indicate percent positive cells in each gate. (B) Percentages of antigen-specific Smarta T cells (tetramer ⁺) in the thymus of eight-week-old control mice (Smarta, CD19-iGP), CD19-iGP_Smarta, Alb-iGP_Smarta and Alb-/CD19-iGP_Smarta.....	45

Figure 10: (A) Representative flow cytometry plots showing antigen-specific Smarta T cells (tetramer⁺) and Foxp3⁺ Tregs of CD4 T cells in the spleen of eight-week-old control mice (Smarta, CD19-iGP), CD19-iGP_Smarta, Alb-iGP_Smarta and Alb-/CD19-iGP_Smarta mice. Numbers in quadrants indicate percent positive cells in each of them.47

Figure 11: Gating strategy of the flow cytometry B cell panel used to stain for CD19⁺ B220⁺ B cells.....48

Figure 12: (A) Representative flow cytometry plots showing CD19⁺ B220⁺ B cells of CD45⁺ cells in spleen and liver of eight-week-old control mice (Smarta, CD19-iGP), CD19-iGP_Smarta, Alb-iGP_Smarta and Alb-/CD19-iGP_Smarta mice. Numbers in quadrants indicate percent positive cells in each of them. (B) Percentages of B cells in spleen and liver of eight-week-old control mice (wildtype, Smarta, CD19-iGP), CD19-iGP_Smarta, Alb-iGP_Smarta and Alb-/CD19-iGP_Smarta mice.....49

Figure 13: Indirect immunofluorescence staining of serum from control mice (CD19-iGP, Alb-iGP) as well as CD19-iGP_Smarta, Alb-iGP_Smarta and Alb-/CD19-iGP_Smarta mice on Hep2 cells at a dilution of 1:160. 400 fold magnification.....50

Figure 14: H&E staining of liver tissue from eight-week-old control mice (Smarta, CD19-iGP) as well as CD19-iGP_Smarta, Alb-iGP_Smarta and Alb-/CD19-iGP Smarta mice. 200 fold magnification. Data of the Alb-iGP_Smarta mice was obtained from Max Preti (Preti, 2019).51

Figure 15: Histology of consecutive liver sections from eight-week-old Alb-/CD19-iGP_Smarta mice. H&E staining and immunohistochemistry staining for B220 (B cells stained in purple) and CD4 (CD4 T cells stained in purple). 100 fold magnification.....52

Figure 16: Measurement of ALT and AST as markers for liver damage in the serum of eight-week-old control mice (Smarta, CD19-iGP), CD19-iGP_Smarta, Alb-iGP_Smarta and Alb-/CD19-iGP_Smarta mice.52

Figure 17: Comparison of flow cytometry data from male vs female Alb-/CD19-iGP_Smarta mice. Shown are percentages of antigen-specific Smarta T cells (tetramer⁺), Tregs, antigen-specific Tregs (tetramer⁺) and B cells in spleen and liver.53

Figure 18: H&E staining of lung tissue from eight-week-old control mice (Smarta, CD19-iGP) as well as CD19-iGP_Smarta and Alb-/CD19-iGP Smarta mice. 200 fold magnification.55

Figure 19: (A) Percentage of mice with ≥ 1 LS in one histological slide of the left lung from eight-week-old control mice (wildtype, Smarta, CD19-iGP) as well as eight-week-old CD19-

iGP_Smarta and Alb-/CD19-iGP_Smarta mice and 20-week-old CD19-iGP_Smarta mice.	56
Figure 20: Histology of consecutive lung sections from 8- and 20-week-old CD19-iGP_Smarta mice. H&E staining and immunohistochemistry staining for B220 (B cells stained in purple) and CD4 (T cells stained in purple). 200 fold magnification.....	56
Figure 21: Percentages of antigen-specific Smarta T cells (tetramer ⁺) in the lung of eight-week-old control mice (Smarta, CD19-iGP) and CD19-iGP_Smarta mice.....	57
Figure 22: Percentages of Tregs and antigen-specific Tregs (tetramer ⁺) in the lung of eight-week-old control mice (Smarta, CD19-iGP) and CD19-iGP_Smarta mice.....	58
Figure 23: Percentages of B cells in the lung of eight-week-old control mice (wildtype, Smarta, CD19-iGP) and CD19-iGP_Smarta mice.....	58
Figure 24: Immunohistochemistry staining of liver tissue from eight-week-old control mice (Smarta, CD19-iGP) and CD19-iGP_Smarta mice for B220 (B cells stained in purple) and CD4 (CD4 T cells stained in purple). 200 fold magnification.....	59
Figure 25: (A) PAS staining of kidney tissue from eight-week-old control mice (Smarta, CD19-iGP) and CD19-iGP_Smarta mice. 400 fold magnification.	60
Figure 26: Disease prevalence of CD19-iGP_Smarta mice compared to CD19-iGP control mice.....	61
Figure 27: Photos of organs from CD19-iGP_Smarta mice displaying severe disease symptoms. (Left) Enlarged spleen, liver and kidney. (Right) Enlarged liver, thymus, normal sized kidney and enlarged spleen.....	62
Figure 28: Histology of tissue from CD19-iGP_Smarta mice older than 20 weeks showing severe disease symptoms. (Up, from left to right) H&E staining of the thymus and spleen. 100 fold magnification. (Middle, from left to right) H&E staining of the liver. 100 fold magnification. PAS staining of the kidney. 400 fold magnification. (Down, from left to right) H&E staining of the lung. 20 and 200 fold magnification.	63
Figure 29: Splenocyte numbers, percentages as well as absolute numbers of T cells in the spleen and absolute numbers of T cells in the liver of 20-week-old control mice (Smarta, CD19-iGP) and CD19-iGP_Smarta mice as well as CD19-iGP_Smarta mice older than 20 weeks with clinical manifestation of disease.	65
Figure 30: (A) Percentages of antigen-specific Smarta T cells (tetramer ⁺) in spleen, liver, lung and kidney of 20-week-old control mice (Smarta, CD19-iGP) and CD19-iGP_Smarta as well as CD19-iGP_Smarta mice older than 20 weeks with clinical manifestation of disease.	66

Figure 31: Percentages of Tregs and antigen-specific Tregs (tetramer⁺) in the spleen, liver, lung and kidney of 20-week-old CD19-iGP_Smarta mice as well as CD19-iGP_Smarta mice older than 20 weeks with clinical manifestation of disease.67

Figure 32: Percentages and absolute numbers of B cells in the spleen and percentages of B cells in the liver, lung and kidney of 20-week-old control mice (Smarta, CD19-iGP) and CD19-iGP_Smarta mice as well as CD19-iGP_Smarta mice older than 20 weeks with clinical manifestation of disease.....68

Figure 33: Gating strategy of the flow cytometry B cell panel for CD19⁺ B220⁺ IgG⁺ CD38⁺ effector and memory B cells isolated from the spleen.69

Figure 34: Percentages of effector and memory B cells in the spleen, liver, lung and kidney of 20-week-old control mice (Smarta, CD19-iGP) and CD19-iGP_Smarta as well as CD19-iGP_Smarta mice older than 20 weeks with clinical manifestation of disease.70

Figure 35: Gating strategy of the flow cytometry B cell panel for B220⁺ Fas (CD95)⁺ Gl-7⁺ germinal centre B cells isolated from the spleen.70

Figure 36: Percentages of germinal centre B cells in the spleen, liver, lung and kidney of 20-week-old control mice (Smarta, CD19-iGP) and CD19-iGP_Smarta mice as well as CD19-iGP_Smarta mice older than 20 weeks with clinical manifestation of disease.71

Figure 37: Gating strategy of the flow cytometry B cell panel for CD19⁺ CD138⁺ plasma cells isolated from the spleen.....72

Figure 38: Percentages of plasma cells in the spleen, liver, lung and kidney of 20-week-old control mice (Smarta, CD19-iGP) and CD19-iGP_Smarta mice as well as CD19-iGP_Smarta mice older than 20 weeks with clinical manifestation of disease.73

Figure 39: MFI as measure for the expression of the activation markers MHC-II and CD69 on CD19⁺ B220⁺ B cells in spleen and liver of 20-week-old control mice (Smarta, CD19-iGP) and CD19-iGP_Smarta as well as CD19-iGP_Smarta mice older than 20 weeks with clinical manifestation of disease.....74

Figure 40: Comparison of flow cytometry data from male vs female CD19-iGP_Smarta mice. Shown are percentages of antigen-specific Smarta T cells (tetramer⁺) and B cells in spleen, liver and lung.75

Figure 41: Disease prevalence of male vs female CD19-iGP_Smarta mice.76

10 List of tables

Table 1: Instruments	28
Table 2: Chemicals	29
Table 3: Consumables	31
Table 4: Kits.....	32
Table 5: Antibodies for histology	32
Table 6: Antibodies and Tetramer for flow cytometry	33
Table 7: Software.....	34
Table 8: Buffer and other solutions	34
Table 9: Mouse Lines.....	36
Table 10: Levels of significance	41

11 Acknowledgements

I would like to extend my sincerest gratitude to all the people who have helped me during my dissertation.

Primarily I would like to thank my supervisors Antonella Carambia and Johannes Herkel who have always supported and helped me throughout my dissertation. I am equally thankful to Max Preti who helped me immensely during this project with all my experiments and was always there to answer questions and give advice. I have learned a great deal from working with him and I am very grateful for his support. I would also like to thank all the members of my lab who always helped and supported me during my dissertation especially to Sabrina Kreß, Gela Schmidt, Marko Hilken, Fenja Schuran, Miriam Schakat and Björn Wieschendorf for their friendship and professional help. Furthermore, I would like to thank Thorsten Wiech for his help and advice with the evaluation of kidney histology. Finally, I would like to thank the Medical Director of the I. Medical Clinic, Ansgar W. Lohse, for providing me with the opportunity to pursue this research project.

On a personal note, I would like to thank my friends and family who have supported me during the time of my dissertation and beyond.

12 Curriculum Vitae

Lebenslauf entfällt aus datenschutzrechtlichen Gründen.

13 Eidesstattliche Versicherung

Ich versichere ausdrücklich, dass ich die Arbeit selbständig und ohne fremde Hilfe verfasst, andere als die von mir angegebenen Quellen und Hilfsmittel nicht benutzt und die aus den benutzten Werken wörtlich oder inhaltlich entnommenen Stellen einzeln nach Ausgabe (Auflage und Jahr des Erscheinens), Band und Seite des benutzten Werkes kenntlich gemacht habe.

Ferner versichere ich, dass ich die Dissertation bisher nicht einem Fachvertreter an einer anderen Hochschule zur Überprüfung vorgelegt oder mich anderweitig um Zulassung zur Promotion beworben habe.

Ich erkläre mich einverstanden, dass meine Dissertation vom Dekanat der Medizinischen Fakultät mit einer gängigen Software zur Erkennung von Plagiaten überprüft werden kann.

Unterschrift: 